

# IVIS2019

14th International Vacuum Insulation Symposium  
September 19 – 20, 2019, Kyoto Research Park, Kyoto, Japan

## **Proceedings of the 14<sup>th</sup> International Vacuum Insulation Symposium (IVIS2019)**

**Editor(s):**

Atsushi Iwamae, Daisuke Ogura, Masaru Abuku



**Proceedings of the 14th International Vacuum Insulation Symposium  
(IVIS2019)**

**Edited by Atsushi Iwamae, Daisuke Ogura, Masaru Abuku**

**Published by Faculty of Architecture, Kindai University**

**3-4-1 Kowakae, Higashi-Osaka, Osaka 577-8502, Japan**

**Date of publication: 19 September 2019**

**All rights reserved. No part of this publication may be reproduced, stored in a retrieval system, or transmitted, in any form or by any means, without the prior permission in writing of the publisher, or as expressly permitted by law, or under terms agreed with the appropriate reprographics rights organization.**

**ISBN: 978-4-600-00218-3**

## **Preface**

**Kyoto is an ancient capital, more than 1,200 years old. Hopefully, the participants will enjoy not only its historical buildings such as temples and shrines but also the natural beauty of the mountains surrounding the city. Autumn is one of the best seasons in Kyoto. The venue of the conference will be at Kyoto Research Park. As well known, Kyoto is 30 minutes by train from Osaka and 1.5 hours by limited express from Kansai international airport (KIX). Kyoto offers many hotels and various sightseeing spots. Here, we would like to welcome the 14th IVIS and its participation.**

**Organized by Kindai University, this two-day event fosters dialogue among scientists, academics and professionals from all around the world who are related to the research, development and production of Super Insulating Materials (SIM). IVIS 2019 will promote the co-operations between manufacturers and researchers and between western and eastern.**

**Atsushi Iwamae (Kindai University)  
Conference Chair**



# CONTENTS

Aerogels - transparent, low-density solids for energy management .....	1
<i>Kazuki Nakanishi, Kazuyoshi Kanamori, Ryota Ueoka and Mamoru Aizawa</i>	
Development of VIP based on core insulators made from textile fibers .....	3
<i>Jiří Zach, Tadej Sekavčnik, Vítězslav Novák, Jan Bubeník, Tomáš Mihelič</i>	
Sawdust based core material for eco-friendly Vacuum Insulation Panels (VIPs).....	7
<i>Mahmood Alam, Harjit Singh</i>	
Impact of artificial ageing on mechanical and hygrothermal properties of Advanced-Porous-Materials (APM) for buildings .....	11
<i>Christoph Sprengard, Sebastian Tremel, Carolin Kokolsky, Susanne Regauer</i>	
Why does the mechanical behaviour of precipitated silica make them unsuitable today for their use in VIP cores? .....	15
<i>Bernard Yrieix, Geneviève Foray, David Jauffres, Belynda Benane, Etienne Guesnet</i>	
Performance advancement of a new sub-micron pore size polymeric foam for vacuum insulation panels .....	19
<i>Flávia A. Almeida, Kenny Rottenbacher, Hermann Beyrichen, Roland Caps, Alexander Müller, Roland Oberhoffer</i>	
Determination of anisotropic thermal conductivity of VIP laminate using transient plane source method .....	23
<i>Bijan Adl-Zarrabi, Pär Johansson, Alireza Marzbanrad</i>	
Development of self-healing films to improve durability of VIPs by in-situ remediation of film defects .....	27
<i>Kaushik Biswas, Tomonori Saito, Pengfei Cao, Natasha Ghezawi, Kelsey Grady, David Wood, Rose Ruther, Dustin Gilmer, Kenisha Gardner</i>	
"Super VIPs" – Vacuum panels with exceptionally low degradation rate .....	31
<i>Yoash Carmi, Eddie Shufer</i>	

Determining the air permeation rate into VIPs in less than 24 hours using Helium permeation .....	37
<i>Eddie Shufer, Yoash Carmi</i>	
Increase of thermal conductivity of vacuum-panels with fumed silica cores in relation to absorbed moisture – hygrothermal simulations and measurements .....	43
<i>Sprengard Christoph, Kerstin Lohr, Carolin Kokolsky, Sebastian Tremel</i>	
A cost-optimal sensitivity analysis of internal VIPs application in buildings .....	47
<i>Márcio Gonçalves, Nuno Simões, Catarina Serra, Shahaboddin Resalati, Kate Brown</i>	
Application of Vacuum Insulation Panel in slim façade: from lab to in-situ experimental evaluations .....	51
<i>F. E. Boafo, SM. Kim, JG. Ahn, HB. Moon, JH. Kim, JT. Kim</i>	
Study on thermal performance of VIP applied wall by installation method in building .....	55
<i>Sang-Myung Kim, Ji-Suk Yu, Kil-Seon Lee, Jin-Hee Kim, Jun-Tae Kim</i>	
Thermal and aging characterization of stand-alone and foam-embedded VIPs for building applications .....	59
<i>K. Biswas, R. Jogineedi, A.O. Desjarlais, D. Smith, J. Jones</i>	
Structural characterization of nanostructured silica ageing: Imaging and analysing particles and pores from a few nanometres up to 100nm .....	63
<i>Bruno Chal, Bernard Yrieix, Lucian Roiban, Karine Masenelli-Varlot, Guilhem Baeza, Geneviève Foray</i>	
Utilization of the vacuum insulation panels in a factory and comparison of long term performance measurement using micro-pressure sensor and prediction value .....	67
<i>Hideya Yamamoto, Daisuke Ogura</i>	
Aging (2011-2019) of glass fiber core VIPs in arctic Canadian climate .....	71
<i>Vivian Chan, Phalguni Mukhopadhyaya, Matthew D. Ooms, Juergen Korn, Douglas MacLean, Stephen Mooney, Shane Andre</i>	

The Wall-ACE project: an overview of the in-field monitoring on the novel Aerogel-based products.....	75
<i>Stefano Fantucci, Elisa Fenoglio, Valentina Serra, Marco Perino, Timea Béjat, Didier Therme, Lori McElroy, Sean Doran, and Jon Hand</i>	
Vacuum insulation panels for fish box.....	79
<i>Sankarshan Verma, Harjit Singh</i>	
Long-term performance of silica aerogel and aerogel based composites: A literature review highlighting pathways for further studies .....	87
<i>Ali Naman Karim, Pär Johansson, Angela Sasic Kalagasidis</i>	
LCA analysis of Vacuum Insulation Panels and their sensitivity to EOL and future grid decarbonisation scenarios .....	91
<i>Shahaboddin Resalati, Kate Brown, Nuno Simões, Márcio Gonçalves, Catarina Serra</i>	
Molecular dynamic measurements, a tools to assess how surface chemistry modifies mechanical properties of mesoporous silica.....	95
<i>Wassim Kassem, Julien Morthomas, Patrice Chantrenne, Genevieve Foray</i>	
Calibration method on the thermal conductivity measurement in the central part of vacuum insulation panels (VIP) by heat flow meter apparatus.....	99
<i>Kensaku Mabuchi, Atsushi Iwamae, Daisuke Ogura, Taichi Tasaka</i>	
Methods for renovation of Kyomachiya dwellings using vacuum insulation panels and evaluation of thermal-insulation performance .....	103
<i>Yui Nakazawa, Daisuke Ogura, Chiemi Iba, Hideya Yamamoto</i>	
Prediction on long-term thermal performance of VIP using glass fiber core considering influence of getter .....	107
<i>Taichi Tasaka, Daisuke Ogura, Atsushi Iwamae, Kensaku Mabuchi, Hideya Yamamoto</i>	
Wood-fibre panels as core material for VIP.....	111
<i>Sebastian Tremel, Max Engelhardt, Elisabeth Windeisen-Holzhauser</i>	
Studying the effect of surface chemistry on the mechanical properties of silica nano-structures through atomistic simulations.....	115
<i>Wassim Kassem, Julien Morthomas, Patrice Chantrenne, Genevieve Foray</i>	

Ultralight carbon-based composites foam with considerable thermal insulation·····	121
<i>Zhang Junxiong, Chen Zhaofeng, Xue Songbai</i>	

## Aerogels - Transparent, Low-density Solids for Energy Management

Kazuki Nakanishi<sup>1,2</sup>, Kazuyoshi Kanamori<sup>2</sup>, Ryota Ueoka<sup>2</sup> and Mamoru Aizawa<sup>3</sup>

<sup>1</sup>Division of Materials Research, Institute of Materials and Systems for Sustainability, Nagoya University

<sup>2</sup>Department of Chemistry, Graduate School of Science, Kyoto University

<sup>3</sup>Tiem Factory Incorporated

dknakanishi@imass.nagoya-u.ac.jp

### Introduction

Aerogels are characterized by low-density, visible-light transparency and superb thermal insulation properties. In the case of most common silica aerogels, their fragile nature and the necessity of using supercritical drying process have kept their practical use unrealistic. We proposed a novel concept of using organic-inorganic hybrid network structure for aerogels, and have been successful in improving the mechanical strength while preserving their fascinating properties as they are. For example, methyl-modified silsesquioxane gels exhibited reversible large deformation under uniaxial compression, which have made ambient drying of large-sized aerogel tiles possible. Aerogels with higher flexural strength have also been prepared accommodating higher fraction of organic networks. Based on the established technology and registered IP's, the venture company is now scaling up the synthesis for industrial applications.

### Experimental Procedures

Methyltrimethoxysilane (MTMS) was used as a single precursor for hydrolysis in the presence of surfactant, urea and dilute aqueous acetic acid. The mixture was stirred to give a homogeneous solution followed by heating up to 60 °C in a closed condition. The ammonia evolved by the hydrolysis of urea raised pH of the reaction solution homogeneously, resulted in the formation of homogeneous gels. After appropriate aging and washing processes, the wet gels were subjected to either supercritical drying or ambient pressure (evaporative) drying. For the resultant polymethylsilsesquioxane (PMSQ) gels, visible light transmittance at the thickness of 10 mm, mechanical behavior under uniaxial compression or 3-point bending, and thermal conductivity at varied gas pressures were measured.

### Results and Discussion

Under the optimized synthesis conditions, monolithic solids larger than 100x100x10 mm<sup>3</sup> have been successfully obtained via ambient pressure drying, with ~0.15 g cm<sup>-3</sup> density corresponding to 90 % porosity, ~90 % transmittance with  $\lambda = 550$  nm visible light, and 12~15 mW m<sup>-1</sup> K<sup>-1</sup> thermal conductivity [1]. These properties are reasonably comparable with those for supercritically dried counterparts. The reversible large deformation of PMSQ network allowed spring-back of once shrunk gel volume upon evaporative drying [2]. Structurally, the trifunctional siloxane network with compact and hydrophobic methyl group attached on each Si atom are contrasted with rigid tetrafunctional silica network with abundant silanol groups. Spectroscopic measurements revealed that the presence of surfactant in the initial stage of hydrolysis/polycondensation of MTMS played a crucial role to regulate the growth and network formation among the PMSQ oligomers. Further extensions of precursor structures and resultant networks to more highly interconnected organic and inorganic bridges have also been done [3, 4].

### References

- [1] K. Kanamori, M. Aizawa, K. Nakanishi, T. Hanada, New transparent methylsilsesquioxane aerogels and xerogels with improved mechanical properties, *Adv. Mater.*, **19**, 1589-1593 (2007).
- [2] G. Hayase, K. Kanamori, A. Maeno, H. Kaji, K. Nakanishi, Dynamic spring-back behavior in evaporative drying of polymethylsilsesquioxane monolithic gels for low-density transparent thermal superinsulators, *J. Non-Cryst. Solids*, **434**, 115-119 (2016).
- [3] (Review) T. Shimizu, K. Kanamori, K. Nakanishi, Silicone-based organic-inorganic hybrid aerogels and xerogels, *Chem. Eur. J.*, **23**, 5176-5187 (2017).
- [4] G. Zu, T. Shimizu, K. Kanamori, Y. Zhu, A. Maeno, H. Kaji, J. Shen, K. Nakanishi, Transparent, superflexible doubly cross-linked polyvinylpolymethylsiloxane aerogel superinsulators via ambient pressure drying, *ACS Nano*, **12**, 521-532 (2018).



## Development of VIP based on core insulators made from textile fibers

Jiří Zach<sup>1,\*</sup>, Tadej Sekavčnik<sup>2</sup>, Vítězslav Novák<sup>1</sup>, Jan Bubeník<sup>1</sup>, Tomaž Mihelič<sup>2</sup>

<sup>1</sup>Brno University of Technology, Faculty of Civil Engineering, Brno, Czech Republic

<sup>2</sup>Turvac, Šoštanj, Slovenija

\*Corresponding e-mail: zach.j@fce.vutbr.cz

### ABSTRACT

Vacuum insulation panels (VIP) are among the most progressive materials in the world. Their consumption grows every year, so it is necessary to find alternative sources of production for their production, which are ecological and sustainable in the long term. Textile fibres (both primary and secondary) belong to universal raw materials available in the world in sufficient quantities, with some of the fibres (for example, cotton fibres) being easily renewable, and a large number of secondary / recycled fibres available on the world market with properties close to primary fibres. The paper describes the results of research on the development of VIP based on core insulators made from textile fibres. This is mainly about the development of insulators based on different types of primary and recycled fibres and the study of their behaviour under reduced pressure (vacuum) and the study of the properties of VIP made of these insulators.

### KEYWORDS

Vacuum insulation, textile fibres, thermal conductivity, alternative core insulator.

### INTRODUCTION

Energy saving is one of the main topics in industry and construction in recent years in the EU area, especially in relation to key documents such as the Energy Performance of Buildings Directive 2010/31/EU as amended by Directive 2018/844/EU [1]. However, the importance of thermal insulation is also in areas where we need to isolate the enclosed space from the effects of high or low external temperatures (shipping containers, boxes, packages), where modern thermal insulations, which are a vacuum insulation panels (VIPs), plays a very important role, because with very low thickness and weight they exhibit very high thermal resistance, which in some cases can be up to 20 times higher than that of conventional insulators (e.g. EPS) of the same thickness. VIP panels are now a common part of most people's lives, because they are built into most cooling home appliances (refrigerators, freezers). Due to the increasing world consumption of VIPs, it is also necessary to deal with their production from a material point of view and to find ways to use secondary and easily renewable raw materials in their production. A number of scientific papers address this issue, for example, researchers from *Vilnius Gediminas Technical University* in Lithuania, have been addressing the use of garnetted grain stalks for VIP production years ago [2, 3]. For example, other works also dealt with the use of man-made organic based fibers for VIP production [4]. Brno university of technology, in cooperation with the Slovenian company Turvac, has been dealing with the possibility of using textile fibers (primary and recycled) for the production of insulating mats usable as core insulation for VIP production for several years. The advantage of these insulators is significantly lower thermal conductivity of primary fibers, which is approx. 4 x lower than the thermal conductivity of glass fibers commonly used for VIP production. The indisputable advantage of textile fibers is their availability, which can be both natural and synthetic fibers and the fiber thickness is very close to the requirements for fibers that are

useful for VIP production, where the limit thickness of the (glass) fibers usable for VIP production is about 10 microns [5].

Fiber thickness regulation in manufacturing is also simpler for synthetic fibers than, for example, glass wool, where the fiber thickness is dependent on the production technology and the use of newer specialized technologies is necessary for the production of very fine fibers. The key parameter for fiber mats is the pressure  $p_{1/2}$  determining the thermal properties of the insulating material under vacuum. This is the pressure at which the gas thermal conductivity reaches the value of one half of the normal thermal conductivity of the air  $\lambda_g$  [6]:

$$p_{1/2} = \frac{T}{\delta} \cdot \frac{2 \cdot \beta \cdot k_B}{\sqrt{2} \cdot \pi \cdot d_g^2}$$

Where:  $\delta$  is medium pore size of the material,  $k_B$  is Boltzman constant,  $d_g$  is diameter of the gas molecules,  $T$  is temperature,  $\beta$  is gas type constant,  $\lambda_g = 25.5 \text{ mW}/(\text{m} \cdot \text{K})$ .

## TEST SAMPLES AND METHODOLOGY

Within research works, a number of both primary and secondary synthetic and natural fibers have been tested for their physical properties as well as their thermal conductivity. Cotton and polyester fibers, which are commercially available (primary and secondary) in thicknesses of about 11 microns have been identified as the most suitable. Primary PES fibers with thickness of 12  $\mu\text{m}$  were selected for the basic work in combination with PES BiCo fibers with thickness of 20  $\mu\text{m}$ .

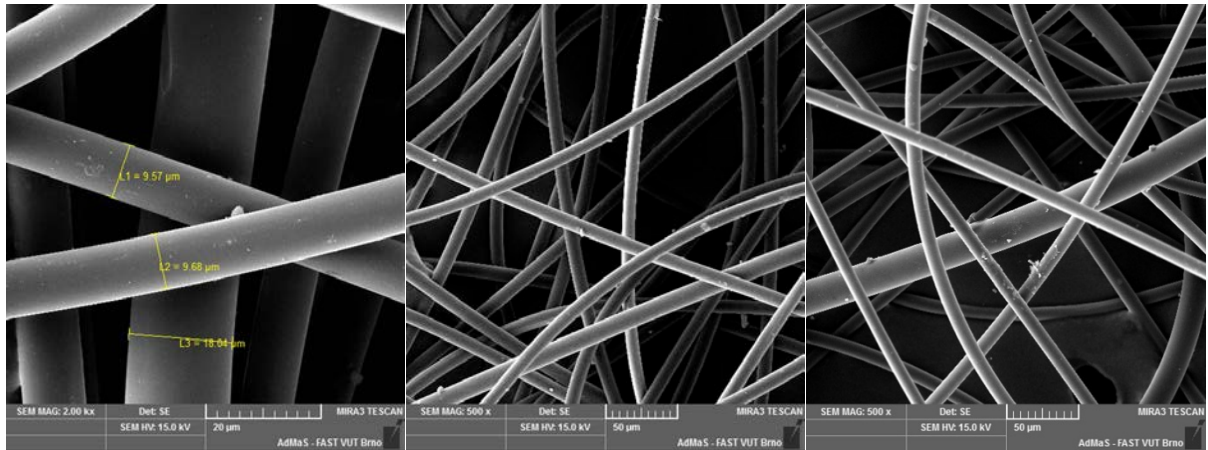


Figure 1: REM photography of insulators structure based on PES fibers (mixture of primary PES fibers and PES BiCo fibers)

These fibers were processed into insulators of varying density and these insulators were subsequently processed in VIP production. The following issues were solved within research works:

- Optimization of density of PES based core insulator,
- Drying the PES-based core insulator to remove the maximum moisture and prevent the VIP properties from deteriorating after vacuuming,
- The issue of outgassing within the VIP with the PES based core insulator and studying the possibilities of using the getters in VIP production.

From the point of view of the test methods, the following were determined for the insulators: linear dimensions and thickness according to EN 822, EN 12085; density according to EN 1602; mass per unit area according to EN 29073-1; thermal conductivity according to EN 12667 and ISO 8301 (including determination of dependence thermal conductivity on pressure).





Figure 2: Photography of equipments for determination of thermal conductivity (FOX 200 Vacuum and FOX 630)

## RESULTS

Drying in a laboratory and industrial drying oven at 200x200mm and 500x500 mm samples was tested in the drying tests. It has been found that the efficiency of the industrial drying oven is significantly higher than that of laboratory driers and therefore significantly less time is needed to dry the samples in the industrial drier. At a temperature of 150 ° C, the drying time of the PES based samples in a laboratory drying oven is at least 90 - 100 minutes depending on the size of the insulator and in an industrial drying oven it is only 30 to 75 minutes depending on the sample size.

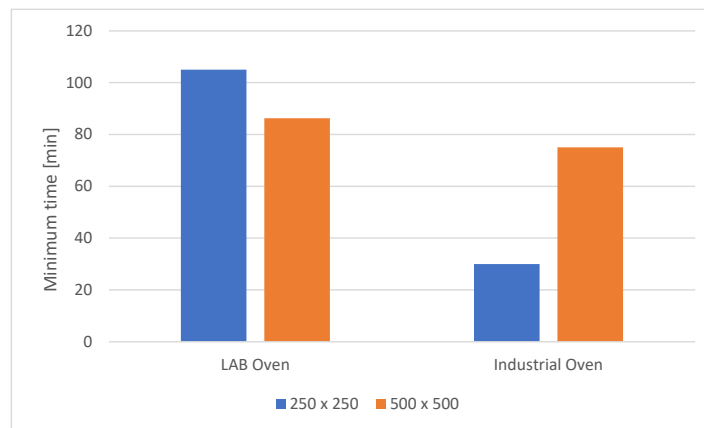


Figure 3: Minimum time required to dry PES based samples according to oven type and sample size

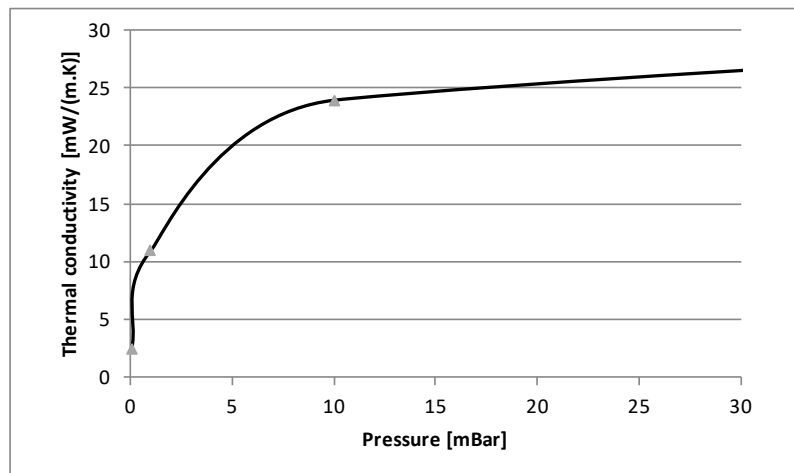


Figure 4: Dependence of thermal conductivity on pressure of core insulator based on PES fibers

Dependence of thermal conductivity on pressure of cose insulator was measured (see fig. 4) pressure  $p_{1/2}$  was from results evaluated  $p_{1/2} = 280$  Pa (for PES based insulator). In addition, the thermal conductivity was determined on the resulting VIPs made from PES-based core insulations depending on the vacuum pressure and type of drying. Measurements were taken after vacuuming, after 24 hours of storage at  $+ 23$  ° C and after 14 days of conditioning at  $+ 70$  ° C. It has been found that samples dried in an industrial dryer show better properties after 14 days. A change in the thermal conductivity was found in the samples, with a very small increase in thermal conductivity in samples vacuumed to a lower pressure of 1 Pa and a decrease in thermal conductivity in samples vacuumed to 5 Pa (see Table 1).

Table 1: Thermal conductivity overview for VIP 500x500 mm samples at different initial pressures

Sample	Pressure [Pa]	$\lambda_{\text{initial}}$ [mW/m.K]	$\lambda_{\text{after 24 h}}$ [mW/m.K]	$\lambda_{\text{14 days, 70°C}}$ [mW/m.K]
PES	1	3,48	3,54	3,62
PES	5	4,26	3,90	3,63

## CONCLUSIONS

As found experimentally, VIP based on PES fibers have very good properties fully comparable to VIP based on glass fibers. From the production point of view, core insulation based on PES fibers is well suited for mass production and when dried in an industrial oven, they achieve better properties than under laboratory conditions. It has also been found that it is not necessary to achieve extremely low pressures in the production of VIPs, with no significant differences in thermal conductivity at 1 and 5 Pa after 14 days. All in all, VIP based on textile fibers represent a full-fledged alternative to classic VIP based on glass fibers, with the advantage of high worldwide availability of textile fibers and the ability to use secondary textile fibers.

## ACKNOWLEDGEMENT

This paper was elaborated with the financial support of the project GA 17-00243S “Study of the behavior of insulating materials under extremely low pressure” and project No. LO1408 “AdMaS UP - Advanced Materials, Structures and Technologies”, supported by the Ministry of Education, Youth and Sports under the “National Sustainability Programme I”.

## REFERENCES

- [1] EU direktive EEB 2010/31/EU (2018/844/EU).
- [2] J. Vėjelienė; Impact of technological factors on the structure and properties of thermal insulation materials from renewable resources; Doctor Dissertation, Vilnius Gediminas Technical University, Lithuania (2012).
- [3] J. Vėjelienė, A. Gailius, S. Vėjelis, et al.; Evaluation of Structure Influence on Thermal Conductivity of Thermal Insulating Materials from Renewable Resources; Materials Science-Medziagotyra, National Conference on Materials Engineering, 17 (2011) 208-212.
- [4] V. Nemanic, M. Žumer; New organic fiber-based core material for vacuum thermal insulation; Energy and Buildings 90 (90) 2015 137-141.
- [5] S. Brunner, K. G. Wakili, T. Stahl, B. Binder; Vacuum insulation panels for building applications—Continuous challenges and developments; Energy and Buildings 85 (2014) 592-596.
- [6] HANITA COATINGS. Thermal Conductivity of VIPs as a Function of Internal Pressure. 2015

## Sawdust based core material for eco-friendly Vacuum Insulation Panels (VIPs)

Mahmood Alam<sup>1,\*</sup>, Harjit Singh<sup>2</sup>

<sup>1</sup>University of Brighton, Brighton, UK

<sup>2</sup>Brunel University London, Uxbridge, UK

*\*Corresponding e-mail: m.alam@brighton.ac.uk*

### ABSTRACT

This study presents an alternative core material developed by using waste sawdust powder for eco-friendly Vacuum Insulation Panels (VIPs). This alternative VIP core material was prepared by using locally sourced waste sawdust powder from woodwork industry. Three samples containing varying mass ratios of sawdust and fumed silica were characterized in terms porosity, pore size, density and thermal conductivity. VIP samples of size 150 × 150 mm were prepared using new alternative core material at a pressure of 0.5 mbar. Center of panel thermal conductivity values of VIP samples were measured just after manufacturing and after storing seven days at room temperature. Test results showed that thermal conductivity (center of panel) values increased with higher contents of sawdust in the VIP core. Reducing sawdust mass% in the VIP core sample from 85% to 30% led to approximately 73% decrease in VIP center of panel thermal conductivity from 21.12 mW/mK to 5.52 mW/mK. Thermal conductivity (center of panel) of VIPs containing 30% sawdust, 55% fumed silica and 15% SiC was measured to be 5.52 mW/mK, which is comparable to commercially available fume silica VIPs. Thermal conductivity results show that sawdust powder in VIP core offers a potentially low cost eco-friendly alternative core material by partially replacing fumed silica, the dominant contributor to the VIP environmental impact.

### KEYWORDS

Vacuum Insulation Panel, Core material, Sawdust powder, Fumed silica, Thermal conductivity

### INTRODUCTION

Vacuum Insulation Panel (VIP), a high thermal performance insulation, is made of inner core board sealed in outer high barrier envelope under vacuum conditions. VIP core is made from porous material retains the vacuum below certain threshold level and physically supports the VIP envelope (Alam et al., 2011). Gaseous heat transfer is suppressed within the core using small size porous materials such as fumed silica. However, fumed silica currently used in the VIP core is an expensive material and have higher associated environmental impact. Global Warming Potential (GWP) of a specified VIP (size 1 m<sup>2</sup>, thickness 25 mm and weight 4.5 kg) at production stage is declared as 42.40 kgCO<sub>2</sub>eq of which 95-99% is contributed by the VIP core (Porextherm Dämmstoffe GmbH, 2014). Among the core materials fumed silica is responsible for at least 90% of the environment impact (Porextherm Dämmstoffe GmbH, 2014). VIP cost and environmental impact reduction can be achieved by fully or partially replacing fumed silica in core board with cheaper natural or renewable alternative materials. Sawdust waste powder is one of the alternative materials which can possibly be incorporated in VIP core as a partial replacement of fumed silica for producing eco-friendly low cost VIPs.

Sawdust is an organic material obtained as waste by-product of the activities of woodworking such as milling, sawing and sanding in wood /furniture industry. Depending upon the nature of

woodworking activity, sawdust can be obtained in different forms and sizes including in the form of very fine powder. It has been used previously for applications such as lightweight cement aggregate (Ahmed et al., 2018) and thermal insulation (Lakrafi et al., 2013) because of its low bulk density, low thermal conductivity and higher porosity. These suitable thermo-physical properties make sawdust an appropriate candidate for VIP core material. This paper presents the development and testing of sawdust and fumed silica composite as VIP core material. The main aim of this work is to optimise thermal and physical properties of sawdust-fumed silica composite as a low cost eco-friendly VIP core material allowing effective recycling of sawdust waste originating from the woodworking industry.

## MATERIALS & METHODS

For this study composites with variable mass ratios of fine sawdust powder, fumed silica and SiC (opacifier) materials were developed by dry mixing. Details of material constituent of different samples are shown in table 1.

Table1. Composition of different investigated samples

Sample	Composition (mass %)		
	Fumed Silica	Sawdust	Silicon Carbide (SiC)
1	0	85	15
2	40	45	15
3	55	30	15

Sawdust used in the study was sourced from a local woodwork company originated as a waste by-product from the sanding operation of reclaimed pine wood. Sawdust waste powder was measured to have the following properties; thermal conductivity 48.68 - 64.08 mW/mK in the temperature range of 10 - 70°C, porosity 79.8%, average pore diameter 7.56µm and bulk density 286 kg/m<sup>3</sup>. Porosity, pore size and density were measured using Mercury Intrusion Porosimetry (MIP) method. VIP samples of size 150 × 150 mm were manufactured with new alternative core materials at a pressure of 0.5 mbar in the vacuum sealing chamber. Center of panel thermal conductivity of developed VIP samples was measured using Heat Flow Meter (HFM 446 Lambda Series- based on ASTM C518).

## RESULTS & DISCUSSION

### Pore size and gaseous thermal conductivity

Three samples 1, 2, and 3 detailed in table 1 were used for MIP measurement. Results of the porosity, average pore size and bulk density are shown in the table 2.

Table 2. Results of MIP measurement

Sample	Average pore diameter × 10 <sup>-6</sup> (m)	Porosity (%)	Bulk density (kg/m <sup>3</sup> )
1	4.100	79.2	335
2	0.239	93.0	116
3	0.237	93.0	91

MIP measurements show that sample 1, no fumed silica, mainly comprising of the sawdust, had the lowest porosity of about 80% and the highest bulk density of 335 kg/m<sup>3</sup>. In composite samples 2 and 3, decreasing the sawdust contents to 45 mass% and 30 mass% led to increase in porosity to 93% and decrease in bulk density to 116 kg/m<sup>3</sup> and 91 kg/m<sup>3</sup> respectively. The

average pore diameter in sample 1 comprising mainly of sawdust powder was  $4.1\mu\text{m}$  while for the composite samples containing both sawdust and fumed silica these values were in the range of 237-239 nm. Using the pore size data (table 1) in equation 1 gaseous thermal conductivity ( $\lambda_G$ ) was calculated.

$$\lambda_G = \lambda_0 / ((1 + (0.032/P\Phi))) \quad (1)$$

Where ( $\lambda_0$ ) is the thermal conductivity of air at atmospheric pressure (W/mK), P is the pressure (Pa) and  $\Phi$  is the pore size (m). Results shown in figure 1 suggests that with composite materials consisting of sawdust and fumed silica (sample 2 and 3) gaseous thermal conductivity can be suppressed to negligible levels below the pressures of 10 mbar while for sample 1 comprising mainly of sawdust powder lower pressures of at least below 0.1 mbar will be needed. In figure 1, curves for sample 2 and 3 are almost identical due to very small difference in their average pore size (table 2).

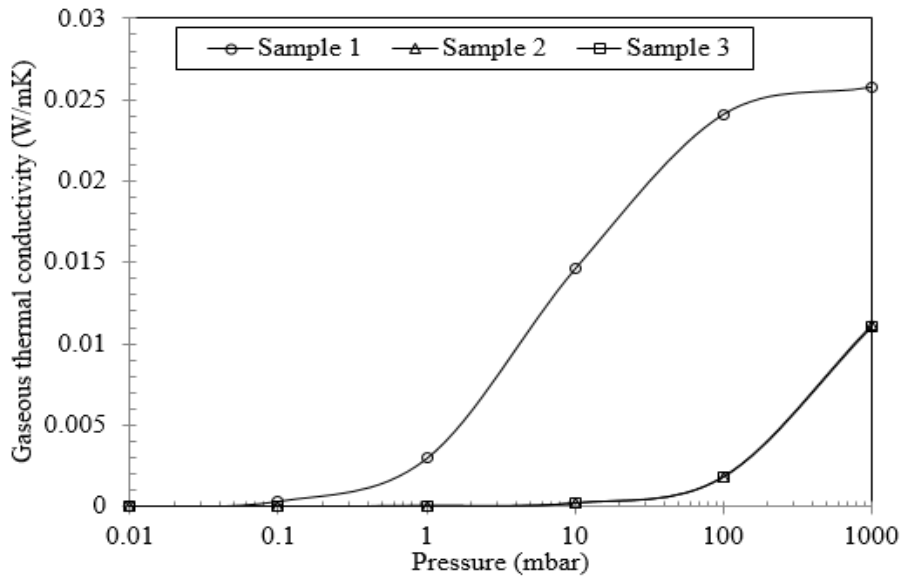


Figure 1. Gaseous thermal conductivity for sawdust and fumed silica composite samples as a function of pressure.

### Thermal conductivity (Center of panel)

Results of experimentally measured center of panel thermal conductivities at mean temperature of  $20^\circ\text{C}$  of VIPs manufactured with samples 1-3 are shown in figure 2. Thermal conductivity values of VIP sample 1 (85% sawdust and 15% SiC) was measured to be 18.18 mW/mK rising to 21.12 mW/mK after 7 days at room conditions. For the VIP sample 2 (45% sawdust, 40% fumed silica and 15% SiC) was measured to be 6.22 mW/mK just after manufacturing increasing to 6.93 mW/mK after 7 days at room temperature. Reducing the sawdust content to 30% and increasing fumed silica content to 55% fumed silica in the sample 3 led to further decrease in the thermal conductivity to 5.10 mW/mK just after manufacturing going up to 5.52 mW/mK after 7 days at room temperature. Lower thermal conductivity of VIP samples can be attributed to the suppression of gaseous and radiative thermal conductivities due to a reduced smaller pore size (237-239nm) and presence of SiC opacifier respectively. The increasing trend of thermal conductivity after storing VIPs at room temperature is assumed to be due to increased pressure inside the VIPs because of outgassing from the sawdust and envelope material. Sawdust was obtained from the reclaimed pine wood which may potentially contain the residual adhesive from earlier use. This assumption was further reinforced from the results in figure 2

which show that the magnitude of thermal conductivity increase with time was found to be higher in samples containing higher mass % of sawdust powder.

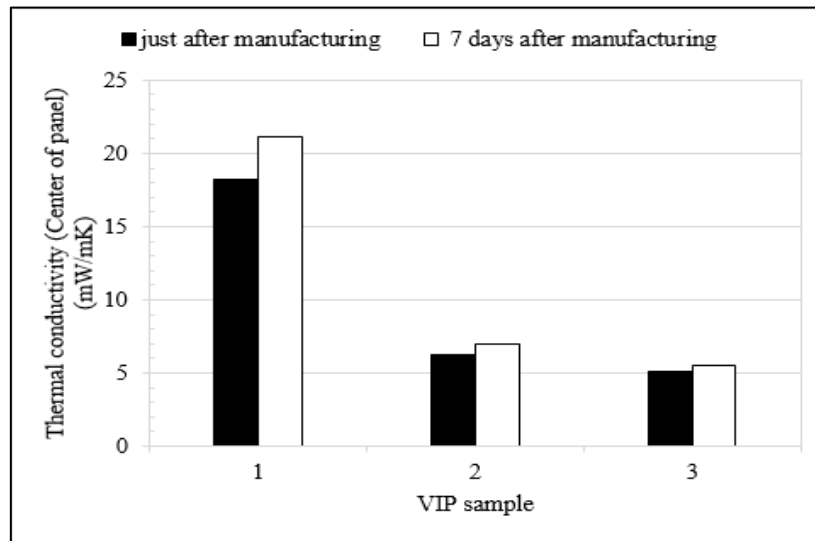


Figure 2. Experimentally measured thermal conductivity for VIP sample (1-3) with core material of sawdust and fumed silica composite

## CONCLUSIONS

In this study application of waste sawdust powder in VIP core has been explored as an eco-friendly alternative core material to partially replace the expensive and high environmental impact fumed silica. Thermal conductivity measurement show the increasing sawdust contents in the sample led to higher thermal conductivity values. The lowest center of panel thermal conductivity value of 5.10 mW/mK was found for VIP sample containing 30 mass % of sawdust along with 55 mass% of fumed silica and 15% SiC which is comparable to that of center of panel thermal conductivity of commercially available fumed silica VIPs. After storing the VIPs at room temperature for 7 days, center of panel thermal conductivity value slightly increased to 5.52 mW/mK. Trend of increase in thermal conductivity with time was measured in all composite samples and attributed to outgassing from sawdust and envelope material. This aspect requires further investigation. It is also recommended to further evaluate the performance of composite materials under different climatic conditions to comprehensively ascertain the thermal performance for range of temperature and humidity conditions.

## REFERENCES

- Alam M., Singh H. and Limbachiya M.C. (2011). Vacuum Insulation Panels (VIPs) for building construction industry - A review of the contemporary developments and future directions, *Applied Energy*, 88, 3592 - 3602.
- Porextherm Dämmstoffe GmbH (2014). Environmental Product Declaration as per ISO 14025 and EN 15804. [http://www.vacuum-panels.co.uk/wp-content/uploads/2016/08/EPD-Porextherm\\_englisch-30.03.2015.pdf](http://www.vacuum-panels.co.uk/wp-content/uploads/2016/08/EPD-Porextherm_englisch-30.03.2015.pdf) Available online [Accessed on 15April 2019]
- Ahmed W., Khushnood RA., Memon SA., Ahmed S., Baloch WL., Usman M., (2018). Effective use of sawdust for the production of eco-friendly and thermal-energy efficient normal weight and lightweight concretes with tailored fracture properties. *Journal of Cleaner Production*, 184, 1016-1027.
- Lakrafli H., Tahiri S., Albizane A., Bouhria M., El Otmanic M.E., (2013). Experimental study of thermal conductivity of leather and carpentry wastes. *Construction and Building Materials*, 48, 566-574.

## **Impact of artificial ageing on mechanical and hygrothermal properties of Advanced-Porous-Materials (APM) for buildings**

Christoph Sprengard<sup>1,\*</sup>, Sebastian Tremel<sup>1</sup>, Carolin Kokolsky<sup>1</sup> and Susanne Regauer<sup>1</sup>

<sup>1</sup>FIW München, Gräfelfing, Germany

\*Corresponding e-mail: sprengard@fiw-muenchen.de

### **ABSTRACT**

Insulating materials based on APMs are the fastest growing group of insulating materials, although the amount of APMs used worldwide as insulating materials in buildings is still very low. In order to foster a wider use of these nano-, meso- and microporous materials, resentments and doubts of potential users and architects about thermal and mechanical performance, long-term behavior and service life have to be removed. FIW completed a research study to show market readiness of these materials and to boost a wider use in the building industry. This paper addresses the investigations on the impact of different methods of artificial ageing on the long-term behavior of mechanical and hygrothermal properties. Several typical products have been selected and tested before and after ageing and showed very promising results for long-term application in buildings without remarkable degradation of performances.

### **KEYWORDS**

APM, Aerogel, ageing, artificial ageing, long-term performance, service life,

### **INTRODUCTION**

There is a large variety of insulating materials available on the market to fulfil current requirements for energy saving regulations. For conventional products, all relevant properties, the long-term-behaviour, types and fields of application are well-known while newly developed products offer new opportunities in terms of space saving and energy efficiency. Especially nanoporous materials with an excellently low thermal conductivity have a large potential for a high energetic level even in difficult cases such as renovations.

The aim of this study was to examine the long-term behaviour of aerogel and APM construction materials thoroughly to establish a basis of available information to support the trust in those materials and to pave the way for a widespread use. The term “Advanced Porous Materials” describes all novel, with specially adapted or newly developed processing methods produced micro-, meso- and nanoporous materials. Aerogels, the widest spread sub-group of APMs, are produced from different inorganic or organic raw materials using the Sol-Gel-Process followed by a (supercritical) drying. Amorphous colloids are used in the construction sector as compressed particles mixed with fibers and binders: Their main representative is fumed silica. Another group are the nano-foams with pore structures in the range of some microns.

Investigations on the relevant properties for building physics and in particular the durability of these novel insulating materials were performed to evaluate the long-term behaviour of the products. Especially the influence of combined temperature and humidity stress relevant in many building applications was a main focus.

## METHODS

Based on a comprehensive study on currently available products on the market and the characterization of their building specific properties, five representative APM and aerogel products were selected for the investigations within the scope of this study.

Table 1. Selected products for investigations about long-term behaviour under artificial ageing

Product code	Raw material	Type	Density (kg/m <sup>3</sup> )
A.1	SiO <sub>2</sub>	Loose	65-85
A.2	PU	Board	150-180
A.3	SiO <sub>2</sub>	Blanket	150
A.4	SiO <sub>2</sub>	Board	130-180
S.1	SiO <sub>2</sub>	Board	165

The investigations have been carried out using common test methods as used for conventional insulating materials. For some tests, the apparatuses and boundary conditions had to be adjusted in order to be able to measure these high-performing insulating materials. Investigating the necessary precautions and adjustments was an important part of the research study and continued the work already reported in the IEA EBC Annex 65 subtask II report (Holm and Sprengard 2019). Prior to the start of the ageing measurements, the fresh values were determined. The same properties were tested after ageing and the results were compared. Results are summed up in the research report (Sprengard, Tremml et.al 2019). Graphs will be presented in the conference. The following ageing methods were used:

- **Hygrothermal Ageing:** accelerated ageing under elevated constant temperature and humidity conditions at 50 °C and 70 % relative humidity over a storage time of nine months. These ageing conditions were agreed on within the work in the IEA EBC Annex 65 project on Super-Insulating-Materials as sufficient but rather severe ageing conditions. Measurements of the relevant properties have been carried out after 3, 6 and 9 months ageing time.
- **Freeze-Thaw-Cycles:** 300 cycles with +20 °C in wet condition and -20 °C in dry condition. The duration of one full cycle was 4 hours. The method is based on EN 12091, but used smaller sample sizes and an adapted sample mounting system. Measurements were carried out after 300 cycles on wet samples and dried samples.
- **UV-Ageing:** Storage at 50 °C and under radiation of UVA 340 lamps with a wavelength of 340 nm over 3000 hours. The ageing procedure is relevant only for translucent applications (loose-fill Material A.1). The method is based on EN 1297 for roofing membranes but used different “mounting” methods, e.g. between window glass, inside PMMA web plate without UV stabilisation and uncovered. Measurements were carried out after 3000 hours only.

The tests were conducted according to the following standards and boundary conditions:

**Thermal conductivity:** according to EN 12667, mean temperature 10 °C and temperature difference 10 K.

**Compressive strength:** according to EN 826 with preload of 250 Pa

**Tensile resistance:** according to EN 1607 with feed speed of 10 mm/min

**Dimensional stability:** according to EN 1604 with storage for 24 hours at 70 °C / 90 % R.H.

**Dynamic stiffness:** according to EN 29052 with and without gypsum layer

**Structural analysis:** SEM-microscopy to detect changes in the structural network

**Hygrothermal Analysis:** Sorption behaviour with Dynamic Vapor Sorption Analysis (DVS)

**Fire behaviour:** according to EN ISO 11925-2 to classify class E, flame application along the edge, on the surface and edge turned 90°



## RESULTS

### Impact of hygrothermal Ageing on:

**a) Thermal conductivity:** Figure 1 shows the evolution of the thermal conductivity over 270 days. The increase during the test duration is in the range of 0.0006 W/m·K and 0.0002 W/m·K. The products show a very stable behavior. For product S.1 the raw density slightly decreased during ageing what may have led to the decreasing thermal conductivity towards the end of the period.

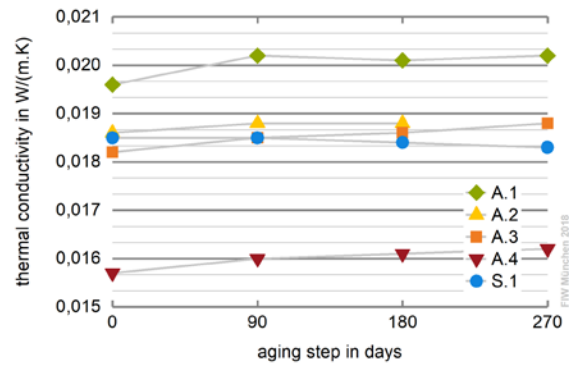


Figure 1. Evolution of thermal conductivity

**b) Tensile Resistance:** A rather big variation of tensile resistance values of the different products could be found e.g. A.3 and S.1 around 2 kPa, A.2 350 kPa and A.4 with 35 kPa. The products also differ in their sensitivity towards the influences of the ageing procedure. Nevertheless, no product showed a clear deterioration with increasing ageing duration, but the scattering of the measurement results within the set of five samples for each test increased.

**c) Compressive Strength:** It was possible to reach the 10% deformation threshold for deformation without previous failure of the material for all samples. Product A.3 showed a non-linear behaviour and for the evaluation the setpoint was at the deformation at a preload of 250 Pa. Two products (A.2 and A.4) have larger scatterings in the measurement values without a clear tendency, but S.1 shows very stable results over all ageing steps.

**d) Dimensional Stability and Dynamic Stiffness:** Both characterization methods lead to the same results. A.3 and S.1 show stable values without scattering while A.2 and A.4 have larger variations within the sets of 3 to 5 samples for one mean value but also don't show any influence from hygrothermal ageing.

**e) Fire resistance:** Five samples of each product were tested after each ageing step and all samples reached the Euroclass E regulation. No influences from ageing could be detected.

### Impact of Freeze-Thaw Cycles:

A visual analysis already showed the strains caused by the ageing. A.2 showed a significantly lower compressive strength especially in the wet condition than in the original state while the raw density did not show a big difference. Material A.4 has similar values for wet and dry samples, which are slightly lower than fresh values, but the density is much higher for wet samples. S.1 does not show any change in the response to pressure.

### Impact of UV-Ageing:

The sample between two panes of common window glass shows a slight deterioration of thermal conductivity during the test phase of 3000 hours from 0.0370 W/(m·K) to 0.0382 W/(m·K), but the cause of this change remains unclear, as also a settlement of the particles could have caused it.

### Structural Analysis

SEM (scanning electron microscope) images give a good indication on structural changes of the material. However, detecting changes in the pore structure is not possible even when using the largest possible enlargement. Assessed effects are limited to the surface appearance of the macro-structure and partly the colour. The UV radiation shows the most noticeable influence

with dark dots on the surface. Hygrothermal ageing and freeze-thaw ageing show weathering on the particle edges and a “dull” surface. Cracks appeared more pronounced with smoother edges.

### **Hygrothermal Analysis:**

No significant changes of the sorption isotherms were detected after applying the ageing procedures.

## **DISCUSSIONS**

The most important findings after the evaluation of the influences occurring from artificial ageing are the small increases in thermal conductivity over time. One product (S.1) showed even a slight decrease, most likely caused by a change of the density by the loss of particles due to dust falling out of the sample during processing. For the products A.2 and A.4 a decreased compressive strength after the freeze-thaw cycles was detected, but all other tests concerning the mechanical properties did not lead to a degradation of the materials tested. Also, the fire testing and the structural analysis could not provide indications that a progressing ageing contributes to a degradation of the specific characteristic.

## **CONCLUSIONS**

In aged conditions, Aerogels and APMs remain high performing insulating materials. The presented results lead to the conclusion that the products are durable and have a good long-term performance concerning hygrothermal and mechanical properties.

A difficulty remains in the handling and testing procedures, e.g. in determining the exact sizes of the samples. Samples are brittle and dusty and sometimes break apart when repeatedly handled in the ageing apparatuses and lab equipment. Contactless measurement procedures with laser sensors proved to work properly and reduced difficulties significantly. Adjustments of the standardized measurement procedures for conventional insulating materials are needed in order to measure properties of APMs with high precision (see Annex 65 report for details).

APMs have reached a high level of fitness for use in building applications, but currently low production volume of aerogels and APMs for the construction is connected to high production and material costs. An increasing demand may lead to a considerable drop of the costs. This would support the economic viability of energetic renovation and concepts for new buildings with APMs.

## **ACKNOWLEDGEMENT**

The project received funding from the Federal Institute for Research on Building, Urban Affairs and Spatial Development, Germany under the ZUKUNFT BAU programme.

## **REFERENCES**

Holm A. and Sprengard C. 2019, EBC Annex 65: Long-term performance of super- insulation materials in building components and systems. Subtask 2 report: characterization of materials and components – laboratory scale. CSTB. France; 2019 (in Press)  
Sprengard C., Tremel S. et al. 2019. Aerogele und APM in der Bauanwendung, FIW München, in press, available July 2019 under <https://www.baufachinformation.de/forschungsberichte>

## Why does the mechanical behaviour of precipitated silica make them unsuitable today for their use in VIP cores?

Bernard YRIEIX<sup>1,\*</sup>, Geneviève FORAY<sup>2</sup>, David JAUFFRES<sup>3</sup>, Belynda BENANE<sup>1,2</sup>, Etienne GUESNET<sup>3</sup>,

<sup>1</sup> EDF R&D les Renardières, Département MMC, F-77250, Moret Loing et Orvanne, France

<sup>2</sup> Univ Lyon, INSA Lyon, CNRS, MATEIS UMR-5510, F-69621, Villeurbanne, France

<sup>3</sup> Univ. Grenoble Alpes, CNRS, Grenoble INP, SIMaP, F-38000 Grenoble, France

\*Corresponding e-mail: [bernard.yrieix@edf.fr](mailto:bernard.yrieix@edf.fr)

### ABSTRACT (Times New Roman Bold 12 pt, UPPERCASE, style: Heading 1)

Cores of vacuum insulation panels (VIP) made of silica use fumed silica rather than precipitated silica despite its lower price. In addition to a thermal performance a bit lower, the main reason is that the cost of the panel is not as low as expected because the density of the compacted panel has to be higher in order to reach the required mechanical strength.

Two extensive works have been undertaken to explain these mechanical behaviors and thus to have ways of improving precipitated silicas. One was mainly experimental, mechanical testing and microstructural characterizations (Hg porosimetry, X-ray tomography, TEM, and SAXS), while the second was only simulations by discrete elements at the aggregate scale where the morphology, the neck size and the surface energy was the main parameters. They succeed to describe the relationships between the mechanical behavior during compression of the powders and their microstructure and surface chemistry. The conclusion is that the two factors contribute in various rates depending on the considered silica, and that the way to use precipitated silicas is not reachable simply and therefore economically.

### KEYWORDS

Precipitated silica, Fumed silica, Aggregate, Mechanical behaviour, Microstructure.

### INTRODUCTION

Cores of vacuum insulation panels (VIP) made of silica use fumed silica (FS) rather than precipitated silica (PS) despite its lower price (Simmler, 2005). Indeed, deriving the objective function (equation (1)) which give the cost of a thermal insulation product designed for a given thermal resistance  $R$  with respect to the material, leads to the performance index of the core  $PI_{core}$  (equation (2)) which have to be minimized for optimal technico-economical balance.

$$Cost = A \cdot R \cdot \lambda \cdot \epsilon_m \cdot \rho \quad (1)$$

$$PI_{core} = \lambda \cdot \epsilon_m \cdot \rho \quad (2)$$

Where  $Cost$ ,  $A$ ,  $\lambda$ ,  $\epsilon_m$ , and  $\rho$  are the overall cost, the area, the conductivity, the mass cost (€/kg) and the density of the core (the only part considered here).

The three materials parameters are not equal for the two kinds of silica. The conductivity of the core is a complex function of the three contributions (infrared radiativity, gaseous and solid conductions) which are themselves function of the density (IEA-EBC). At the same density, the conductivity at medium pressure of PS core is a bit higher than that of FS (Simmler, 2005). On the other hand, the mass cost of PS is lower than that of FS. At this stage we may understand that a larger gain on the mass cost can easily compensate the little difference of conductivity and then be profitable. This is the main driving force for considering the alternative of PS. The difficulty comes from the third parameter: the density. The manufacturer is not free to minimise

this parameter because the density has to be high enough to give i) a sufficient compression strength to hold the atmospheric pressure and also ii) a sufficient flexion strength to ensure a safe manipulation during the manufacturing. At this point a huge difference can be seen between the behaviours of the two silicas. In order to reach the required mechanical strength, the density of the compacted panel have to be higher for PS (200 to 250 kg/m<sup>3</sup>) compared to 140 to 200 kg/m<sup>3</sup> only for FS. Finally, thanks to the poor mechanical behaviour of the PS, the cost of the panel made with this silica is not as low as expected and its performance index is a bit higher than that of FS. The question that arises then is: why such behaviour? and how to modify it favourably? Answer to these questions is the aim of this communication.

## METHODS

Two extensive works have been undertaken to explain these mechanical behaviors and thus to have ways of improving precipitated silicas. One was mainly experimental (Benane 2018), mechanical testing and microstructural characterizations. The second was only modeling and simulations by discrete elements at the aggregate scale (Guesnet 2018) where the fractal dimension, the number of particles and the surface energy was the main studied parameters.

Two commercial silica powders were extensively studied, one PS and one FS. Table 1 gives some of their characteristics. These silicas are typical of the two families so they are referenced as FS and PS. Their specific areas ( $S_{BET}$ ) are close as their intrinsic densities ( $\rho_s$ ), FS is hydrophobic while PS is hydrophilic (respectively low and high surface silanols rate  $n_{OH}/nm^2$ ), the elementary particle size (diameter  $\phi$ ) is lower for FS than for PS.

Note that for each different scale exist: the particles, the aggregate (tenth to hundreds of particles strongly linked), agglomerates made of many aggregates weakly linked, and grains which are the scale observable with naked eyes. Tests are performed on pure silica without fibers and opacifier.

Table 1 – powders' characteristics (\* measured in this work)

Reference	Silica			Grains	Particles	
	$S_{BET}$ (m <sup>2</sup> /g)*	$n_{OH}/nm^2$	€/kg	D50 (μm)*	$\rho_s$ (g/cm <sup>3</sup> )*	$\phi$ (nm)*
FS	187	1	3.5	70	1.9	14
PS	207	4.6	2.7	10	1.9 – 2.1	24

**The mechanical behavior** was characterized by oedometric compression performed on samples stabilised at 23°C and 44% RH whose final dimensions are 20 mm diameter and about 2 mm in height. The test comprised three steps: first, a filling step by gravity flow of 200 mg of powder; then, a loading phase to compact it, followed by an unloading phase. Instrumented indentation was also performed on the obtained compacts.

Several technics were performed for **microstructural characterizations**: small-angle X-ray scattering experiments combined with transmission electron microscopy, electron-tomography and mercury intrusion porosimetry.

**Modeling and simulations** of the compaction behavior and of the tensile behavior at the compacted state were made at the aggregate scale by Discrete Elements Method (DEM) with Hertzian and bonded contacts. Simulations used a set of numerically generated silica aggregates with varying morphology (fractal dimension and number of particles), neck size and surface energy which are representative of the two studied silicas. The calculations used 30,000 particles, leading to a gas of at least 200 aggregates, and a simulation box of  $\approx 1 \mu m^3$ .

## RESULTS AND DISCUSSION

### Mechanical testing - Comparison of the FS and PS silicas

Oedometric compression (Figure 1) as well as instrumented indentation allow a clear comparison between the two silicas and confirm the previous knowledge coming from manufacturers. First, the as filled PS is much denser than FS. Second, at a given load PS is always denser than FS and finally the compacted FS is twice as stiff and harder as PS.

**The influence of natural and accelerated ageing** was also investigated by testing the two silicas after 6, 12 and 18 months of storage in the laboratory (23 °C – 33 % HR). A continuous shift towards higher density up to 10 % after 18 months for the both was observed (Figure 2). We know from Chal (2019) that the main evolution of FS is an increase of its hygrophilicity and that the main evolution of PS is a decrease of specific area as well as an increase of the pore size. So, at this stage, the origins of the evolutions of the mechanical behavior could be different. To explore the influence of the surface chemistry, we aged the FS 24 h at 70 °C – 90 %HR. This accelerated ageing leads only to an increase of the hygrophilicity without significant decrease of the specific surface (measured  $S_{\text{BET}} = 173 \text{ m}^2/\text{g}$ ). The impact on the mechanical behavior is an increase of the density of 22 % (Figure 2), higher than those observed after natural ageing. This shown that the increase of the hydroxylation of the surface bring the FS closer to PS. In that case the aged FS has more or less the same behavior than PS.

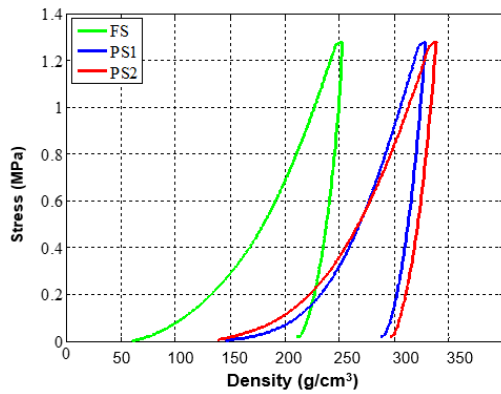


Figure 1. Oedometric compaction of the silica powders

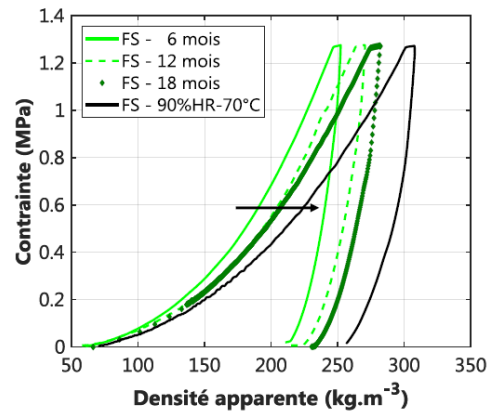


Figure 2. Influence of ageing on the oedometric compaction of FS

### Microstructural characterizations

Thanks to the several technics used, including SAXS (Benane, 2019), many differences between the two silicas was observed and quantified with a high degree of confidence. Besides the particle size already mentioned, the microstructural characteristics are summarized Table 2 and illustrated Figure 3. In short, the aggregates of FS are more anisotropic, larger, and less compact than those of PS. At the initial state, these differences could explain their different mechanical behavior by a better percolated solid net for FS than PS. But the behavior after ageing emphasize the important role of the surface chemistry and then of the energy of surface.

Table 2 – Microstructural powders' characteristics

	Aggregates				Particles	
	Shape	Compacity	Fractal dimension	Radius of gyration	Surface	$\phi$ (nm)
FS	Flakes	0.29	1.85 - 2	64 nm	Smooth	14
PS	Isotropic		> 2.4	35 nm	Rough	24

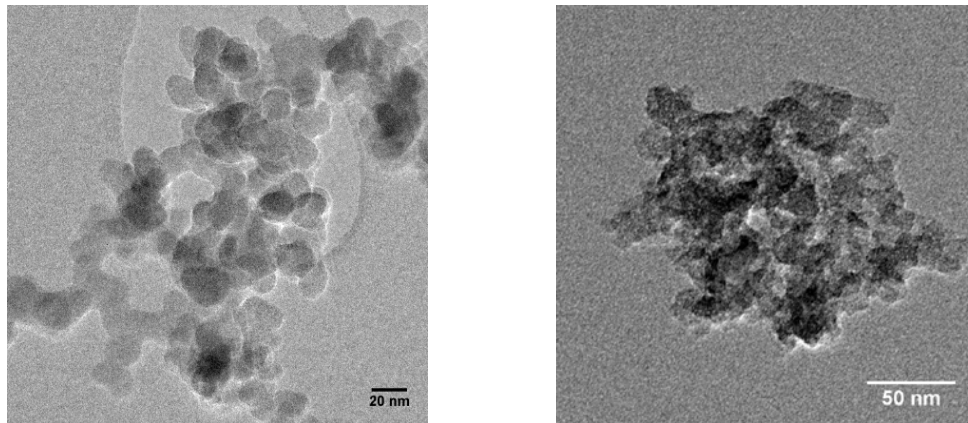


Figure 3. Transmission electron microscopy examination of the silicas, FS left, PS right

### Modeling and simulations

The parametric study has shown that neck size and surface energy have more influence on the mechanical behaviour than the aggregate morphology in the simulations. While the compaction behaviour is largely influenced by the neck size, the surface energy is the first governing parameter for strength. These conclusions are only partially in accordance with the experimental data but we have to consider that the simulations are made at the scale of the aggregates while the experimental is at the agglomerates and grains scales. A future study will have to be done at this scale.

### CONCLUSIONS

These studies make it possible to imagine the ideal silica for VIP cores. It is a precipitated silica for its lower cost, the particles are small with a high neck size, it has few silanols on the surface, and finally it has anisotropic aggregates with low compacity. Some of these characteristics are antagonistic, which explains why fumed silicas are better and that changing a precipitated silica in this way will be difficult technically but also economically, which is possibly the greatest limitation.

### REFERENCES

- Benane B., 2018, Mécanique des lits de silices granulaires pour l'optimisation des coeurs de panneaux isolants sous vide (PIV), *Ph.D. thesis*, INSA de Lyon. NNT : 2018LYSEI007
- Benane, B. et al, 2019, Multiscale Structure of Super Insulation Nano-Fumed Silicas Studied by SAXS, Tomography and Porosimetry. *Acta Mater.* 168, 401–410. doi:10.1016/j.actamat.2019.02.024.
- Chal, B. et al, 2019, Nanostructured silica used in super-insulation materials (SIM), hygrothermal ageing followed by sorption characterizations. *Energy Build.* 183, 626–638.
- Guesnet E., 2018, Modélisation du comportement mécanique et thermique des silices nano-architecturées, *Ph.D. thesis*, Université Grenoble Alpes, Français. NNT : 2018GREAI075. tel-01982891
- IEA-EBC, to be published, *Annex 65*, Long term performance of super-insulating materials in building components and systems.
- Simmler H. et al, 2005, Vacuum Insulation Panels: Study on VIP-Components and Panels for Service Life Prediction of VIP in Building Applications Subtask A. *Final Report IEA/ECBCS Annex 39*.

## Performance advancement of a new sub-micron pore size polymeric foam for vacuum insulation panels

Flávia A. Almeida<sup>1,\*</sup>, Kenny Rottenbacher<sup>1</sup>, Hermann Beyrichen<sup>1</sup>, Roland Caps<sup>1</sup>, Alexander Müller<sup>2</sup> and Roland Oberhoffer<sup>2</sup>

<sup>1</sup>va-Q-tec AG, Würzburg, Germany

<sup>2</sup>SUMTEQ GmbH, Düren, Germany

\*Corresponding e-mail: [flavia.almeida@va-q-tec.com](mailto:flavia.almeida@va-q-tec.com)

### ABSTRACT

This work demonstrates the advancements towards the use of a submicron- pore size polymeric foams (SUMFOAM) as core for Vacuum Insulation Panels (VIPs). The results of the 3<sup>rd</sup> generation foam show a remarkable total thermal conductivity below 5 mW/m·K in vacuum. Under atmospheric conditions, values similar to the thermal conductivity of still air (26 mW/m·K) are achieved. The suitability of SUMFOAM as core for VIPs was evaluated for a real sized transport box, resulting in similar thermal performance compared to the box made with standard fumed silica cores.

### KEYWORDS

vacuum insulation panel, polymeric foam, thermal conductivity, sub-micron pore sizes, open porous materials

### INTRODUCTION

In Europe, buildings account for almost 40% of total energy consumption with the majority being spent by the heating sector (space and water heating and appliances - refrigerators and freezers). In cold chain logistics, there is an increasing need for high autonomy (passive cooling solutions), high temperature maintenance time of the goods to be delivered and an optimal volume capacity by shipment. By being up to 10 times better than existing solutions, VIPs save considerably valuable space and resources.

The newly developed sub-micron pore size polymeric foam, by the company SUMTEQ, is the first high-performance and scalable polymeric material to industrial applications. In contrast to aerogels, a time-consuming drying process is not needed. Results of the 1<sup>st</sup> and 2<sup>nd</sup> generation foams were shown by Almeida et al. (2017). The former revealed open pores below 1  $\mu\text{m}$ , but the thermal conductivities  $\lambda$  in vacuum were still too high (up to 20 mW/m·K). The 2<sup>nd</sup> generation foams were prepared with opacifiers, which decreased  $\lambda$  to values of  $\sim 7$  mW/m·K. But these presented larger pore sizes of about 5  $\mu\text{m}$ , which is considered too high for long-term applications in comparison to fumed silica. Advances towards the 3<sup>rd</sup> generation foam and its suitability as core material for VIPs are presented here.

### METHODS

SUMFOAM (SF) was produced by the company SUMTEQ GmbH following the method developed by Strey et al. (2015). Several foams of different co-polymer composition (as PS- and PMMA-based), additives, autoclave parameters (pressure, temperature and time) and foam expansion rate were tested. All the foams were prepared containing carbon based opacifier material. Samples in the sizes of (12x12x1.5) cm<sup>3</sup> were manufactured and characterized in terms of thermal conductivity dependence on air pressure. For this, the same procedure and equations



as described by Almeida et. al (2017) are used. For building the prototype transport box, 4 panels of  $(30 \times 27.5 \times 3) \text{ cm}^3$  and 2 panels of  $(32 \times 32 \times 3) \text{ cm}^3$  were produced. Figure 1 shows a representative real size core and VIP panel made of SF and its assembly as a transport box system.



Figure 1. Real size panels made of SUMFOAM before and after evacuation and the assembly of the transport box.

**Heat loss value (Q value) test:** The test uses a fan heater for introducing thermal energy into the packaging system. The electrical power used to keep the inner temperature of the box along the test time divided by the temperature difference of inside and outside the box, determine the Q value of the component. The box was placed inside a cooling chamber at  $0^\circ\text{C}$  while the inside temperature was set to  $30^\circ\text{C}$  ( $\Delta T = 30 \text{ K}$ ).

**Performance test:** The qualification of the box is done according to the International Safe Transit Association 7D summer scenario (ISTA 7D, 2007). The target of this test is the evaluation of the duration of temperature stability of the inner temperature between  $+2.0^\circ\text{C}$  and  $+8.0^\circ\text{C}$ . To stabilize the temperature inside the box, phase change materials (PCMs) pre-conditioned to  $\sim 3^\circ\text{C}$  were placed inside the boxes.

## RESULTS AND DISCUSSION

### Thermal conductivity measurements

Gas pressure influence on the thermal conductivity of several types of SUMFOAM (SF) and conventional cores for VIPs is presented in Figure 2. Fumed silica (FS) still has the smallest gas pressure dependence on thermal conductivity of all the core materials. It has a total thermal conductivity in vacuum of  $4 \text{ mW/m}\cdot\text{K}$ , which doubles at gas pressures as high as 100 mbar. The major difference compared to the other commercial cores is the pore size. While FS has pores in the nanometric scale ( $\sim 0.4 \mu\text{m}$ ), thus in the same order of magnitude of the mean free path of air molecules, PU foam and glass fibre have considerable larger pore diameters ( $\sim 130 \mu\text{m}$  and  $60 \mu\text{m}$ , respectively). Besides that, glass fibres presented the so-called “coupling effect”, related to the gas in between the intermediate spaces of the fibres creating additional pathways to heat conduction (Fricke et al., 2006).

The curves of the 1<sup>st</sup>, SF-(1G) and the 2<sup>nd</sup>, SF-(2G) generations of polymeric foams presented by Almeida et al. (2017) are plotted on Figure 2 for comparison. As reported, the high radiation and solid thermal contributions of SF of the 1<sup>st</sup> generation yield a total thermal conductivity in vacuum of more than  $20 \text{ mW/m}\cdot\text{K}$ . The macro-defects in between the foam granules cause the rise of the thermal conductivity at gas pressures below 10 mbar, but the very small pore sizes of this foam ( $\sim 0.4 \mu\text{m}$ ) are able to suppress the gas conductivity in a similar way as FS. This can be visible by the shape of the data fitting, where the second inflection point of the “S-shape” curve happens at gas pressures above 1000 mbar for both materials. On the other hand, the thermal conductivity of the 2<sup>nd</sup> generation SF in vacuum presents much lower values, close to



the start value of PU. However, these foams do not have pores at the sub-micrometer level and gas conductivity starts to rise at gas pressures below 10 mbar.

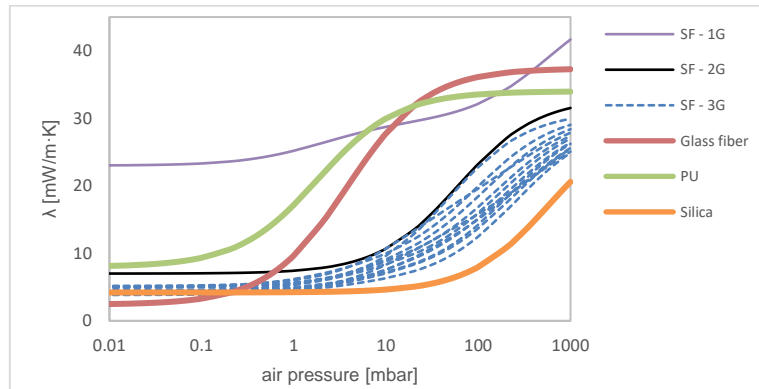


Figure 2. Thermal conductivity as function of internal gas (air) pressure for the SUMFOAM cores of the 1<sup>st</sup> (1G), 2<sup>nd</sup> (2G) and 3<sup>rd</sup> (3G) generation in comparison to conventional core materials.

Advancements by keeping the fine structure of SUMFOAM while keeping a low total thermal conductivity can be seen in Figure 2. All the SF materials of the 3<sup>rd</sup> generation have a thermal conductivity in vacuum very similar to fumed silica (~ 4 to 5 mW/m·K). As a result of their small pores (mostly below 1  $\mu\text{m}$ ), the thermal conductivities of the majority of the SF foams at atmospheric conditions are similar to or even below that of still air (~ 26 mW/m·K). However, the foams also have micrometric gaps in between the foam particles, mostly in between 12  $\mu\text{m}$  and 50  $\mu\text{m}$  size and 10% to 20% in volume. Despite this and in order to keep the thermal conductivity below 10 mW/m·K, the internal gas pressure can be extended up to 50 mbar.

### Thermal performance of SUMFOAM transport box prototype

**Heat loss value (Q-value) test:** It describes the energy loss of a component per time and temperature difference. The smaller the Q value, the better are the insulation properties. The test was carried out for about 67 hours to analyze a longer-term thermal behavior of the tested box. The average temperatures in and out of the box were 32.7 °C and 0.1 °C, respectively. With an injected electric power given by the heater of 4.02 W, the calculated Q-value of the SF-box is 0.12 W/K. The Q-value of the standard transport boxes made with fumed silica panels is  $0.11 \pm 0.01$  W/K, similar to SF-box.

**Performance test:** Figure 3 presents the test protocol of temperature over time of the transport boxes built with SF-VIPs (bluish curves) and fumed silica VIPs (black curves), respectively. Inside and outside temperatures are plotted. It shows the dynamic response of the temperatures inside the boxes when subjected to the external multi-level summer temperature profiles in the range of 22 °C to 35 °C (night and days summer simulation) along the time. It can be seen that the inner temperatures of both boxes are very similar and have comparable response to the external profile.

Figure 3 also shows that the performance time, i.e. the time span until the average value of the temperature sensors inside the box exceeds the +8.0°C, is very similar for both boxes: 40 hours for the SF-box and 42 hours for the fumed silica one. With a deviation of only 5%, it can be considered that this first SUMFOAM box prototype performs similar to the conventional ones under the tested conditions. However, more tests are needed to get statistically valid data for a new transport box built with SUMFOAM-VIPs.

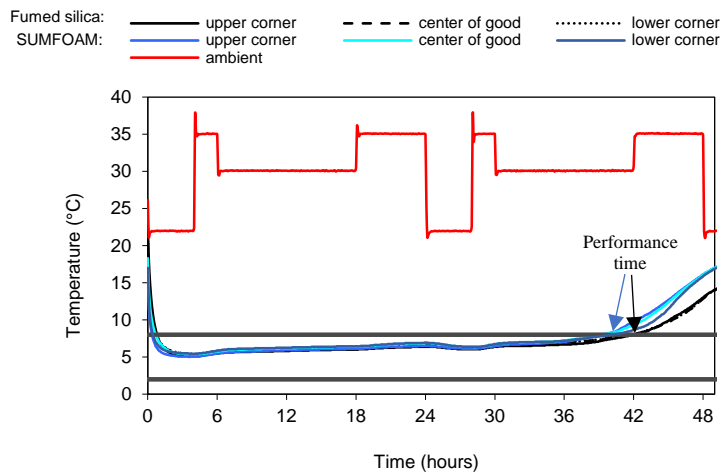


Figure 3. Performance test of transport boxes built with fumed silica VIPs (black curves) and SUMFOAM-VIPs (bluish curves) under ISTA 7D (2007) summer profile.

## CONCLUSIONS

The thermal conductivity measurements of the 3<sup>rd</sup> generation SUMFOAM have shown that low thermal conductivities in the range of 4 to 5 mW/m·K can be achieved, which is similar to fumed silica boards. Real size prototype SUMFOAM-VIPs were produced and integrated into a standard transport box from the va-Q-tec portfolio. All the necessary steps for the production of such a commercial box turned out to be applicable with SUMFOAM panels as well, meaning that there are no changes in the production process.

The prototype box was tested under established internal procedures and compared to boxes with fumed silica panels. Heat loss (Q-Value test) and performance (ISTA 7D summer scenario) tests of SUMFOAM-VIP prototype box revealed similar values to the conventional fumed silica ones. This is due to the comparable thermal conductivity in vacuum of both types of cores, as well as to the identical assembly of the box system.

Further research is being conducted for the suitability of SUMFOAM-VIPs for building applications. Also, aging factors in addition to the gas pressure increase are under investigation.

## ACKNOWLEDGEMENTS

This work has received funding from the European Union's Horizon 2020 research and innovation programme under the grant agreement No 748256 and 768576.

## REFERENCES

- Almeida F.A., Dodamani N., Beyrichen H., Caps R., Grassberger L., Müller A., Oberhoffer R. 2017. A New Sub-Micron Size Polystyrene Foam as Core Material for Vacuum Insulations. In: *Proceedings of the 13th International Vacuum Insulation Symposium (IVIS 2017)*, Paris, France, September 20–21, 2017, pp. 19-20.
- Fricke J., Schwab H., Heinemann U. 2006. Vacuum Insulation Panels – Exciting Thermal Properties and Most Challenging Applications, *International Journal of Thermophysics*, 27, 1123-1139.
- ISTA – International Safe Transit Association, 2007. 7D: Development Tests, effect of external temperature exposures of individual packaged-products.
- Strey R. 2015. Production of porous materials by the expansion of polymer gels. *Patent*, WO2015071463A3.

## **Determination of Anisotropic Thermal Conductivity of VIP Laminate using Transient Plane Source Method**

Bijan Adl-Zarrabi<sup>1,\*</sup>, Pär Johansson<sup>1</sup>, Alireza Marzbanrad<sup>1</sup>

<sup>1</sup>Chalmers University of Technology, Gothenburg, Sweden

*\*Corresponding e-mail: zarrabi@chalmers.se*

### **ABSTRACT**

The use of super insulation materials, such as vacuum insulation panels (VIP), is expected to increase in buildings in the future. One key aspect for successful implementation is the quality control. At the factory, the thermal performance can easily be controlled by measuring the internal pressure of the VIP. Preferably, the performance should be controlled again at the construction site before installation. The thermal conductivity of a VIP is possible to measure by using the transient plane source method (TPS). This method uses a sensor which measure the temperature increase during a heat pulse. For the analysis of the measurement, information on the thermal conductivity of the metalized multi-layer polymer laminate, used around the VIP, is needed. This paper presents the results obtained from different measurement setups of the laminate. The aim of the study is to identify a practical approach to analyse the results, and to give recommendations on the best measurement setup. Two measurement submodules were used; 'anisotropic' and 'thin film'. The thermal conductivity of the laminate was measured in-plane and perpendicular to in-plane. The volumetric heat capacity was measured by differential scanning calorimeter (DSC). The measurement results were compared to calculations. The results from the 'anisotropic' module was in best agreement with the calculated results. It was also illustrated that the TPS may be used for relative measurements to find damaged VIP.

### **KEYWORDS**

VIP, laminate, thermal conductivity, TPS, measurement

### **INTRODUCTION**

There is a large focus on reducing the energy demand for heating of buildings in Europe. The European Union has targeted an overall energy efficiency improvement by at least 32.5% by 2030 to achieve a highly energy efficient and decarbonised building stock by 2050. To reach these targets, the existing building stock needs energy retrofitting measures. One possible way of reducing the energy demand for heating is to use super insulation panels in the building envelope. An insulation material can be defined as a super insulation material when the thermal conductivity of the material is lower than 20 mW/(m·K). Super insulation materials yield a step-change in performance over conventional insulation materials but at significantly higher cost.

A construction site is generally a rough environment for all type of materials. Due to the fragility of the laminate surrounding the VIP, punctures before installation into building components on a construction site may lead to loss of the excellent insulation property. Therefore, controlling the function of the VIP at the construction site can be part of the quality assurance process for achieving a good quality of the building component. The transient plane source method (TPS) is an established method to measure thermal properties which could be used for fast determination of the functionality of VIP on a construction site. Previous studies on EPS covered by aluminum foil showed that there is a challenge to evaluate materials with highly anisotropic properties (Johansson et al., 2011; Johansson et al., 2012). For this purpose, an

analytical solution was developed by Claesson (2012) which was compared to numerical simulations and TPS measurements for five setups; EPS, EPS covered by aluminum foil and VIP laminate respectively, and VIP (evacuated and punctured) (Johansson and Claesson, 2014). It was found that the material properties of the VIP laminate had to be better determined to make the TPS method applicable. Therefore, this paper presents results obtained from different measurement setups of the laminate using TPS. The aim of this study is to identify a practical approach to analyse the results, and to give recommendations on the best measuring setup.

## METHODS

The TPS method, ISO 22007-2, uses a circular double nickel spiral, 10  $\mu\text{m}$  thick, sandwiched between two layers of Kapton (polyimide film), each 25  $\mu\text{m}$  thick, in contact with the material sample. The sensor is clamped between two samples of the same material and a constant electric power is conducted through the spiral. The heat raises the temperature and thus the resistance of the spiral. The rate of this temperature increase depends on how quickly the heat developed in the spiral is conducted away through the surrounding material. Heating is continued for a period of time, with the voltage across the coil being registered. As the power is held constant, the voltage changes in proportion to changes in the resistance of the coil. With knowledge of the voltage variation with time i.e., variation of temperature with time and the heat flow, it is possible to calculate the thermal conductivity and volumetric heat capacity of the material. The mathematical solution used in the TPS method is described by Gustafsson (1991).



Figure 1. TPS sensor on a functioning VIP (left) and measurement setup with the sensor clamped between two VIP (right).

The TPS method offers several submodules that make it possible to measure isotropic and anisotropic material. Furthermore, it is possible to measure the thermal conductivity of thin films. However, the commercially available software for analysing the measured data by TPS method is not suitable for determination of the thermal conductivity of VIP. Thus, two approaches were investigated. In the first approach, ‘relative measurement’ of evacuated and punctured samples was used. The second approach needs accurate determination of thermal properties of VIP i.e. protection layer and the core material of a VIP. Furthermore, the measured data by TPS method should be analysed by a heat transfer software.

## RESULTS

Measurement results obtained by the relative measurements and two different setups are presented in the following sections.

### Results from the relative measurement

The TPS method, submodule ‘isotropic’, was used for the determination of the thermal conductivity of two VIP samples, one evacuated and one punctured. The selected submodule is used as baseline for all other measurements. The measurement time was 160s. The measurement results are presented in Table 1 as mean values of eight repeated measurements.

Table 1. Measured thermal properties of evacuated and punctured VIP.

Samples VIP	Thermal conductivity (W/(m·K))	Thermal diffusivity (mm <sup>2</sup> /s)	Volumetric heat capacity (MJ/m <sup>3</sup> K)	Penetration depth (mm)
Evacuated	0.026	0.127	0.202	8.57
Punctured	0.040	0.153	0.259	9.39

The measurement results deviate significantly from the expected thermal conductivity. The deviation is caused by the unknown properties of the VIP laminate which is highly conductive and anisotropic, compared to the VIP core material. However, the results in Table 1 also show a significant difference between the evacuated and punctured sample. Therefore, the method could be used as a ‘relative method’ for identification of damaged VIP. The measurement time was 160 seconds which could be reduced to 80 seconds with the same measurement results.

### Characteristics of the VIP laminate

In the second approach, the thermal conductivity of the laminate and core material should be determined. The protection layer in this type of VIP is a thin metalized multi-layer polymer laminate, see Figure 2, with a thickness of about 100  $\mu\text{m}$ . Determining thermal properties of thin films is a challenge, especially when the film is anisotropic.

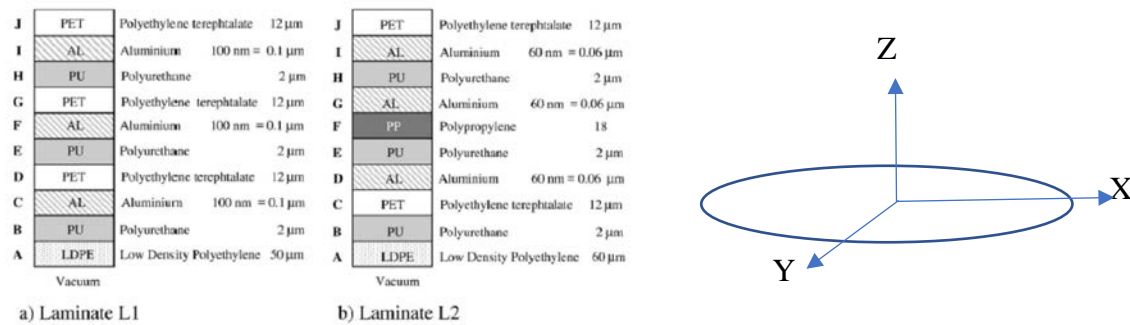


Figure 2. Examples of composition of VIP laminate (left). Illustration of the anisotropy (right).

### Theoretically determined thermal properties of the VIP laminate

The thermal properties of laminate L1 and L2 were calculated to be used as a reference value for the measurement results. The calculations are based on literature values and series/parallel coupled thermal resistance (electrical circuit model), see results in Table 2. The ranges are caused by the variation of thermal properties of the different layers found in the literature.

Table 2. Calculated thermal properties for the laminates under observation

Thermal properties	Laminate L1	Laminate L2
$\lambda_z$ (W/(m·K))	0.133-0.17	0.144-0.165
$\lambda_{xy}$ (W/(m·K))	0.97-1.07	0.61-0.68
$C_p$ (MJ/m <sup>3</sup> K)	1.619	1.733

### Measured thermal properties of the VIP laminate

The thermal properties of the VIP laminate were measured by using two different TPS method submodules; ‘thin film’ and ‘anisotropic’. The ‘thin film’ module provides the thermal conductivity ( $\lambda_z$ ) perpendicular to the surface of the thin film. The mean value of  $\lambda_z$  for four repeated measurement was 0.19 W/(m·K) which was about 10% higher than the maximum calculated values in Table 2.

The ‘anisotropic’ module needs information on the volumetric heat capacity of the laminate. Therefore, the heat capacity was measured using differential scanning calorimeter (DSC). The measured volumetric heat capacity was 1.745 MJ/(m<sup>3</sup>K). This is in good agreement with the calculations for L1 and L2 in Table 2. The results of the anisotropic measurements are presented in Table 3.

Table 3. Calculated and measured thermal properties by the ‘anisotropic’ module.

Thermal properties	Calculated L1	Calculated L2	Measurement
$\lambda_z$ (W/(m·K))	0.133-0.17	0.144-0.165	0.175
$\lambda_{xy}$ (W/(m·K))	0.97-1.07	0.61-0.68	0.958
$C_p$ (MJ/m <sup>3</sup> K)	1.619	1.733	1.745

## CONCLUSIONS

A quality assurance procedure is needed for controlling the performance of VIPs at the construction site. The results of the measurement presented in this paper indicate the TPS method can be used as an in-situ measurement method, using a relative measurement procedure. More research is needed to use the TPS method for absolute measurements of the thermal conductivity of a VIP.

Two TPS measurement modules were used to determine the thermal conductivity of the multi-layer aluminum laminate around a VIP. The setup ‘anisotropic’ was in very good agreement with the calculations.

## ACKNOWLEDGEMENT

The work is supported by the Swedish Energy Agency (42856-1). Thanks to Jimmy Forsberg and Remi Sørensen for performing a part of the TPS measurements in their Bachelor’s degree project.

## REFERENCES

- Claesson, J. 2012. Mathematical report: heated disk in contact with insulation material covered by thin highly conductive layer (No. 2012:11). Chalmers University of Technology, Department of Civil and Environmental Engineering (Gothenburg, Sweden).
- Gustafsson, S. E. 1991. Transient plane source techniques for thermal conductivity and thermal diffusivity measurements of solid materials. *Review of Scientific Instruments*, 62(3), 797-804.
- ISO. 2008. *ISO 22007-2:2008*, Plastics - Determination of thermal conductivity and thermal diffusivity - Part 2: Transient plane heat source (hot disc) method.
- Johansson, P., Adl-Zarrabi, B., Hagentoft, C.-E. 2011. Measurements of Thermal Properties of Vacuum Insulation Panels by using Transient Plane Source Sensor. In: *Proceedings of the 10th International Vacuum Insulation Symposium*, Ottawa, Canada, September 15-16, 2011.
- Johansson, P., Adl-Zarrabi, B., Hagentoft, C.-E. 2012. Using transient plane source sensor for determination of thermal properties of vacuum insulation panels. *Frontiers of Architectural Research*, 1(4), 334-340.
- Johansson, P., Claesson, J. 2014. Analytical model to calculate the temperature increase in a low conductive material covered by a highly conductive film. In: *Proceedings of the 10th Nordic Symposium on Building Physics*, Lund, Sweden, June 15-19, 2014.

## **Development of self-healing films to improve durability of VIPs by in-situ remediation of film defects**

Kaushik Biswas, PhD; Tomonori Saito, PhD; Pengfei Cao, PhD; Natasha Ghezawi; Kelsey Grady; David Wood, PhD; Rose Ruther, PhD; Dustin Gilmer; Kenisha Gardner

Oak Ridge National Laboratory, Oak Ridge, TN USA

*\*Corresponding e-mail: biswask@ornl.gov*

### **ABSTRACT**

The integrity of the VIP barrier film or envelope is a critical for maintaining the ultra-low thermal conductivity of VIPs. Here, the concept of a self-healing barrier film is described and demonstrated. The self-healing concept is based on an addition reaction between two chemicals, without the need for any external stimuli. The chemicals are incorporated as coatings in a multi-layered film and are initially kept separate with a partition layer. In case of damage, the chemicals would mix, react and heal the damage. Tests of small-scale film samples in a custom vacuum pump apparatus by puncturing the samples demonstrated the proof-of-concept. The tests indicated that the chemicals reacted and healed the puncture immediately to maintain the system vacuum. The intact and punctured self-healing films showed near-identical behaviour, while a control sample allowed the pressure to rise to atmospheric levels on puncturing.

Development of films with coated chemicals using tape casting and slot die coating methods is also described. These are low-cost and mature technologies, which are commonly used by various industries. The proposed chemicals are low-cost, commercially available materials. Thus, the self-healing technology is expected to be inexpensive and scalable.

**KEYWORDS:** self-healing film, multi-layered barrier film, roll-to-roll manufacturing, durability of VIPs

### **INTRODUCTION**

Self-healing strategies can be classified as intrinsic (one-part chemistry) and extrinsic (two-part chemistry) mechanisms [1]. One-part healing chemistry, based on reversible covalent bond or supramolecular chemistry, typically requires external stimuli, such as light or heat, which may not be applicable for VIPs in building applications (usually VIPs are covered by multiple layers of materials). Extrinsic self-healing occurs with the help of a healing agent and catalyst. The present work evaluated a vacuum assisted, two-part addition reaction as the self-healing process for barrier films of vacuum insulation panels (VIPs). Addition reaction involves short reaction time, which are desired so that the films can heal themselves from damage before the VIPs lose their internal vacuum.

In this study, reaction kinetics were investigated with multiple combinations of chemicals to identify the most promising pair of epoxy and curing agent for subsequent proof-of-concept testing. Small-scale coated film samples with the self-healing chemicals were produced and tested in a vacuum pump apparatus. The self-healing film samples were punctured and the ability of the healed film samples to maintain the system vacuum was observed using a pressure gauge. Further, scalable roll-to-roll (R2R) manufacturing trials were performed to create multi-layered coated films in a continuous process.



## MATERIALS

Fig. 1 shows the schematic of the multi-layered self-healing film [2]. We started our investigations of chemicals for reaction kinetics and suitability as coating agents. The team discussed different film materials that are commercially available and started experimenting with polyethylene terephthalate (PET), polyethylene (PE) and co-extruded polymer films. PET and metallized-PET (mPET) films are currently used for barrier films of VIPs. Based on available information, the oxygen transmission rates of PET and mPET films are in the ranges 31-93 and 0.16-1.7 cc/m<sup>2</sup>/day.<sup>1</sup> For reference, the OTRs of typical VIP barrier films are 0.07-0.0005 cm<sup>3</sup>/m<sup>2</sup>/day. The multi-layered films with the self-healing chemicals and nanoclay additive are expected to achieve similar OTRs as VIP barrier films [2].

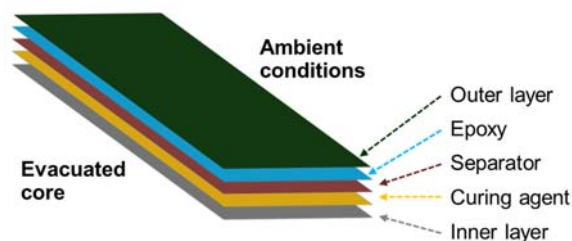


Fig. 1. Schematic of self-healing film.

An addition reaction with epoxy and curing agent (CA) resulted in a fast healing reaction. A commercial epoxy, EPON 8111<sup>2</sup>, and polyethyleneimine (PEI)-based curing agents (PEI-10K and PEI 800) are used; 10K and 800 refer to the molecular weights of the chemicals. The chemicals were mixed with a nanoclay (NC) for viscosity control and processability. Fig. 2 shows the measured viscosities of different slurries at different shear rates. Development of shear thinning slurries at typical R2R coating shear rates (100-1000 s<sup>-1</sup>) is critical for good coating quality and all slurries exhibited viscosities in the current range. Initial coating trials were done with small-scale tape caster with different slurries and substrates. Fig. 3 shows the tape casting method and some sample coatings. The coatings were observed to retain their shape even when held vertically.

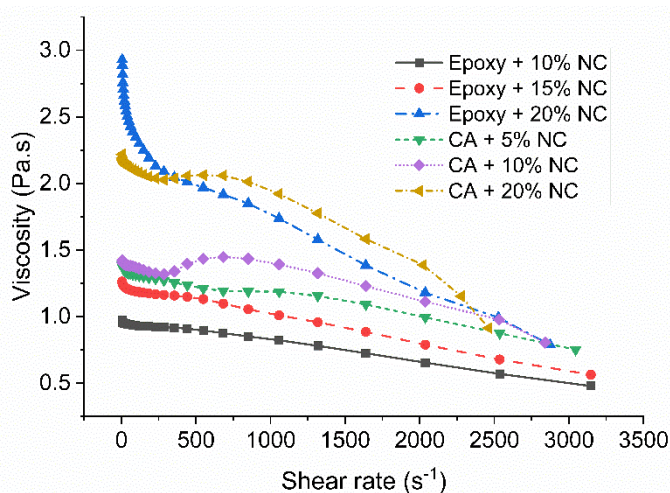


Fig. 2. Measured viscosities of slurries.

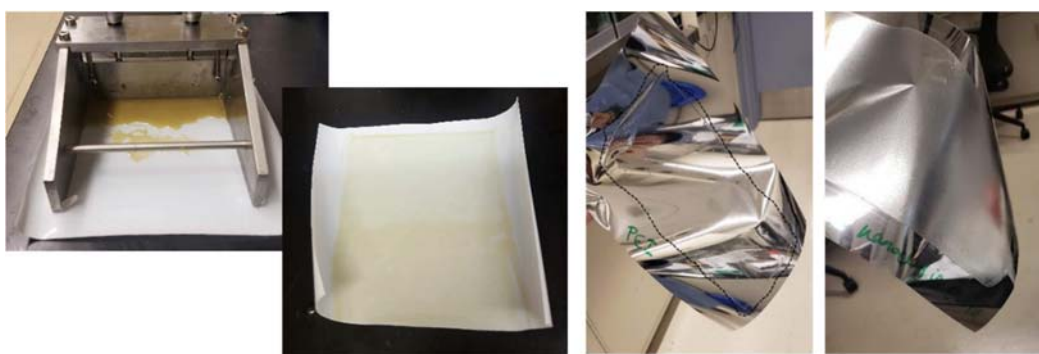


Fig. 3. Left: Tape casting method; Right: Sample coatings.

<sup>1</sup> <http://www.polyprint.com/flexographic-otr.htm>

<sup>2</sup> <http://www.hexion.com/en-us/brand/epon>



## SELF-HEALING EXPERIMENTS

Hand-assembled self-healing samples were tested via puncture experiments in a custom vacuum apparatus, see fig. 4. The apparatus consists of the sample holder that exposes the film samples to the atmosphere on one side and a partial vacuum on the other. The sample holder is connected to a vacuum pump and a pressure gauge via tubes; the vacuum is held within the tubes.

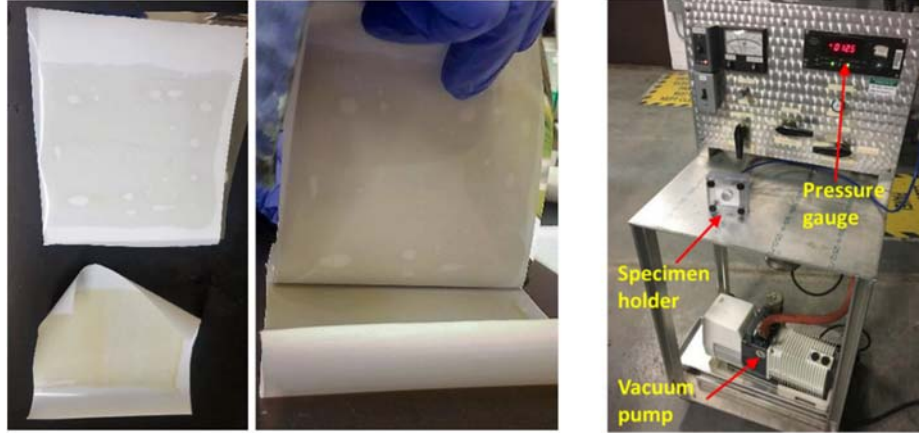


**Fig. 4.** Left: Hand-assembled self-healing film samples; Right: Custom vacuum apparatus.

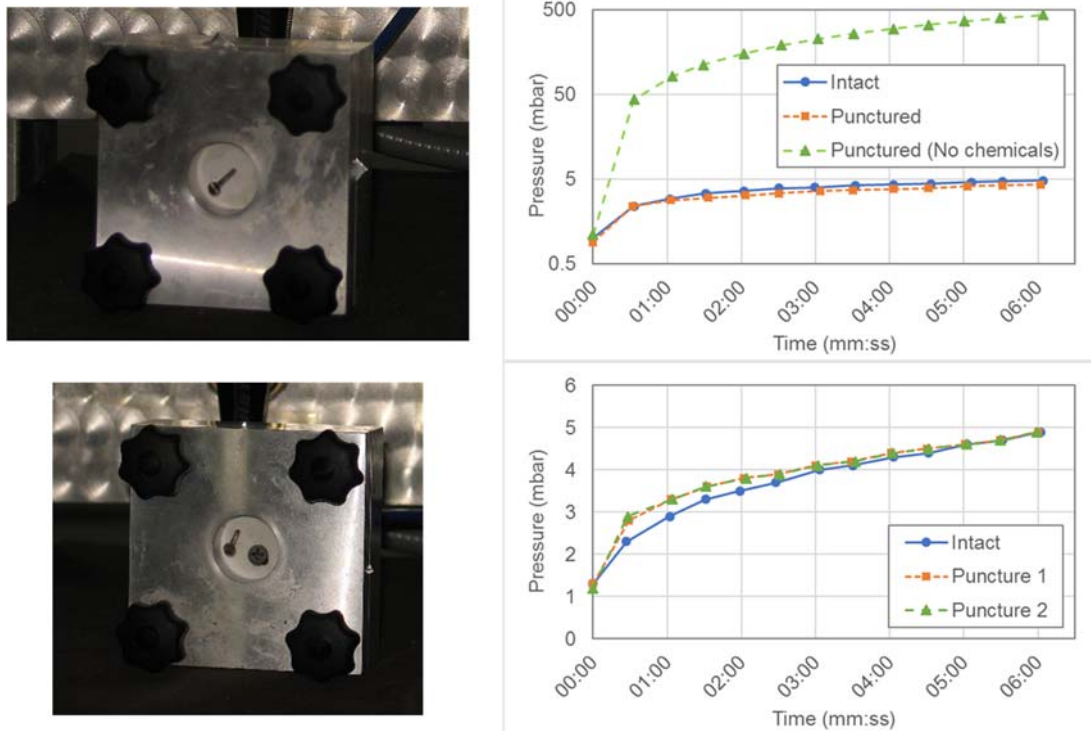


**Fig. 5.** Left: Punctured self-healing film samples; Right: Pressure increase with time.

For testing, the film samples were installed in the sample holder. Next, the vacuum pump was turned on to evacuate the system to 1 mbar. The pump was then turned off and the pressure was monitored for several minutes with the test sample remaining intact to gather the baseline pressure data. Next, the vacuum pump was turned on again to re-evacuate the system to 1 mbar and then turned off and the test sample was punctured. The system pressure was again monitored and recorded for several minutes or till the system pressure rose to the atmospheric pressure. Samples with and without the self-healing chemicals were tested. Fig. 5 shows samples that were punctured with a needle and a screw and the resulting pressure increase. The

results showed that, with self-healing chemicals, the punctured films maintained the low system pressure similar to intact films. It is noted that the system is not hermetically sealed, so there is some pressure increase due to air leakages even with the intact films. Without the self-healing chemicals, the system pressure rose quickly when the films were punctured.

## R2R TRIALS

Finally, the team has started performing trials to create self-healing films in an industry-scalable manner using a slot die coating machine. Fig. 6 shows one of the coating trials to create multi-layered film with interleaved substrates and coatings. In this scenario both epoxy and curing agent coatings were applied to the opposing surfaces of the separator layer (see fig. 1). The inner and outer layers are interleaved sequentially to create the overall multi-layered structure.

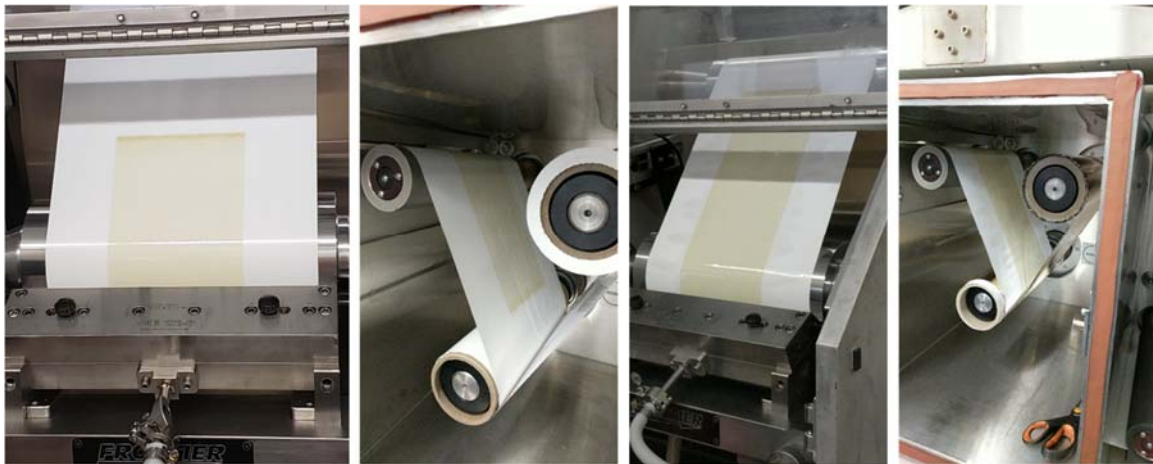


**Fig. 6.** Multi-layered slot die coating trial. From left-to-right: (i) first layer on coating on first substrate (which becomes the separator layer shown in fig. 1), (ii) an interleaved layer (which becomes the inner layer), (iii) second coating on the exposed face of the separator layer, and (iv) final interleaved outer layer.

## CONCLUSIONS AND FUTURE WORK

The current work showed the ability of prototype self-healing films to heal quickly and maintain the film impermeability, evidenced by puncture tests in a custom vacuum apparatus. Some preliminary trials were performed to create multi-layered, coated films using a continuous roll-to-roll manufacturing process.

## ACKNOWLEDGEMENT

This work was supported by the Building Technologies Office of the U. S. Department of Energy (DOE) under Contract No. DE-AC05-00OR22725 with UT-Battelle, LLC. The authors acknowledge the funding support from Mr. Sven Mumme of the U.S. DOE. Thanks are due to Mr. Jerald Atchley of ORNL for his help with puncture experiments and Mr. William Blake Hawley of the University of Tennessee, Knoxville for his help with viscosity measurements.

## REFERENCES

1. Zhu, D.Y., M.Z. Rong, and M.Q. Zhang, *Self-healing polymeric materials based on microencapsulated healing agents: From design to preparation*. Progress in Polymer Science, 2015. **49-50**: p. 175-220.
2. Biswas, K., D. Gilmer, N. Ghezawi, P. Cao, and T.J.V. Saito, *Demonstration of self-healing barrier films for vacuum insulation panels*. 2019.

## “Super VIPs” – Vacuum Panels with Exceptionally Low Degradation Rate

Yoash Carmi<sup>1,\*</sup>, Eddie Shufer<sup>1</sup>

<sup>1</sup>Avery Dennison Hanita, Israel

\*Corresponding email: [yoash.carmi@eu.averydennison.com](mailto:yoash.carmi@eu.averydennison.com)

### ABSTRACT

The article describes three new technologies developed by Avery Dennison Hanita to meet the demands for achieving nearly zero ageing panels:

A. **PST (Proprietary Surface Treatment) technology** – helps to reduce the air permeation through the skin of metallized films to less than  $0.5\text{cc/m}^2\text{year}$  at ambient conditions.

B. **Al Foil Patches** - extremely low water intake levels of about  $0.03\text{g/m}^2\text{day}$  at  $40^\circ\text{C}$ , 90%RH were achieved by laminating Al foil patches to the envelope. The patches were designed not to reach the edges of the panels in order to avoid additional thermal bridging.

C. **USW (Ultrasonic Welding Technique)** - a smart ultrasonic welding technique was developed to allow leak tight welding of metallized PET films and removing the need for a PE seal layer in the structure of the encapsulating laminates. Without the PE layers, the panels can be used at a much higher temperature, and the side air permeation is substantially reduced. By combining the ultrasonic welding technique with the PST technology, the overall air permeation can be reduced down to  $0.5\text{cc/m}^2\text{year}$  at ambient conditions, leading to an annual pressure increase for 12.5mm thick panels of only  $4\text{Pa/year}$ . This corresponds to a very small increase in thermal conductivity for such fiberglass (FG) panels inside the refrigerator walls of only  $\Delta\lambda = 1.4\text{mW/mK}$  over **10 years**. In building applications using fumed silica (FS) panels with the Al foil patch technique, thermal conductivity of typical panel is expected to increase by only  $0.13\text{mW/mK}$  over **50 years**.

The development of these three new technologies was partially funded by the H2020 EU project: INNOVIP (723441)

### KEYWORDS

Proprietary Surface Treatment (PST), Ultrasonic Welding, Al foil patches, Air and Moisture permeation rates, Thermal Conductivity

### INTRODUCTION

Manufacturers of VIP laminates face three major challenges in their quest to offer better performing envelopes: minimal air and moisture vapour permeation through the envelope skin, minimal air permeation through the seals (side permeation) and the development of good working solutions for high temperature applications such as EV cars and district heating. All of these should be achieved with minimal thermal bridging, and at low production cost.

To meet the requirement of minimal air skin permeation, Avery Dennison Hanita introduced the PST (Proprietary Surface Treatment) approach, which helped to reduce the skin air permeation rate to a level similar to that of Al foils. We used the fact that the moisture vapour permeation rate through Al foils is extremely low and developed an efficient production process for laminating Al foil patches to the high barrier laminates. The Al foil patches are designed to cover most of the envelope, but without reaching the edges of the panels in order to avoid thermal bridging, as shown schematically in Fig.1

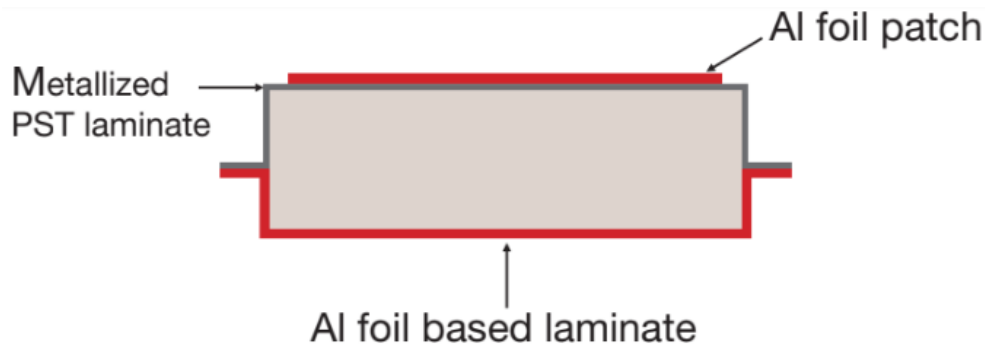


*Fig.1 – Schematic of Al foil patched VIP with hybrid envelope of Al foil based laminate on one side and metallized Polyester laminate on the other.*

In most of the VIP laminates PE (polyethylene) films are used as the seal layer. Unlike PET films, PE films can easily be heat sealed to provide very reliable and leak tight seals. However they suffer from two major disadvantages: PE films melt at temperatures around  $100^{\circ}\text{C}$ , so they cannot be used for high temperature applications, and in addition, PE films provide a poor barrier to air permeation, therefore allowing the substantial side permeation responsible for most of the ageing process of fiberglass panels. In order to overcome the two limitations of the PE seal layers, we developed a new sealing technique based on ultrasonic welding technology (USW). It was found that with specially designed ultrasonic horns, the metallized PET films used to provide the barrier can be welded together to provide leak-tight seals with good seal strength. Since PET films have much better barrier to air permeation compared to PE films, the USW technology reduces the side permeation to a very low level. In addition, as these new laminates do not contain PE films, they can function very well at much higher temperatures than standard VIP laminates.

## METHODS

### PST technology

PST technology is based on a roll to roll surface treatment procedure applied to the PET films before the vacuum metallization process. This surface treatment has an excellent effect on the barrier to air permeation via the vacuum deposited Al layers. Typical PST laminates contain only two metallized films, and have skin air permeability of around  $0.5\text{cc}/\text{m}^2\text{year}$  at  $23^{\circ}\text{C}/50\%\text{RH}$ , similar to Al foil based laminates. The skin air permeation rate was determined by measuring the evolution of the thermal conductivity of fiberglass panels and thus calculating the internal pressure increase rate using the previously measured  $\lambda$ vsP curve of the FG (fiberglass) core material. To eliminate the effect of the side air permeation, the panels were produced with double seal lines with evacuated space between them. This allowed almost zero pressure difference along the internal seal lines, leading to a negligible side permeation rate.

### B. The Al foil patch technology

The Al foil patch technology is based on roll to roll lamination of Al-foil patches of pre-designed dimensions on the external surface of high barrier laminates. Normally the length and width of the patches should be three to four centimeter smaller than the core material to maximize the covered surface area, whilst at the same time avoiding extra thermal bridging. The encapsulating bags should be produced in a registered mode to ensure that the patches are located at the center of the core, with strips of bare laminate of around 1.5cm wide surrounding the edges of the panel.

### C. The Ultrasonic Welding technology

Several FG panels with PST laminates were produced using the USW sealing technique. The laminates used did not contain PE films and the internal PET films of both sides of the bags were sealed together to form a leak-tight envelope. The evacuated panels were stored at 23°C/50% and at 100°C for several months and their thermal conductivity was measured every few weeks. The air permeation rate at each of the storing conditions was calculated using the previously measured  $\lambda$ vsP curve of the FG core.

## RESULTS

### A. Water Intake test results of Panels with Al foil patches

The permeation rate of water molecules through metallized films is several orders of magnitude faster than that of air molecules, therefore it is possible to calculate the permeation rate from the weight increase of the panels along storage time. In order to measure the effect of the laminated Al foil patches on the moisture permeation, fiberglass panels with different encapsulation bags were prepared and stored at 40°C/95%RH. All contained desiccants to keep the internal water vapour close to zero.

The average water intake of three reference panels with dimensions of 250mm X 250mm X 100mm was 31.5mg/m<sup>2</sup>day. These panels had PST metallized films on both sides of the encapsulating bags. The table below shows the average readings of water intake of three types of panel groups, each with a different percentage of the envelope surface covered by Al foil. The hybrid group contained envelopes with Al foil based laminates on one side and metallized laminates on the other side. In this case the covered part by Al foil included the Al foil laminate plus the Al foil patch laminated to the metallized laminate on the other side of the bag. It can be seen that the measured water intake levels were higher by only a small margin than the Water Intake levels based on the assumption of zero moisture permeation through the covered by Al foils areas.

	Type	% of Envelope surface covered by Al foil	Average water intake (mg/m <sup>2</sup> day)	Expected water intake(mg/m <sup>2</sup> day)
1	Reference	0%	31.5	31.5
2	Metallized both sides	46%	18.6	17.1
3	Metallized both sides	58%	15.6	13.2
4	Hybrid	79.9%	7	6.7

*Table1 The Water Intake levels of FG panels with metallized PST laminates and hybrid bags containing Al foil patches. The reduction factor of the water intake reading found to be very similar to the ratio between the overall surface area of the envelope to surface area of the envelopes parts not covered by Al foil.*

### B. Air permeability through PST envelopes sealed with the Ultrasonic Welding technique

Several fiberglass panels (300 X 300 X 10mm) were prepared with metallized PST laminates not containing PE seal layers. All four seals of the bags were made by the specially designed ultrasonic welding unit. The panels were stored at 23°C/50%RH for almost a year and their thermal conductivity was measured every few weeks. Fig.2 below shows the internal pressure of one of those panels as a function of the storage time. In the first fifty days the pressure increase rate was faster due air outgassing from the laminate. The steady state air permeation rate (Permeability) was calculated from the slope of the curve and found to be 0.52cc/m<sup>2</sup>year.

Typically the Permeability of identical panels with the same PST laminates and PE seals is  $1.6\text{cc/m}^2\text{year}$ . By reducing to a minimum the air side permeation, the USW seal technique was able to reduce the overall air permeability rate by as much as 68%. In this specific example, the use of the USW sealing technique can triple the lifetime of the FG panels compared to standard PE sealing.

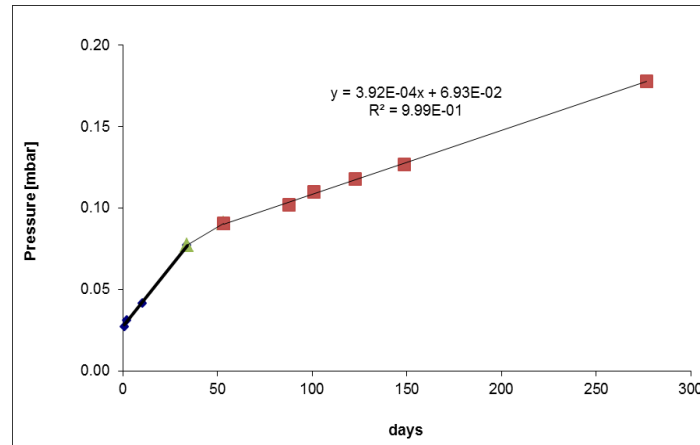


Fig.2 The internal pressure as a function of time of an FG panel produced with the USW sealing technique and stored at  $23^{\circ}\text{C}/50\%\text{RH}$ . The steady state air permeation rate calculated from the slope of the curve was found to be  $0.52\text{cc/m}^2\text{year}$ . This permeability level is about one third of similar panels with PE seals.

## DISCUSSION

### A. Al foil patches

- The most important finding discovered in the Al foil patch tests is that the Water Intake improvement factor is directly connected to the percentage of the laminate surface area covered by Al foils. For example, a panel which 80% of its envelope is covered with Al foil is expected to have close to a five times smaller moisture vapour permeation rate compared to a similar panel with formed with only metallized laminates.
- The potential of the Al foil patches can be demonstrated in the following example: Typical FS panels for the construction industry have dimensions of  $600\text{mm} \times 600\text{mm} \times 25\text{mm}$ . With a hybrid bag and an Al patch on the metallized surface, an 85% coverage of the bag surface by Al foil can be achieved with very small extra thermal bridging. Only 15% of the encapsulating envelope will be exposed to moisture permeation. The typical water intake rate of standard metallized laminates at the reference conditions ( $23^{\circ}\text{C}/50\%\text{RH}$ ) of the CEN standard for VIPs for buildings is  $1.7\text{mg/m}^2\text{day}$ , which translates to a moisture permeation rate into the Al foil patched hybrid,  $600\text{mm} \times 600\text{mm}$  panel of  $86\text{mg/year}$ , or only  $4.3\text{g}$  in fifty years. In fifty years the weight of this  $1.6\text{Kg}$  panel is expected to increase by only 0.26% due the permeated water molecules. According to the CEN standard the thermal conductivity of this Al foil patched panel will increase by only  $0.13\text{mW/mK}$  after fifty years due to moisture permeation – almost undetectable ageing after fifty years inside the building wall.

### B. Ultrasonic Welding and the PST technologies

- The advantage of the combination of the Ultrasonic Welding and the PST technologies can be demonstrated in the following example of a typical FG panel  $12.5\text{mm}$  thick: Using the Ultrasonic Welding and the PST in the encapsulation, air permeability as low as  $0.5\text{cc/m}^2\text{year}$  can be achieved. For a  $12.5\text{mm}$  thick panel, such air permeability



rate will induce an extremely low annual pressure increase of 4.0Pa/year, corresponding to a very slow ageing rate and an annual increase of the thermal conductivity of only 0.14mW/mK.

- High temperature applications – At high temperatures, the permeation rate of both water molecules and air molecules can be an order of magnitude higher than at ambient conditions. For example, the air permeability of standard PETMET panels is around 200cc/m<sup>2</sup>year, causing quite a fast rate of degradation, even when FS cores are used. The air permeability of USW+PST is only 45cc/m<sup>2</sup>year at 100<sup>0</sup>C, therefore these two technologies can be very useful for high temperature applications. At high temperatures, the moisture vapour permeation rate is also much faster than at ambient conditions. Accordingly, Al foil patches and hybrid bags can of great help in reducing the ageing rate of both FS and FG panels. At high temperatures, the hybrid and the Al foil patches can reduce substantially the air permeation rate even when the PST technology is applied.

## CONCLUSIONS

- The PST technology is shown to be a very efficient means for reducing the air permeation rate of metallized laminates. This is particularly useful for cores with low P<sub>1/2</sub> values such as fiberglass, Perlite or open cell PU foams, and for fumed silica cores in high temperature applications.
- The Al foil patches when combined with the hybrid solution can reduce by a factor of seven the water intake rate of metallized envelopes with minimal thermal bridging. These are especially effective for long term application such the construction industry, and for high temperature applications.
- The Ultrasonic Welding technology enables the use of VIPs for applications above 80<sup>0</sup>C by sealing together the PET films with no need for PE seal layers. By reducing to a minimum the side permeation of air, the technique is very useful for cores with small P<sub>1/2</sub>, or any core in high temperature applications.

## ACKNOWLEDGEMENT

The studies presented in this article were partially funded by the EU Commission as part of the H2020 project INNOVIP (723441).





# Determining the air permeation rate into VIPs in less than 24 hours using Helium permeation

Eddie Shufer<sup>1</sup>, Yoash Carmi<sup>1,\*</sup>

<sup>1</sup>Avery Dennison Hanita \*Corresponding e-mail: [yoash.carmi@eu.averydennison.com](mailto:yoash.carmi@eu.averydennison.com)

## ABSTRACT

The existing method of measuring the rate of air permeability through VIP laminates entails measuring the thermal conductivity of fiberglass (FG) core panels with a known  $P_{1/2}$  value for several weeks until steady-state is reached. The thermal conductivity readings as a function of time are then converted to the pressure readings necessary to calculate the steady state air permeation rate. This very accurate technique was adopted as the CEN and the ISO standard for determining the air permeability rate of VIP laminates at different temperatures and levels of relative humidity.

The main disadvantage of this technology is that due to outgassing, the steady pressure increase rate is reached after about 60 days at ambient conditions, or even longer. This measurement time can be shortened to less than 24 hours by exposing the panels to Helium (He) atmosphere, due to the fact that He atoms permeate three orders of magnitude faster than air molecules. The He permeation rate is determined by inserting the panels into a bag full of He gas and placing it between the two plates of a lambda machine for only 12 hours. The article describes this testing technique, and also several correlation curves between the He and the air permeation rates under different storage conditions.

## KEYWORDS

Permeation rate, He, VIP ageing, thermal conductivity

## INTRODUCTION

Permeation of air molecules through the encapsulating envelope of VIPs together with moisture permeation are the two mechanisms that dominate the ageing process of VIPs. The permeation rate of the water molecules can be measured relatively easy by commercial devices like Mocon units, or by gravimetric techniques. Measuring the air permeation rate through the envelope is much more complicated because there are no commercial devices built for measuring air permeation, and additionally, the air permeation rate through evacuated envelopes is substantially higher than through a flat laminate. The reason for this is that with evacuated panels, the envelopes are continuously under the stress of atmospheric pressure. Less than a decade ago, Avery Dennison Hanita developed very accurate and easy to operate technique for measuring the air permeation rate through evacuated laminates by measuring the increase rate of the thermal conductivity of fiberglass VIPs with pre-measured  $P_{1/2}$  along the storage duration, and using this data for calculating the internal pressure increase rate and the air permeability rate. This technique was adopted by the European and the ISO standards for VIPs in buildings.

Right after evacuation, the internal air pressure increases not only due to permeation through the envelope but also due to the release of air molecules (outgassing) from the encapsulating

laminate into the evacuated area. This outgassing process can last for more than two months at ambient conditions and during this time it is not possible to calculate the steady-state air permeation rate because the internal pressure increase rate is also affected by the outgassing mechanism. It is, therefore, necessary to extend the air permeation tests at ambient conditions to three months or even longer. At 100°C accelerated tests, the outgassing from the laminates stops after about two weeks, and therefore the steady-state air permeation rate can be determined after about one month, still a very long time. Both VIP manufactures and laminate manufacturers could benefit if the steady-state air permeation through the ultra-high barrier laminate could be determined in less than twenty-four hours.

We found in recent studies made by measuring the thermal conductivity of FG panels exposed to He atmosphere that the goal of determining the air permeation rate in just twelve hours is achievable once the correlation line between the He permeation rate and the air permeation rate is established.

## METHODS

### A. Determining the $\lambda$ vsP curves for air and for He

The dependence of the thermal conductivity of the FG core used in the tests as a function of the air internal pressure or the He internal pressure was determined by using mVIP systems, where a leak-tight connector was attached to the envelope, allowing simultaneous measurements of internal pressure and thermal conductivity. By adding small amounts of the gases through the connector, the entire  $\lambda$ vsP curves of the two gases were established.



Fig.1 Right – a picture of an mVIP system used for simultaneous measurements of the internal pressure and the thermal conductivity of panels. Left – The mVIP system set up together with a heat fluxmeter device.

### B. Measuring the permeation rate of air

FG panels with dimensions of 300 X 300 X 10mm with envelopes made out of different laminates were prepared and stored at 23°C/50%RH and at 100°C and ambient RH. The thermal conductivity of the panels was measured every few days and the steady-state air permeation was calculated using the relation  $\lambda$ vsP of the core for calculating the increase rate of the internal pressure.

### C. Measuring the permeation rate of He

The same evacuated panels were inserted inside another sealed envelope full with pure He gas and placed between the cold (10°C) and the hot (35°C) plates of LaserComp Fox310 heat fluxmeter. The increasing thermal conductivity of the panels was measured for about twelve

hours. The speedy permeation of the He atoms through the encapsulating envelopes induced a fast enough thermal conductivity increase rate with a linear dependence on time, which was converted to linear pressure increase rate using the  $\lambda$ vsP dependence of the FG core used for He. By using this method, the steady-state He permeation rate could be determined very accurately in just twelve hours.

#### D. Establishing the correlation functions between the air permeation of different laminates to their He permeation rates.

The He permeation rates of tens of different high barrier laminates were plotted against their air permeation rate, both at ambient conditions and at 100°C. The correlation curves of the metallized polyester (PETMET) laminates and separately of PST laminates were then best fitted to third-degree polynomial function.

## RESULTS

#### A. The $\lambda$ vsP curves for air and He of the tested FG core

The two graphs below describe the dependence of the thermal conductivity of the fiberglass core used in this research. From the air permeation test results the  $P_{1/2}$  value for air of this core was found to be 7mbar. Both curves fitted very well to third-degree polynomial functions.

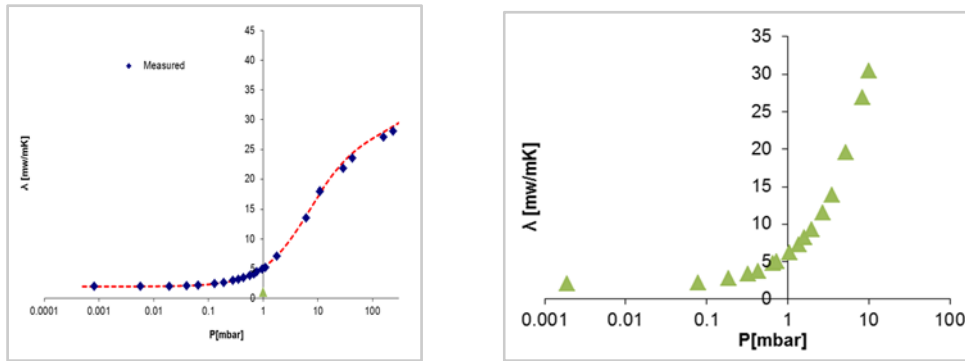


Fig.2. Left: thermal conductivity as a function of air pressure for the tested FG core. Right: the same curve for He pressure. Both graphs have logarithmic pressure axis.

Fig.3 below describes the  $\lambda$ vsP curves of Fig.2 with linear pressure axis. It can be clearly seen how the light He atoms contribute to the thermal conductivity more than the heavier air molecules. The higher the internal pressure, the greater the difference.

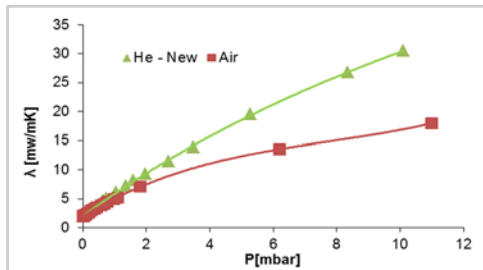


Fig.3 The  $\lambda$ vsP curves of air (lower red curve) and He (upper green curve) with linear pressure axis. For the same pressure levels, the contribution of the He atoms to the overall thermal conductivity of the panels is larger than that of the air molecules. Also at higher pressure levels, the thermal conductivity increases when the pores of the FG core contain He atoms.

### B. Typical air permeation test results at 23°C and 100°C

The dependence of the thermal conductivity of FG panels at 23°C and at 100°C is shown in Fig.4. In both cases, the slope of the curves is much steeper at the first few weeks, and constant increase rate is reached only after the outgassing eventually stops, and only the steady-state permeation is responsible for the internal pressure ramp up. The length of these tests is a clear disadvantage which calls for the development of a much faster way to determine the steady state air permeation rate through the laminate.

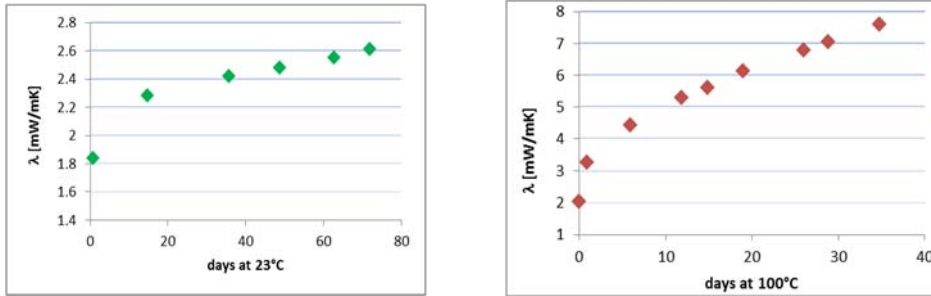


Fig 4. Typical thermal conductivity tests results of FG panels stored at 23°C (left) and at 100°C. At 100°C the air permeation rate is substantially higher than at ambient conditions and also the steady-state conditions (linear curve) are reached after a much shorter time.

### C. Typical He permeation rate

Fig.5 shows the thermal conductivity of an FG panel placed between the cold and the hot plate of a heat fluxmeter device and exposed to 1000mbar He atmosphere. The effect of the air outgassing from the laminate is completely obscured by the fast permeation mechanism of the He atoms and a steady-state situation is reached after less than one hour, allowing accurate determination of the He permeation rate in less than twelve hours.

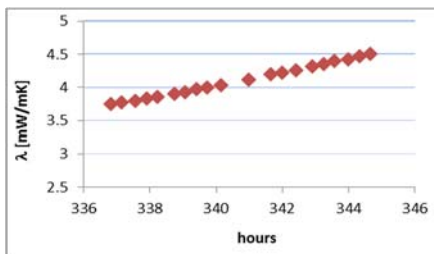


Fig.5 The thermal conductivity of an FG panel exposed to 1000mbar of He and placed between the cold (10°C) and the hot (35°C) plates of a heat fluxmeter device. In less than twelve hours the steady-state, He permeation rate through the tested envelope can be very accurately determined.

### D. The correlation functions between air and He permeation rate for PST films at 23°C and 100°C

A pretty good linear correlation between the air permeation rate and the He permeation rate at ambient was found for PST films. At 100°C, a completely different relation of third-degree polynomial function was found for these laminates.

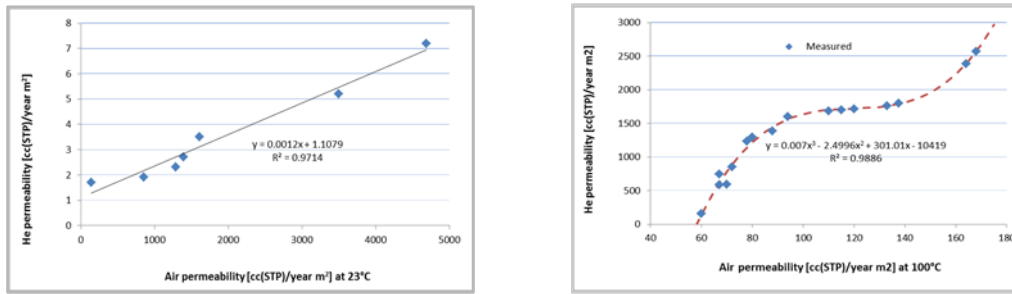


Fig.6 The graph on the left describes the linear correlation function between the air permeation rate through PST films to the He permeation. Right: a totally different correlation function was found at 100°C.

### E. The correlation functions between air and He permeation rate for PETMET laminates at 100°C

For standard PETMET laminates at 100°C, different third-degree polynomial correlation functions are shown between the air and the He permeation rates. It is pretty clear that a specific correlation curve should be established for each of the different group of laminates. The correlation curve for PETMET laminates at 100°C is shown in Fig.7.

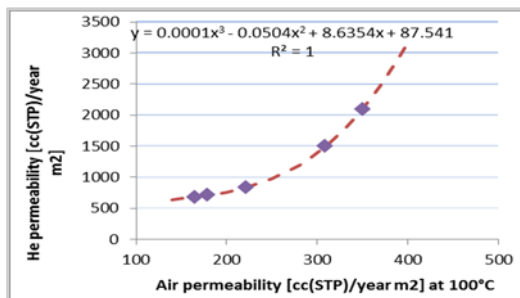


Fig.7 He vs Air permeation rate correlation curve for standard PETMET laminates at 100°C. Very good agreement with a third-degree polynomial function. The He/air correlation curve of the standard PETMET laminates is very different from that of the PST laminates.

## ANALYSIS OF FINDINGS

- In somewhat more sophisticated tests we found that the side permeation rate of He atoms through the seals was substantially smaller than the He skin permeation rate.
- In this work, we couldn't find one "universal" correlation curve between the permeation rate of air and He. However, several good correlation curves could be established for specific types of laminates at specific temperatures.
- The He permeation rate was determined by exposing half of the envelope to 10°C (cold plate) and the other half to 35°C. More work should be done to determine the optimal set of temperatures for getting a better correlation to the air permeation rate, especially at ambient conditions.

## CONCLUSIONS

- After establishing correlation functions between He and air permeation rate to a specific family of laminates it would be possible to replace the weeks-long air permeation test by overnight He permeation tests.



## **Increase of thermal conductivity of vacuum-panels with fumed silica cores in relation to absorbed moisture – hygrothermal simulations and measurements**

Sprengard Christoph<sup>1,\*</sup>, Kerstin Lohr<sup>1</sup>, Carolin Kokolsky<sup>1</sup> and Sebastian Tremel<sup>1</sup>

<sup>1</sup>FIW München, Munich, Germany

\*Corresponding e-mail: [sprengard@fiw-muenchen.de](mailto:sprengard@fiw-muenchen.de)

### **ABSTRACT**

The goal of this study is an investigation on the effect of moisture content and its distribution on the thermal conductivity of VIPs with fumed silica cores. Measurements from Carmi and Shufer (2017) show that the thermal conductivity of VIPs increases slower from a certain water content onwards. In an extended study at FIW, measured material parameters are taken as input data for hygrothermal simulations (WUFI<sup>®</sup> Pro) of VIPs. Simulations of the measurement setup in a guarded-hot-plate apparatus at different mean temperatures and with different temperature gradients are carried out. The moisture distribution as well as condensation effects within the core are observed closely to explain the unsteady functionality of the thermal conductivity of VIPs as a function of the moisture content first described by Carmi and Shufer (2017). Additionally, simulations for different temperature gradients show a slower increase of the moisture dependent thermal conductivity with larger temperature gradients due to earlier condensation processes on the cold side of the panel (at lower moisture contents).

### **KEYWORDS**

VIP, Core Material, Thermal Conductivity, Absorbed Moisture, Moisture Content Simulation

### **INTRODUCTION**

Moisture permeation through the barrier foil affects the ageing process in Vacuum Insulation Panels (VIPs) with fumed silica cores. Therefore, understanding the effect that adsorbed moisture has on the thermal conductivity of VIPs is of high importance. This paper is based on a study conducted by Carmi and Shufer (2017) in which the thermal conductivity of different fumed silica powders at various moisture contents was measured under stationary temperature gradients. For all investigated materials, the thermal conductivity as a function of water content increased faster at low water contents and more moderately at higher levels of water content. It is assumed that this effect is due to condensation and redistribution processes of the moisture on the cold side of the VIP. This paper aims to further investigate this effect by measuring certain material properties of fumed silica cores regarding the heat and moisture transport in an evacuated environment as well as conducting further simulations of the effect of moisture content on the thermal conductivity in VIPs with WUFI<sup>®</sup> Pro.

### **METHODS**

This work is divided into four main steps: 1) Measurements on VIP core materials were conducted to be used as input for hygrothermal simulations under stationary temperature gradients. These include the density, porosity and sorption properties. 2) The measurements are used together with material parameters ( $\lambda_{\text{dry}}$  and thickness) used by Carmi and Shufer (2017) and generic properties for VIPs provided in the WUFI<sup>®</sup> database to conduct simulations which recreate the experiment in the guarded-hot-plate apparatus at different plate temperatures. 3) Both literature research and measurements of further material parameters are

conducted to determine the effect that the evacuated environment has on certain moisture transport mechanisms, including vapor diffusion, capillary conduction and the moisture distribution within the VIP. From these results, it will be determined whether or not it is possible to conduct WUFI® simulations that sufficiently represent the effect of an evacuated environment instead of a normal atmospheric pressure under transient conditions. 4) If possible, transient WUFI® simulations depicting real-use conditions are conducted for the VIPs. This way, the effect of moisture content on the thermal conductivity of VIPs can be assessed under more realistic conditions. The results and methods used for steps 1) and 2) are outlined here. Steps 3) and 4), on the other hand, are still ongoing and the results cannot be fully presented yet, but first insights will also be discussed.

### Theoretical investigation and basis for further research steps

Investigations by Carmi and Shufer (2017) have shown a linear increase of the thermal conductivity of the VIP up to a certain mass related moisture content (MC) after which it clearly flattens out, with the curve showing a sharp bend. In order to predict this bend, theoretical principles were investigated. For this purpose, the p-v diagram of water and the sorption curve of VIP cores were examined. Carmi and Shufer (2017) discovered that the water vapor partial pressure remains constant from the buckling onwards despite increasing water content. The following theory is used to predict the bend: In a vacuum, the total pressure measured corresponds to the partial water vapor pressure in the VIP. If the water vapor partial pressure exceeds the saturation vapor pressure on the cold side, condensation occurs resulting in the bend in the course of the related change of the moisture distribution over the panel thickness. In the case of Carmi and Shufer (2017), 2°C were present on the cold side and 18°C on the warm side. The saturation vapor pressure at 2°C corresponds to 7.05 mbar. Knowing the temperature distribution in the panel for a vapor pressure of 7.05 mbar one can determine the total water content in the panel by calculating the relative humidity for each point in the panel and assigning the corresponding equilibrium moisture content of the sorption isotherm. This also means that for different temperature settings, the bend lies elsewhere as condensation occurs at a different water vapor pressure and consequently at a different water content in the VIP.

### Simulations and Measurements

Simulations were conducted in WUFI® Pro, a software that allows dynamic simulations of the one-dimensional coupled heat and moisture transfer in building components. Since WUFI® is designed for simulation under atmospheric pressure, it is to be expected that the speed of certain moisture transport mechanisms under evacuated conditions varies from standard values provided by WUFI®. This needs to be assessed in more detail in the future. Until then, only stationary measurements where the component has reached steady-state conditions and the speed of the moisture transport does not matter anymore are carried out.

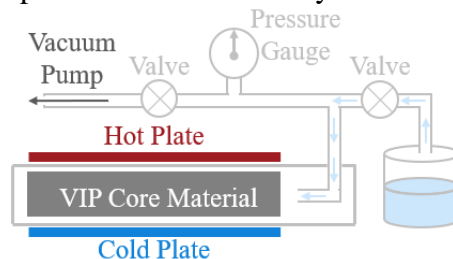


Figure 1. Experimental setup used by Carmi and Shufer (2017) and reconstructed in WUFI®.

The measurement setup used by Carmi and Shufer (2017) and modelled in WUFI® is depicted in Figure 1. The VIP core material is surrounded by a leak-tight foil to which a vacuum pump



is connected. A measured quantity of water vapor is allowed within the system to reach certain moisture contents within the core material. Thermal conductivity is measured with the heat flow meter method. The simulation in WUFI® Pro is performed at different temperature gradients ( $-2-22^{\circ}\text{C}$ ,  $2-18^{\circ}\text{C}$ ,  $5-15^{\circ}\text{C}$ ) with a mean temperature of  $10^{\circ}\text{C}$  to assess the influence of possible phase changes of water from vapor to liquid or solid on the thermal conductivity. Some basic material parameters ( $\lambda_{\text{dry}}$  and thickness) provided by Carmi and Shufer (2017) used in the simulations are summarized in Figure 2. Additionally, the sorption isotherms, bulk density and porosity of two different VIP cores were measured and used instead of the generic data from the WUFI® database (see Figure 2). The porosity is a required input value for WUFI® Pro, as it is an indicator for the maximum water content. It was determined by knowing the real density (measured with a helium pycnometer) and bulk density of the materials. The sorption isotherms were measured at  $23^{\circ}\text{C}$  up to a relative humidity of 98%. It is to be noted that in current simulations, no liquid transport coefficients have yet been taken into account.

	$\lambda_{\text{dry}}$	Density	Porosity	Thickness
	mW/(m.K)	g/cm <sup>3</sup>	m <sup>3</sup> /m <sup>3</sup>	mm
Core I	4.9	0.179	0.9187	15.4
Core II	4.9	0.170	0.9253	15.4

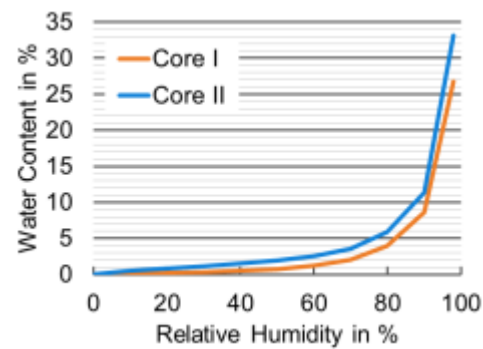


Figure 2. Material parameters used in WUFI® Pro (left) and adsorption isotherm for two different Cores measured by FIW (right).

In the model, the VIP core material is divided into five different layers. By assessing the heat flow between each of the simulated layers, it is possible to calculate the thermal conductivity for each layer independently and to better understand the influence of moisture in certain areas of the VIP.

## RESULTS

The performed simulations confirm the results measured by Carmi and Shufer (2017), although the sharp bend is not as visible in the simulations as it was in the measurements. Nevertheless, the moisture dependent thermal conductivity curve flattens evidently with increasing moisture content. Figure 3 shows the impact of the applied temperature gradient on the point at which the curve begins to flatten.

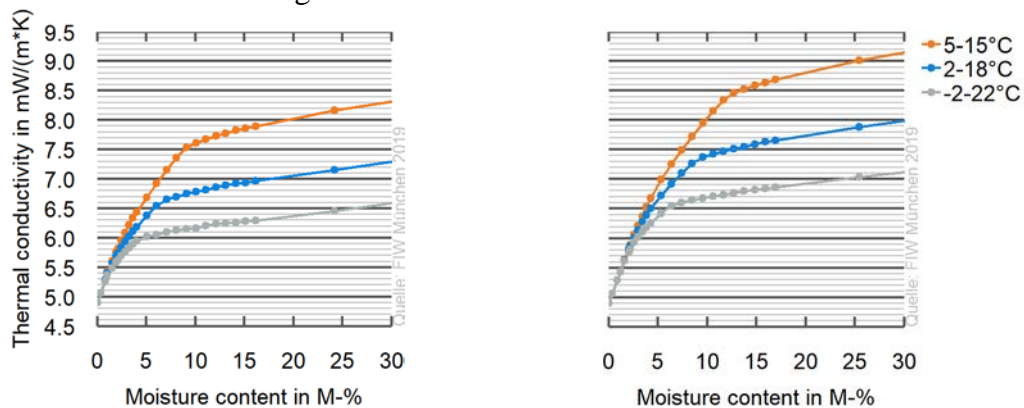


Figure 3. Simulation Results for moisture dependent thermal conductivity of VIP Core I (left) and Core II (right) at different temperature gradients.

Figure 4 shows that the moisture dependent thermal conductivity increases much more significantly in the VIP layer on the cold side (L1) than in all other panel layers (L2-L5). While in the beginning all layers show an increase of the thermal conductivity, the thermal conductivities of L2-L5 remain almost constant from certain moisture content onwards.

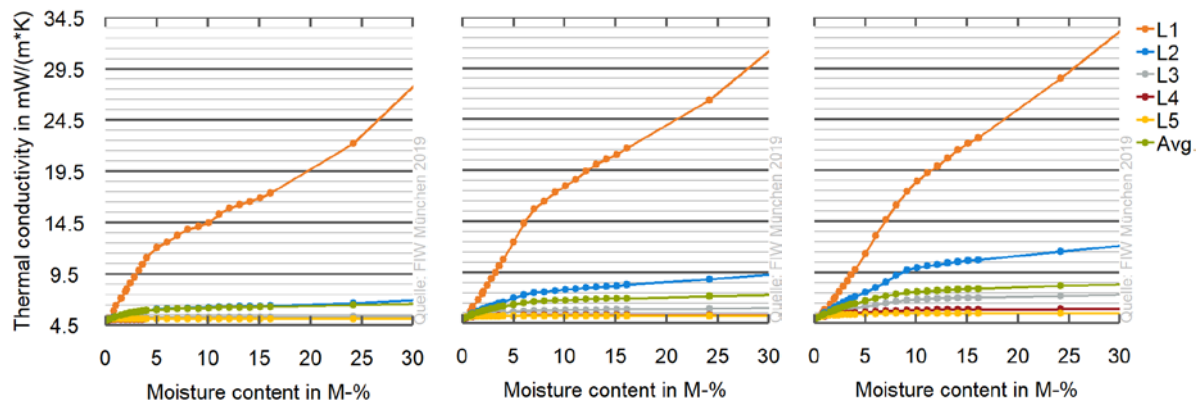


Figure 4. Moisture dependent thermal conductivity for different layers (L1: cold side, L5: warm side) of VIP Core I (exemplary) for temperatures -2–22°C (left), 2–18°C (middle) and 5–15°C (right).

## DISCUSSIONS

It can be derived from Figure 3 that the performance of the VIP is better with larger temperature gradients as the curve of the moisture dependent thermal conductivity starts flattening at lower moisture contents. A closer look on the water vapor pressure inside the VIP panel shows that the flattening occurs exactly when the saturation pressure at the cold side of the VIP is reached. Another observation confirms the assumption that condensate mainly forms in the layers close to the cold side: when reaching their saturation pressure, simulations with higher water contents show only a negligible increase in the water vapor pressure in the other VIP layers. With stagnating vapor content, the moisture inside the panel must be either liquid or solid (for temperatures lower than 0°C).

For higher moisture contents, Figure 4 indicates that water accumulates only in the outer layer on the cold side of the VIP (L1). Therefore, only L1 contributes to an increase of the total thermal conductivity, while for lower moisture contents (only gaseous phase), all layers contribute to an increase of the thermal conductivity indicating that water vapor is distributed more evenly than liquid water. However, further investigations will be carried out within the framework of the study in this regard.

It must be mentioned that the simulation results currently only allow a qualitative statement, since not all measurements of required material input parameters have yet been completed and liquid transport coefficients have so far been neglected. Until the final presentation, all missing parameters will be examined.

## CONCLUSIONS

This study contributes to a better understanding of the material behavior of VIPs with fumed silica cores. Based on the results of this study, statements can be made about the performance of VIPs in construction practice. One first conclusion is that the use of VIPs in cold countries is more suitable due to the increased performance of the component (lower thermal conductivity with increasing moisture contents) than in warmer countries (higher thermal conductivity with increasing moisture contents).

## REFERENCES

Carmi Y., Shufer E. 2017. An Advanced Technique for Measuring the Effect of Moisture content on the Thermal Conductivity of Fumed Silica VIPs, *A VIPA funded Project*.

## A cost-optimal sensitivity analysis of internal VIPs application in buildings

Márcio Gonçalves<sup>1,2\*</sup>, Nuno Simões<sup>1,2</sup>, Catarina Serra<sup>1,2</sup>,  
Shahaboddin Resalati<sup>3</sup>, Kate Brown<sup>3</sup>

<sup>1</sup>ADAI – LAETA, Department of Civil Engineering, University of Coimbra, Portugal

<sup>2</sup>Itecons - Institute for Research and Technological Development in Construction, Energy, Environment and Sustainability, Coimbra, Portugal

<sup>3</sup>Oxford Brookes University, Oxford, UK

\*Corresponding e-mail: [marcio.goncalves@itecons.uc.pt](mailto:marcio.goncalves@itecons.uc.pt)

### ABSTRACT

The building sector is known to be one of the most significant consumers of energy. To address this, the Energy Performance of Buildings Directive (EPBD) was published with the main goal of promoting the improvement of the energy performance of buildings. This directive also imposed the need for Member States to set cost optimal levels of minimum energy requirements taking into account their local climatic conditions.

In this context, the present study investigates the cost-optimality of applying Vacuum Insulation Panels (VIPs) when internally insulating residential buildings. Economic calculations are performed based on the cost-optimal methodology framework established in the Commission Delegated Regulation no. 244/2012. The calculations are performed using dynamic thermal simulation for different climatic zones in the EU. The cost analysis considers a rentable floor area analysis for low, medium and high rental values.

The results assess the range of prices for which the VIP solution may be considered a viable alternative to conventional insulation materials. This work is particularly useful for VIP manufacturers looking to market competitive products in regions with different climatic and economic conditions.

### KEYWORDS

Cost-optimal analysis; VIP; Internal wall insulation; Residential buildings.

### INTRODUCTION

The Energy Performance of Buildings Directive (EPBD), first published in 2002 (European Parliament, 2002) and recently replaced by Directive 2018/844 (European Parliament, 2018), aimed at promoting the energy performance of buildings. The EPBD focused on the improvement of building energy performance by setting minimum requirements for buildings and establishing nearly-zero energy buildings (nZEB) targets (Loukaidou, *et al.*, 2017). In addition, the EPBD introduced the determination of cost-optimal requirements on the basis of a methodology published in EU Delegated Regulation 244/2012 (European Parliament, 2012), which specifies how to compare energy efficiency measures in relation to their energy performance during life cycle.

One of the keys for achieving nZEB requirements can be through the use of highly efficient thermal insulation materials, such as vacuum insulation panels (VIPs). Due their low thermal conductivity, when compared with traditional insulation materials, VIPs allow for reduced thickness walls, enabling a better use of space in buildings. The economic benefits of thin walls when compared to other conventional insulation solutions could be particularly relevant where the available space for construction is limited, or where the rental prices are high. In fact, energy efficiency measures may lead to renting prices increase, which can be beneficial for landlords (Kamal *et al.*, 2019).

Some authors have been studying the economic feasibility of VIP application in buildings following different approaches. Some results have shown VIP to not be an economical alternative when compared to EPS (Mujeebu *et al.*, 2016). However, if area savings are taken into account, the VIP investment could be profitable as (Alam *et al.*, 2017) and (Fantucci *et al.*, 2019) have demonstrated. Cho *et al.* (2014) performed a life cycle cost analysis, showing the economic benefit of VIPs over conventional insulation materials. However, they compared different levels of insulation (thermal resistance of VIP  $\approx 4.4$  (m<sup>2</sup>.K)/W against 2.1 (m<sup>2</sup>.K)/W of conventional insulation material) which will lead to different levels of thermal comfort. This work will complement those studies, by presenting a cost-optimal analysis of internal VIPs application in buildings based on the Commission's cost-optimal methodology framework. Included were all factors which can affect the economic calculations, namely the VIPs' performance degradation with time, the panel size (edge effect) and the economic benefits of area savings. The energy performance of the reference building was achieved using dynamic simulations, since quasi-steady state methods for calculating energy needs are less precise (Tadeu *et al.*, 2014). In order to assess the cost-effectiveness of vacuum technology, the results were compared to those with expanded polystyrene (EPS), the most commonly used insulation material.

## METHODOLOGY AND CASE STUDY DEFINITION

This study was carried out considering a new multifamily building located in Berlin, Germany. The building data was collected using Tabula Webtool (TABULA, 2016), and the envelope thermal quality meets the German requirements. The calculations were performed for an intermediate floor apartment. The system for space heating and cooling is a heat pump with a Coefficient of Performance (COP) for heating of 3.4 and an Energy Efficiency Rating (EER) for cooling of 2.8. In this study, only the internal application of insulation in walls was studied, using different thicknesses of thermal insulation products. Since the goal was evaluate the economic viability of VIPs, the results were compared with a widely used insulation material, namely EPS. Other components such as windows, roof and floor insulation, systems, etc. remained unchanged in the simulations.

Table 1: Properties of thermal insulation materials.

Insulation	Thickness (m)	Conductivity (W/m.K)	Material cost (€/m <sup>3</sup> )	Installation cost (€/m <sup>2</sup> )
VIP	0.01 – 0.06	0.007	3000	20
EPS	0.05 – 0.31	0.036	120	10

The energy demand results for the several thermal insulation application measures was calculated using the dynamic thermal simulation software *DesignBuilder*, version 4.7.0.027. The set point temperatures were 20 °C for heating and 25 °C for cooling. The building airtightness is 0.6 ac/h (air change rate per hour). The final energy consumption was converted into primary energy by using a factor of 2.0 kWh<sub>PE</sub>/kWh for electricity (Eurelectric, 2017). The global cost,  $GC$ , over the calculation period,  $p$  (30 years), for a financial perspective is calculated by:

$$GC(p) = \sum_j \frac{[C_{I,j} + \sum_{i=1}^p (C_{a,i} \cdot D_f) - (V_{p,j} \cdot D_f)]}{A_{u,j}} \quad [\text{€/m}^2] \quad (1)$$

where,  $C_{I,j}$  is the initial investment cost for each measure  $j$ ;  $C_{a,i}$  is the annual cost during year  $i$  for measure  $j$ , calculated as:

$$C_{a,i} = C_e + C_m - \Delta R \quad [\text{€/year}] \quad (2)$$

where,  $C_e$  is the annual energy cost for heating and cooling;  $C_m$  is the annual maintenance cost, defined as 1% of initial investment;  $\Delta R$  is the additional rental income (corresponding to the floor area savings of VIP in comparison with EPS, for the same U-value);  $V_{p,j}$  is the residual value of measure  $j$  at the end of the calculation period;  $A_u$  is the useful floor area for measure

$j$ ;  $D_f$  is the discount factor for year  $i$  based on the real discount rate  $r$ . A discount rate of 5 % (Germany Banks, 2019) and an electricity cost of 0.30 €/kWh (Eurostat, 2019) were assumed. All applicable taxes including VAT were considered. A 100 €/m<sup>2</sup>.year rental cost (Thomschke, 2015) was kept constant over time. Other economical parameters were studied, namely the return on investment, the internal rate of return and the discounted payback period.

## RESULTS

Cost-optimal calculations showed that VIP is not a profitable solution when the rental benefits were not included (Figure 1a). However, if we consider rental incomes (Figure 1b) VIPs could be a cost-optimal solution, especially when transitioning to lower energy demands (nZEB targets). According these calculations, if the cost of VIPs is reduced to less than 2500 €/m<sup>3</sup>, it will become a competitive solution against EPS.

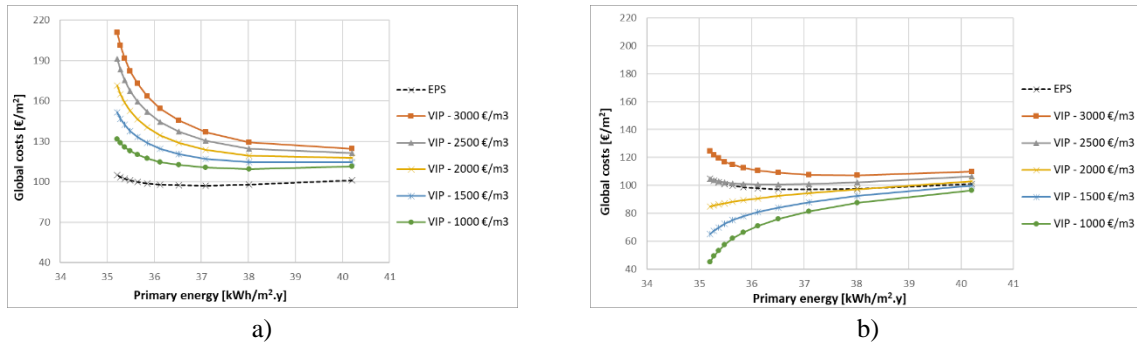


Figure 1. Cost-optimal curves of VIP and EPS: a) global cost calculation without rental benefits; b) global cost calculations with rental benefits.

Even with the estimated current VIP cost (3000 €/m<sup>3</sup>), investments could be economically profitable if the rental values are high enough. Figure 2a shows that zones with rental prices of 150 €/m<sup>2</sup> have already lower global costs than the EPS insulation with the same U-values. A sensitivity analysis for different climate zones was performed considering a VIP cost of 3000 €/m<sup>3</sup> and a rental price of 100 €/m<sup>2</sup>. The results presented in Figure 2b shows the cost-optimal curve for each city, and as expected, the optimal level of insulation changes with the climate data. For example, while in London the optimal solution means a U-value of 0.38 W/(m<sup>2</sup>.K), in the coldest city (Helsinki) the optimal U-value is 0.30 W/(m<sup>2</sup>.K). Please note that electricity prices were adjusted for each country (Berlin = 0.30 €/kWh; London = 0.20 €/kWh and Helsinki = 0.17 €/kWh), which explains the high global costs in Berlin.

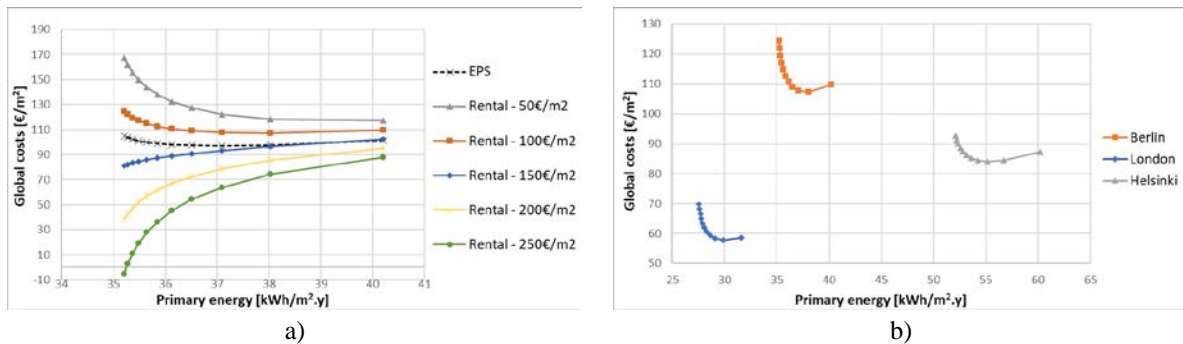


Figure 2. Cost-optimal curves: a) VIP as a function of rental prices; b) VIP in three different locations.

## CONCLUSION

This work presented a cost-optimality analysis for internal application of VIPs in the walls of a multifamily building. Economic calculations were performed based on the cost-optimal methodology framework, and rental income was included.

The results showed that VIP solutions can be economically profitable when compared with conventional insulation material, particularly if high thermal insulation levels are needed (e.g. nZEB targets). The benefits of area savings pay off the higher investment costs of vacuum technology. The VIP cost, the rental prices and the climate data are decisive when assessing the cost-optimality of VIPs. Accurate economic data is essential for performing an adequate cost-optimal assessment.

## ACKNOWLEDGEMENTS

This work has been developed under the European Union's Horizon 2020 research project INNOVIP, under grant agreement No 723441. This work has also been supported by the Portuguese Foundation for Science and Technology (FCT), under PhD grant PD/BD/135194/2017 under the Eco-Construction and Rehabilitation Programme.

## REFERENCES

- Alam M., Singh H., Suresh S., Redpath, D.A.G. 2017. Energy and economic analysis of Vacuum Insulation Panels (VIPs) used in non-domestic buildings, *Applied Energy*, 188, 1–8. doi:10.1016/j.apenergy.2016.11.115.
- Banks Germany. 2019. Available at: <https://banks-germany.com/> (accessed in May 2019).
- Cho K., Hong Y., Seo, J. 2014. Assessment of the economic performance of vacuum insulation panels for housing projects, *Energy and Buildings*, 70, 45–51. doi: 10.1016/j.enbuild.2013.11.073.
- Eurelectric 2017. European Commission proposal to revise the Energy Efficiency Directive. Brussels.
- Eurostat. 2019. Electricity price statistics. Available at: <https://ec.europa.eu/eurostat/web/energy/data/database> (accessed in May 2019).
- Fantucci S. Garbaccio, S., Lorenzati A. Perino M. 2019. Thermo-economic analysis of building energy retrofits using VIP - Vacuum Insulation Panels, *Energy and Buildings*, 196, 269–279. doi: 10.1016/j.enbuild.2019.05.019.
- Intelligent Energy Europe projects TABULA and EPISCOPE. 2016. Tabula Webtool. Available at: <http://webtool.building-typology.eu/#bm> (accessed in May 2019).
- Kamal A., Al-Ghamdy S. G., Koc, M.. 2019. Revaluing the costs and benefits of energy efficiency: A systematic review, *Energy Research and Social Science*. 54, 68–84. doi: 10.1016/j.erss.2019.03.012.
- Loukaidou K., Michopoulos A., Zachariadis T. 2017. Nearly-zero Energy Buildings: Cost-optimal Analysis of Building Envelope Characteristics, *Procedia Environmental Sciences*, 38, 20–27. doi: 10.1016/j.proenv.2017.03.069.
- Mujeebu, M. A., Ashraf N., Alsawayigh, A. 2016. Energy performance and economic viability of nano aerogel glazing and nano vacuum insulation panel in multi-story office building, *Energy*, 113 949–956. doi: <http://dx.doi.org/10.1016/j.energy.2016.07.136>.
- European Parliament. 2002. Directive 2002/91/EC of the European Parliament and of the Council of 16 December 2002 on the energy performance of buildings, L 1/65 – L 1/71.
- European Parliament. 2012. Commission Delegated Regulation 244/2012 of 16 January 2012 supplementing Directive 2010/31/EU of the European Parliament and of the Council on the energy performance of buildings by establishing a comparative methodology framework for calculating cost-optimal levels of minimum energy performance requirements for buildings, L81/18 – L 81/36.
- European Parliament. 2018. Directive (EU) 2018/844 of the European Parliament and of the Council of 30 May 2018 amending Directive 2010/31/EU on the energy performance of buildings and Directive 2012/27/EU on energy efficiency, 75–91.
- Tadeu S., Tadeu A., Simões N., Gonçalves M. 2014. The Impact of Thermal Insulation Cost on the Profitability of Energy Rehabilitation of Buildings, in 40<sup>th</sup> IAHS World Congress on Housing, 1–10.
- Thomschke L. 2015. Changes in the distribution of rental prices in Berlin, *Regional Science and Urban Economics*, 51, 88–100. doi: 10.1016/j.regsciurbeco.2015.01.001.

## **Application of Vacuum Insulation Panel in Slim Façade: from Lab to In-situ Experimental Evaluations**

F. E. Boaf<sup>1</sup>, S.M. Kim<sup>1</sup>, J.G. Ahn<sup>1</sup>, H.B. Moon<sup>1</sup>, J.H. Kim<sup>2</sup>, J.T. Kim<sup>1,3,\*</sup>

<sup>1</sup>Dept. of Energy Systems Engr., Kongju National Univ., Cheonan, Republic of Korea

<sup>2</sup>Green Energy Tech. Research Center, Kongju National Univ., Cheonan, Republic of Korea

<sup>3</sup>Dept. of Architectural Engr., Kongju National Univ., Cheonan, Republic of Korea

*\*Corresponding e-mail: jtkim@kongju.ac.kr*

### **ABSTRACT**

Buildings with curtain wall systems (CWS) are prominent in contemporary architecture, especially for commercial purposes. To improve their energy consumption footprint, CWS are prefabricated with glazed (i.e. transparent vision) and spandrel (i.e. non-vision/opaque) sections; spandrel areas incorporate insulation to curtail fluctuating heat fluxes. Nonetheless to meet local stringent building energy codes, thick traditional insulation materials (> 150 mm) are required behind monolithic glazing/spandrel panel and hidden from view between adjacent floor (slab/plenum) areas, otherwise they compromise aesthetics; thus, restricting the overall area to install insulation. On the other hand, high-performance vacuum insulation panel (VIP) serves as a feasible slim spandrel insulation. This study is a continuation of an ongoing project investigating application of VIP in slim curtain wall façades. Particularly in this study, mock-up modules were fabricated based on optimum numerical results, and the thermal performance of the system was investigated under dynamic outdoor conditions.

### **KEYWORDS**

Vacuum insulation panel, Curtain wall systems, Slim facade, Thermal performance.

### **INTRODUCTION**

Glass façades, commonly referred to as curtain wall system (CWS), is one key signature of modern building construction; due to improved daylighting levels and aesthetics, increased speed and quality of construction, smaller wall footprint, among others [1]. However, energy demand to ensure comfortable indoor thermal environment is greater in highly glazed curtain walled buildings as compared to conventional buildings, especially during peak summer and winter; since glazed systems have lower thermal resistance than opaque walls [2]. Alternatively, CWS with vision and spandrel (non-vision/opaque) components potentially reduces heat fluxes. Consequently, spandrel insulation is significant but restricted due to small/slim area to apply insulation. Some authors have studied thermal performance of spandrels with rigid foam insulation in [3, 4] and durability of VIP as spandrel insulation under accelerated aging conditions [5]. The concept represents a strategy to extend the service life and in-service durability of VIP. Based on prior numerical evaluations, this study presents initial experimental findings for slim curtain wall spandrel system with integrated VIP. This work is part of a continuous study on VIP applications in slim façades, previously reported at the 12<sup>th</sup> and 13<sup>th</sup> IVIS [6, 7]. The aim is to experimentally evaluate thermal behavior of CWS with VIP spandrel.

### **METHODS**

#### **Initial modeling and spandrel alternatives**

Firstly, numerical investigations using Physibel BISCO/TRISCO were carried out to propose and examine optimized configurations for slim curtain wall spandrel system with integrated



VIP. Except for minor changes in configurations, the numerical methods were similar to procedures already reported in [9]. Based on the numerical studies, two alternative scenarios were considered to mitigate thermal bridges, in addition to a control base case; the material configuration and dimensions of the spandrel scenarios are depicted in Figure 1.

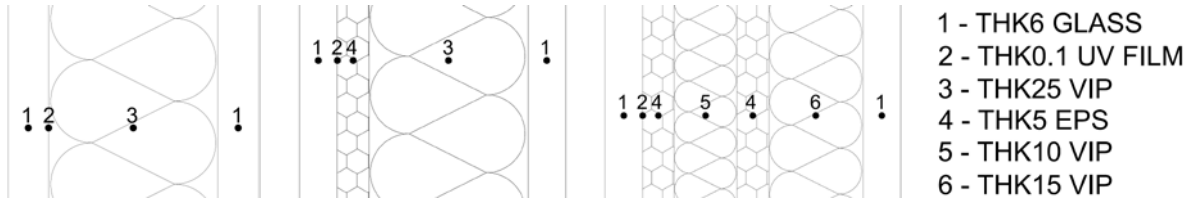


Figure 1. Schematic diagram showing details of spandrel sections: base case 1 (C1), alternative case 2 (C2) and alternative case 3 (C3); from left to right.

### Overview of mock-up test

Using a stick-aluminum frame system, spandrels measuring 1355 mm by 1355 mm were fabricated; each spandrel scenario consisted of 4 air-tight spandrel sections (see Figure 2). In-situ tests were conducted in June 2019. The mock-up test facility is presented in Figure 3.

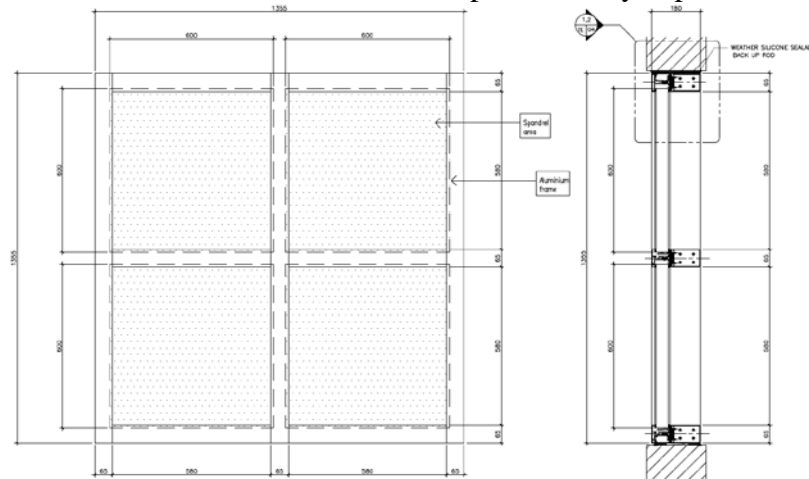


Figure 2. Schematic diagram: details of stick spandrel (left) and sectional view (right).



Figure 3. Schematic plan (left) and actual test facility (right).

In all, 16 fumed silica-based VIPs with metalized barrier envelope (size 600 mm<sup>2</sup>) thicknesses indicated in Figure 1, were installed. The center of panel thermal conductivity of the VIPs ranged from 3.79-4.56 [ $10^{-3}$  (W/mK)]. The external wall of the facility was made of 100 mm EPS sandwiched panel, 50 mm glass wool insulation and 19 mm 2-ply gypsum board (from outside to inside). Three openings measuring 1360 mm by 1360 mm each, were provided on the south-facing wall of the facility to accommodate the spandrel specimens. Additionally, the



test facility had a buffer area that also doubled as a control room. The internal and external surface temperature of spandrel specimens, indoor temperature of each test room, and cavity temperatures of VIP surface towards exterior and interior environments were measured at intervals of 5 minutes. Detailed technical and uncertainty specifications of test equipment are listed in Table 1.

Table 1. Specification of measuring apparatus

Type (model)	Specification
Thermocouple (Yokogawa KX-F 0.32)	Measurement range: -200 to 1372 Accuracy: $\pm 0.50$ (at -200 °C to -50 °C), $\pm 0.25$ (at -50 °C to 1372 °C)
Infrared thermal camera (Fluke Ti32)	Operating temperature: -10 °C to 50 °C Infrared spectral band: 7.5 $\mu\text{m}$ to 14 $\mu\text{m}$ Measurement range: -20 °C to 600 °C Thermal sensitivity: $\leq 0.05$ °C Accuracy: $\pm 2$ °C or $\pm 2\%$
Data logger (Graphtec GL800)	Clock accuracy: $\pm 0.002\%$ (ambient temperature 23 °C) Measurement accuracy: $\pm (0.05\%$ of reading + 2 °C) at -200 °C to -100 °C; $\pm (0.05\%$ of reading + 1 °C) at -100 °C to 1370 °C.

## RESULTS AND DISCUSSION

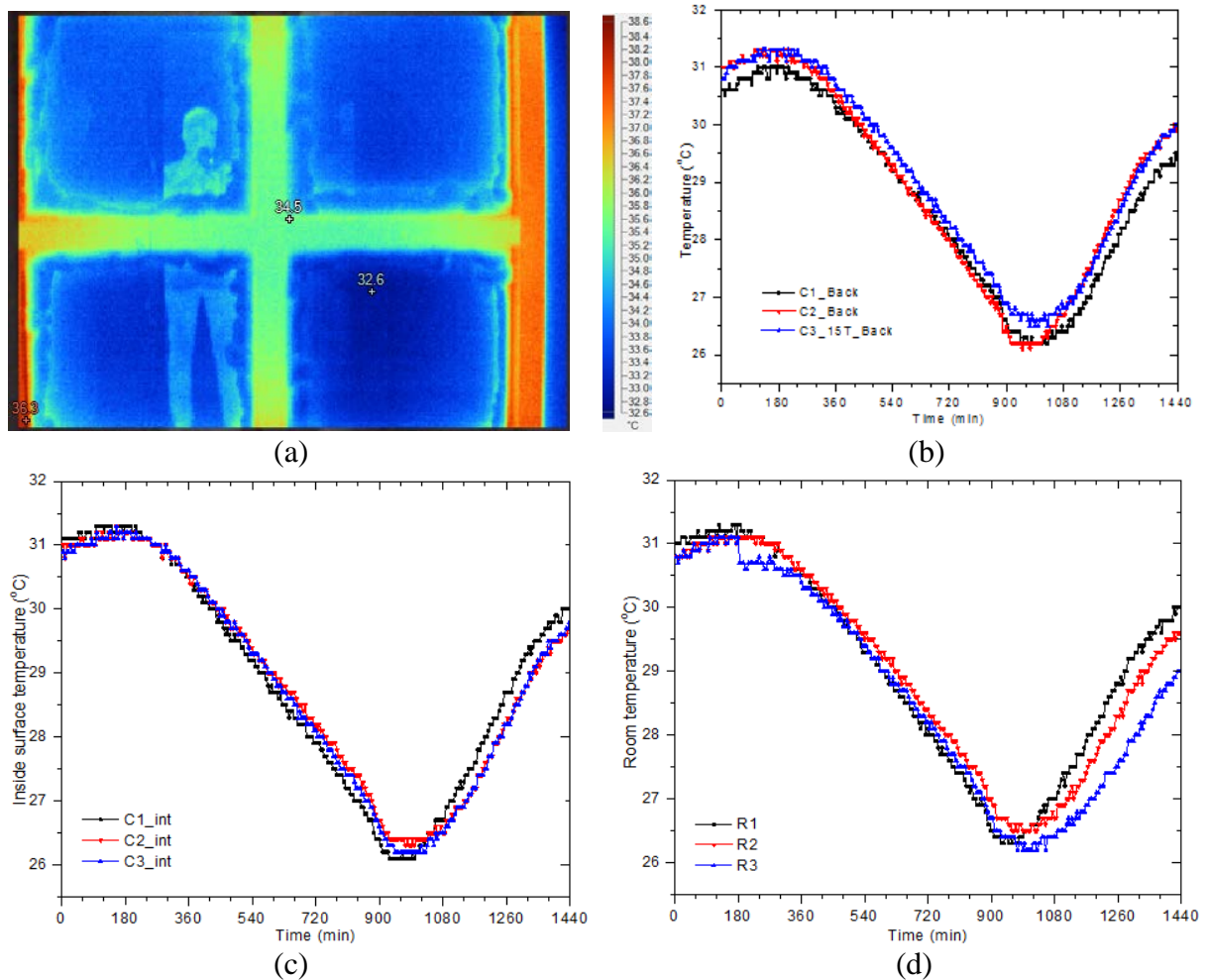


Figure 4. Surface temperature distributions: (a) thermal image of interior facing spandrel, (b) VIP surface towards interior, (c) internal spandrel surface and (d) room temperature.

Considering a representative 24-hour summer day (ie. 8<sup>th</sup> July at 4pm to 9<sup>th</sup> July at 4pm), the temperature distribution dynamics are presented in Figure 4. Under non-air-conditioned mode, around 12 noon the outside surface temperatures were 37.5 °C, 37.7 °C and 36.9 °C for base case 1 (C1), alternative case 2 (C2) and alternative case 3 (C3), respectively; corresponding to inside surface temperatures of 28 °C, 27.6 °C and 27.5 °C for C1, C2 and C3. In all scenarios, around 12 noon, the VIP front surface temperature was higher than the VIP back surface temperature within the spandrel cavity; 38.8 °C and 27.5 °C for C1, 39.4 °C and 28 °C for C2, 38.6 °C and 31.8 °C for the exterior facing 10T VIP of C3, and 31.5 °C and 27.9 °C for the interior facing 15T VIP of C3. Around 12 midnight the outside surface temperatures were 21.8 °C, 21.8 °C and 21.6 °C for C1, C2 and C3, respectively; corresponding to inside surface temperatures of 29.5 °C, 29.7 °C and 29.7 °C for C1, C2 and C3. In all scenarios, around 12 midnight, the VIP front surface temperature was lower than the VIP back surface temperature within the spandrel cavity; 22.8 °C and 29.6 °C for C1, 22.4 °C and 29.7 °C for C2, 22.6 °C and 26.2 °C for the exterior facing 10T VIP of C3, and 26.6 °C and 30 °C for the interior facing 15T VIP of C3. The mean temperature fluctuations between the front and back VIP surface were more pronounced for C2 (ie. 12.2 °C) and C1 (11.9 °C), but lower for the exterior facing 10T VIP of C3 (ie. 6.2 °C) and 4.8 °C for the interior facing 15T VIP of C3. Generally, the mean spandrel surface temperature was lower than the frame temperature (see Figure 4a). Noticeable areas of heat loss were at the edge of frame junctions.

## CONCLUSIONS

In this study, thermal behavior of curtain wall system with VIP integrated as spandrel insulation has been examined, experimentally; by considering alternatives towards improved thermal performance. Results depict that Case 3 showed the least temperature fluctuations across the VIP. Further study considering air-conditioned mode is ongoing, to understand the system.

## ACKNOWLEDGEMENT

This work was supported by the Ministry of Education and National Research Foundation of Republic of Korea through Basic Science Research Program (No. 2018R1D1A1A09083870).

## REFERENCES

- [1] Kazmierczak, K. and Hershfi, M. Review of Curtain Walls, Focusing on Design Problems and Solutions. *Proceedings of BEST2 Conference*. 2010.
- [2] Torgal, F.P. et al. Nearly zero energy building refurbishment. 2013: *Springer*.
- [3] Behr, R.A. On-site investigations of spandrel glass microenvironments. *Building and Environment*, 30 (1995) 61-72.
- [4] Richman, R. and Pressnail, K. A more sustainable curtain wall system: analytical modeling of the solar dynamic buffer zone (SDBZ) curtain wall. *Building and Environment*, 44 (2009) 1-10.
- [5] Gubbels, F. et al. Durability of vacuum insulation panels in the cavity of an insulating glass unit. *Journal of Building Physics*, 2014.
- [6] Boafu, F.E., et al. Impact of VIP envelope reflectance on the performance of curtain wall system. In: *Proceedings of 11th International Vacuum Insulation Symposium (IVIS 2015)*, Nanjing, China, September 19-21, 2015, pp. 158-163.
- [7] Boafu, F.E., Kim, S.-M. and Kim, J.-T. Application of VIP in slim façade: thermal bridge evaluation. In: *Proceedings of 12th International Vacuum Insulation Symposium*, Paris, France, September 20-21, 2017, pp. 33-34.
- [8] Boafu, F.E., Kim, J.-H. and Kim J.-T. Numerical study of slim curtain wall spandrel with integrated vacuum insulation panel: Concept, performance evaluation and challenges. *Energy and Buildings*, 183 (2019) 139-150.

## Study on thermal performance of VIP applied wall by installation method in building

Sang-Myung Kim<sup>1</sup>, Ji-Suk Yu<sup>1</sup>, Kil-Seon Lee<sup>1</sup>, Jin-Hee Kim<sup>2</sup> and Jun-Tae Kim<sup>3,\*</sup>

<sup>1</sup>Department of Energy System Engineering, Kongju National University, Cheonan, Korea

<sup>2</sup>Green Energy Technology Center, Kongju National University, Cheonan, Korea

<sup>3</sup>Department of Architecture, Kongju National University, Cheonan, Korea

\*Corresponding e-mail: [jtkim@kongju.ac.kr](mailto:jtkim@kongju.ac.kr)

### ABSTRACT

To reduce building energy, Korea insulation regulations have continuously been strengthened, and the insulation thickness of building exterior walls is also increasing to satisfy the regulation. Vacuum insulation panel (VIP) is a high-performance insulation which has lower thermal conductivity compared to existing insulation material. In addition, VIP satisfies the said regulations with relatively thin thickness. VIP is not a homogeneous material but composed of different materials. So, its insulation performance can deteriorate due to ensuing thermal bridges when applied in the buildings. Particularly, since the edge of VIP is not completely uniform/flat, air gaps are generated between adjacent panels and heat losses may occur when the panel is integrated to a wall. In this study, the effect of the air gap between panels on the thermal performance of a VIP integrated wall is analyzed by simulation program and experiment. The VIP applied walls were designed based on different installation methods. The thermal performance of the system was analyzed using thermal analysis program. In addition, the thermal characteristics of the VIP applied walls were investigated by experiment.

### KEYWORDS

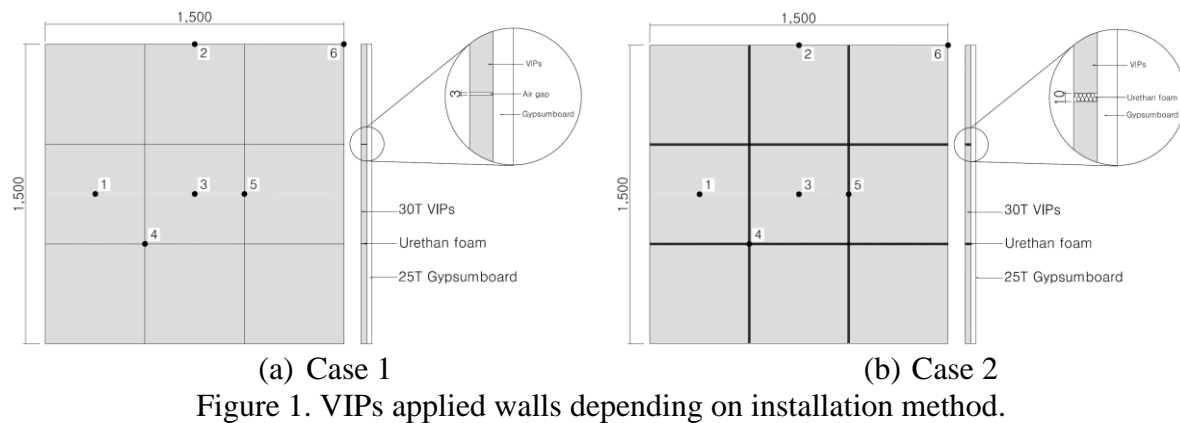
Vacuum Insulation Panel (VIP), Thermal bridges, Building application, Thermal performance

### INTRODUCTION

The green gas emission is globally one of major issue and lot of efforts to reduce emission have been done. Since building is one of main consumer of energy, many alternatives have been proposed and progressed to reduce energy demands in building sector. In case of Korea, the thermal transmittance of exterior wall has gradually strengthened to reduce the energy demand of buildings. In 2010, the thermal transmittance of exterior wall was  $0.36\text{W/m}^2\text{K}$  and it currently intensified  $0.15\text{W/m}^2\text{K}$  more than twice. To satisfy enhanced insulation regulation building insulation thickness is increased, and it causes building areas are reduced. For this reason, the high-performance insulation materials are required to meet higher insulation performance of building. VIP is one of high-performance insulation which has lower thermal conductivity about 8 to 10 times than existing insulation materials for building. Therefore, it satisfies said regulations with relatively thin thickness. VIP is not a homogeneous material, but composed of different materials such as core, envelope and getter. When applied buildings, it causes thermal bridge, and thermal bridge deteriorates insulation performance of building. Especially, since the surface of VIPs is completely not uniform and flat, air gaps are generated between adjacent VIPs. And the heat losses occurred through air gap between adjacent panels. For this reason, it should be considered how to install VIPs when VIPs are applied in building. In this study the thermal characteristics of VIPs wall depending on method to installed VIPs was investigated. For this study, the walls applied VIPs were modelled and manufactured by different installation methods, and it were analyzed by using the thermal analysis simulation program and experiment.

## METHODS

In this study, it is analyzed that thermal bridge and thermal characteristics of VIP-walls depending on the installation methods of VIPs. For this study, two types of VIP-walls were modelled and manufactured for simulation and experiment. Fig. 1 show the schematics of VIP-walls according to the installation methods. One is VIPs were attached in gypsum board and the air gap was occurred between adjacent VIPs (a). The other is VIPs were fixed in gypsum board with constant space of 10mm between VIPs, and the space between VIPs was filled in urethane foam to prevent heat loss (b).



To analysis the thermal performance of VIPs applied wall, the thermal analysis simulations and experiment were completed. Simulation programs called BISCO and TRISCO which analysis steady-state heat transfer at different boundary conditions were used to calculate the linear thermal transmittance and effective thermal transmittance. BISCO is for two-dimensional objects made of different materials, and TRISCO is three-dimensional. In the simulation the boundary condition and the thermal conductivity of materials are shown in the Table 1.

Table 1. Thermal conductivity of materials and boundary condition

Indoor	25 °C	Outdoor	-10 °C
VIP	0.0045 W/mK	Gypsum board	0.144 W/mK
Urethane foam	0.05 W/mK		

Figure 2 showed the manufactured VIPs walls according to different installation methods, and the test of thermal transmittance was conducted. The test was proceeded in the guarded hot box test facility based on the ISO 8990 [Thermal insulation – Determination of steady-state thermal transmission properties- Calibrated and guarded hot box]. Figure 3 is schematics of experiment set-up. The set temperature of cold box was -10°C, and the temperature of guard box set up 25°C. Besides, to analyse thermal characteristics of VIPs-wall, the temperature points which are located in the edge and between VIPs were additionally measured shown as Figure 1 (1~6).



Figure 2. Experiment for VIPs applied walls

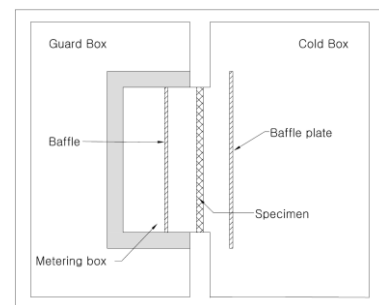


Figure 3. Experiment setup

## RESULTS

Table 1 shows the simulation results of VIPs applied wall according to the building installation methods. The table include the temperature distribution, one-dimensional U-value ( $U_{1d}$ ), linear thermal transmittance ( $\psi$ ) and effective thermal transmittance ( $U_{eff}$ ). In the results of the temperature distributions the heat flows were different depending on the installation method at the adjacent VIPs. In case 1, it is confirmed that the heat losses happened at the air gap occurred between adjacent VIPs. In the case 2 the urethane foam was filled at the regular intervals between VIPs to prevent heat losses through air gap. However, the temperature distribution of case 2 shows that the heat losses and thermal bridge were occurred through urethane foam between VIPs. Because the thermal conductivity of urethane foam is higher than VIPs, the difference of thermal conductivities affected the thermal bridge. The result of linear thermal transmittances of case 1 and case 2 were 0.006, 0.108 W/mK. The linear thermal transmittance is the numerical data which show effect on thermal bridge, and it means the thermal bridge of the case 2 was bigger than case 1. The reason of the higher thermal bridge of case 2 than case 1 is analyzed not only difference of thermal conductivity, but also the width of the space between adjacent VIPs. The case 2 was designed 10mm width space in order to fill in urethane foam than air gap of case 1. By filling urethane foam which has higher thermal conductivity than VIPs into broader width space, many heat losses was happened and it caused bigger thermal bridge. For this reason, the effective thermal transmittances which consider thermal bridge were also case 2 was higher than case 1.

Table 2. Simulation results

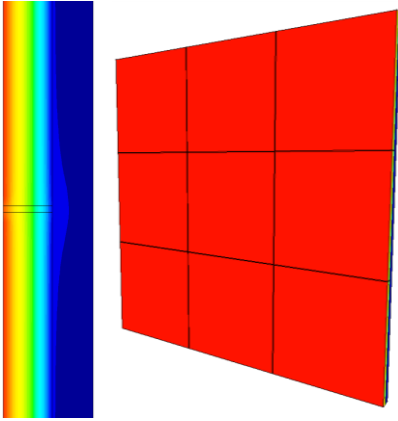
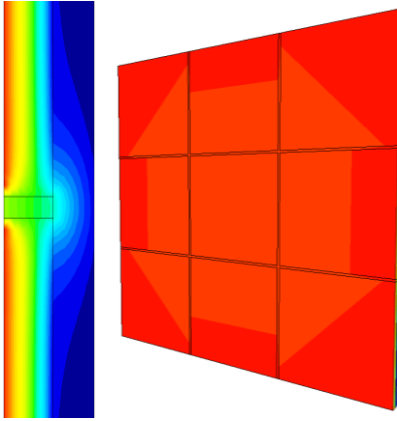

	Case 1	Case 2	Legend
Temperature distribution			
$U_{1d}$ (W/m <sup>2</sup> K)	0.143	0.143	
$\psi$ (W/mK)	0.006	0.108	
$U_{2d}$ (W/m <sup>2</sup> K)	0.146	0.215	
$U_{eff}$ (W/m <sup>2</sup> K)	0.194	0.221	

Table 3 is results of experiment which measured the surface temperature and thermal transmittance of the manufactured VIPs walls. It shows overall surface temperature of case 1 was higher than case 2. Because the heat losses of the case 1 is lower than case 2, the surface temperature of case 1 was kept higher than case 2. Also, the thermal transmittances of VIPs applied walls were measured and calculated based on the ISO 8990. The thermal transmittances of case 1 and 2 were 0.236, 0.244 W/m<sup>2</sup>K. The thermal transmittance of case 1 was lower 0.008 W/m<sup>2</sup> K and it was confirmed that the installation method of case 1 was kept higher thermal performance than case 2.

Table 3. Experiment results

Case	Experiment	Point Temperature					
		1	2	3	4	5	6
Case 1	Average temperature (°C)	24.5	23.3	24.7	22.5	22.9	23.6
	Thermal transmittance (W/m <sup>2</sup> K)	0.236					
Case 2	Average temperature (°C)	24.4	22.8	24.2	22.1	22.5	23.5
	Thermal transmittance (W/m <sup>2</sup> K)	0.244					

## DISCUSSIONS

In the results it was analysed that thermal performance of VIPs applied wall can be changed depending on the building installation methods for VIPs even though it designed and manufactured same one-dimensional u-value. Through the simulation and experiment it was confirmed the thermal performance of VIPs-wall can be decreased by thermal bridge, and thermal bridge affected how to install VIPs for building. The same size VIPs-walls was investigated and when it has broader width interval between adjacent VIPs, the thermal bridge was occurred even if the interval was filled as insulation materials.

To prevent decreasing thermal performance, it is considered the space between VIPs and the properties of materials which is composed with VIPs in the wall. Because when the materials which have higher thermal conductivity than VIPs are used with VIPs, lot of heat can escape through higher materials.

## CONCLUSIONS

In this study, it was investigated the effect of VIP installation methods on thermal performance for building. VIP is composed with different materials and have different characteristics with different insulation materials. For this reason when VIP is applied for building, it is essential to consider how to install. To keep the high thermal performance of VIPs applied wall, the efforts of reducing thermal bridge are considered such as intervals between adjacent VIPs and the properties of materials which combined together with VIPs. To revitalize VIP industry for building, the research which investigate to minimize the occurred thermal bridge of VIPs in building application and propose the optimal installation methods are required

## ACKNOWLEDGEMENT

This work was financially supported by the Ministry of Education (MOE) and National Research Foundation (NRF) of Korea through the Basic Science Research Program (No. 2018R1D1A1A09083870).

## REFERENCES

- Asdrubali, F., Baldinelli, G. 2011. Thermal transmittance measurements with the hot box method: Calibration, experimental procedures, and uncertainty analyses of three different approaches, *Energy and Buildings*, 43(7), 1618-1626.
- Boafo, F. E., Kim, J. T. and et al. 2019. Numerical study of slim curtain wall spandrel with integrated vacuum insulation panel: Concept, performance evaluation and challenges, *Energy and Buildings*, 183, 139-150.
- Min, D. H., Kim, S. M. and et al. 2019. The thermal bridge characteristic of wall with vacuum insulation panels according to the thermal bridge reduction method, *KIEAE Journal*, 19(2), 81-86
- ISO. 2017. *ISO 8990:1994*, Thermal insulation – Determination of steady-state thermal transmission properties – Calibrated and guarded hot box.

## Thermal and aging characterization of stand-alone and foam-embedded VIPs for building applications

K. Biswas<sup>1,\*</sup>, R. Jogineedi<sup>1,2</sup>, A.O. Desjarlais<sup>1</sup>, D. Smith<sup>3</sup> and J. Jones<sup>3</sup>

<sup>1</sup> Oak Ridge National Laboratory (ORNL), 1 Bethel Valley Rd., Oak Ridge, Tennessee, USA

<sup>2</sup> Department of MEEP, Southern Illinois University, Carbondale, IL, USA

<sup>3</sup> NanoPore Incorporated, 2525 Alamo Ave. SE, Albuquerque, NM, USA

\* [biswask@ornl.gov](mailto:biswask@ornl.gov), Tel.: +1 (865) 574-0917

**ABSTRACT:** Understanding the performance of vacuum insulation panels (VIPs) and VIP-based composites under laboratory conditions as well as in real building applications is needed to enable broad adoption of VIPs in buildings. Stand-alone VIPs and VIPs fully encapsulated by foam insulation were aged under natural weatherization, room and accelerated aging conditions; the accelerated aging was done under elevated temperature and/or humidity. The change in performance of the VIPs and foam-VIP composites were investigated using direct measurements of thermal resistance in the laboratory as well as in situ measurements of heat flows in the natural weatherization tests. In addition, the impact of different barrier films, metallized vs. polymeric, on the overall thermal performance of composite foam-VIP insulation boards were investigated.

**KEYWORDS:** natural aging, accelerated aging, composite foam insulation, heat flow meter.

**INTRODUCTION:** ORNL and NanoPore have been collaborating to develop composite foam boards containing low-cost vacuum insulation panels (VIPs), which can achieve 2-3 times the thermal resistance of current building insulation materials [1]. Current efforts are focused on evaluating the long-term performance of the foam-VIP composites. The barrier film is a critical component of the VIPs. The film impacts the long-term performance of VIPs by its ability to maintain the internal vacuum within VIPs and the overall thermal performance of VIPs when considering the edge effects. Most of the past work on the foam-VIP composites were with VIPs containing a polymeric film made of ethylene vinyl alcohol (EvOH). Recently, we have also started investigating metallic barrier films.

**LABORATORY AND NATURAL AGING:** Aging studies are being performed at multiple locations under different conditions and are described below. The foam-VIP composites used in the aging were all created in factory using a typical foam board manufacturing process. The composites consist of an array of 1 inch (2.54 cm) VIPs that are sandwiched by 0.5 inch (1.3 cm) foam sheets on either side. To make the composite boards, the VIPs were initially adhered to a 1.3 cm high-density (HD) polyisocyanurate (PIR) coverboard, which was then fed onto to a foaming line for spray-application of 1.3 cm of regular PIR [1].

**Oak Ridge, TN:** At ORNL, VIP and foam-VIP composites (with EvOH barrier films) are being aged under natural, room and accelerated aging conditions. The room aging is being done in a temperature and relative humidity (RH) controlled space. The accelerated aging was done in two environmental chambers that were maintained at 24°C/80% RH and 70°C/50%RH. The natural aging is being done on a low-slope roof. Two set of VIPs and foam-VIP composites are being aged; one set is installed under a black roof membrane and the other under a white roof membrane. VIPs of dimensions 11.5"×11.5"×0.5", 11.5"×11.5"×1", and 22"×22"×1" are being aged. The composites contain 22"×22"×1" VIPs



and the overall dimensions of the composites are 24"×24"×2". All samples are periodically tested using heat flow meters (HFM) according to ASTM C518 [2].

Figure 1 shows the measured thermal resistance of the VIPs and foam-VIP composites as a function of time. As expected, the more stringent conditions of 70°C and 50% RH caused the resistance of the samples to drop the most, while the measured resistances were relatively stable under room conditions. It is interesting to note the similarities in the aging curves of the roof samples and the samples aged at 24°C and 80% RH. Further testing is needed, but preliminary findings indicate that aging of VIPs at 24°C and 80% RH can be a surrogate for natural aging under the mixed-humid climate conditions of Oak Ridge, TN. The 70°C/50%RH aging was terminated once the thermal resistance of the samples dropped by about 50% of the original value and seemed to become stable (after about 250 days). The samples were removed and stored under room conditions. Further testing suggested a recovery (increase) in thermal resistance; see fig. 1 (bottom row). Testing of all samples are being continued.

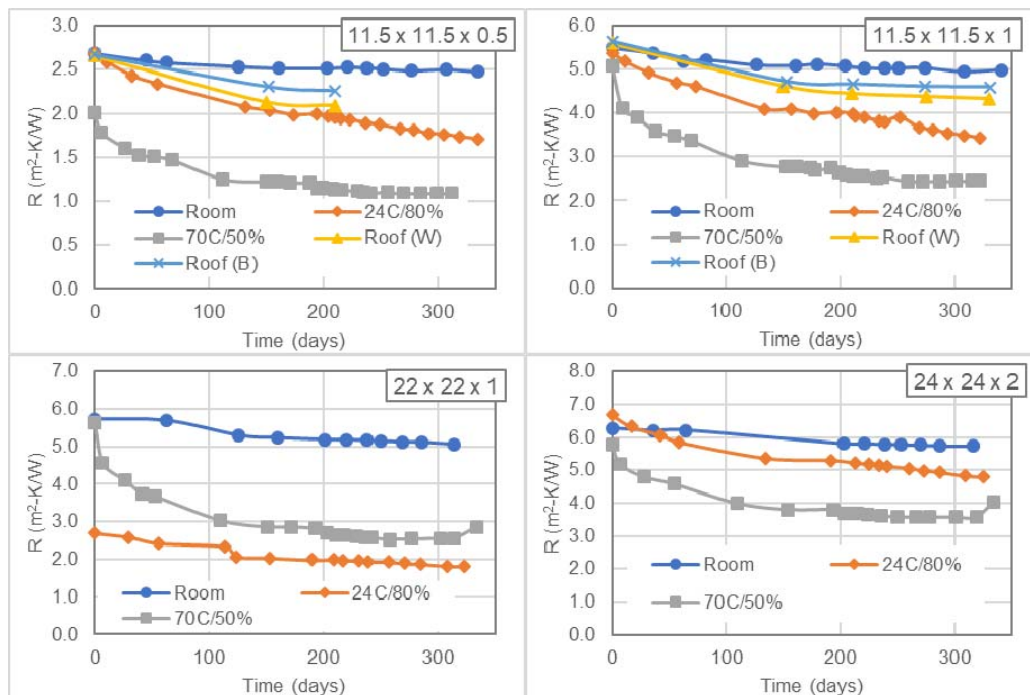


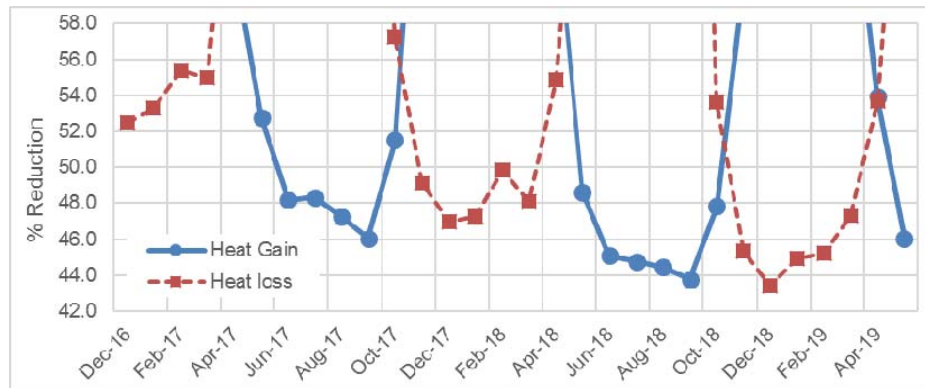
**Fig. 1:** Measured thermal resistance of aged VIPs and foam-VIP composite over time.

**Charleston, SC:** A natural exposure test (NET) facility in Charleston, South Carolina (SC) was also part of the aging study. The NET facility is designed to accommodate side-by-side wall assemblies for long term testing under real building conditions. Tests wall are typically 2.64 m high and 1.22 m wide. They are instrumented with thermistors and heat flow transducers (HFTs). For this aging study, two side-by-side test walls were installed: one with the 5.1 cm composite foam-VIP board (1) as the exterior continuous insulation (CI) layer and another with 5.1 cm of regular PIR board as the CI. Both test walls were built identically (except the exterior CI layer): interior 1.3 cm gypsum board, wood framing (studs), cavity insulation (fiberglass batts) and exterior 1.3 cm oriented strand board (OSB).

The measured heat flows at the OSB-cavity interface of each test wall showed that the foam-MAI composite, with its higher thermal resistance, significantly reduced the heat flow into and out of the building. It is noted that this HFT measured the heat flows through a small area that is coincident with the center of the VIPs and doesn't represent the overall performance of the foam-VIP composite. However, these measurements are useful in understanding the long-term behavior of the foam-encapsulated VIPs.

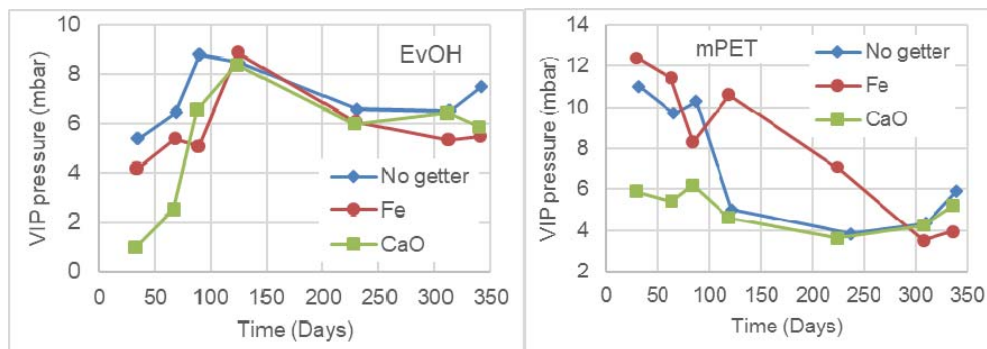


Fig. 2 shows the percent reduction in monthly integrated heat gains and heat losses from the foam-VIP composite compared to regular PIR. Reductions in heat gain during the summer months (Jun-Sep) and reductions in heat losses during the winter months (Dec-Mar) are of primary interest. A small degradation is observed in the foam-VIP composite performance relative to the regular PIR. The average percent reduction during the first winter period (Dec 2016 – Mar 2017) was 54%, but during the subsequent winter periods (2017-18 and 2018-19), the percent reductions dropped to 48% and 45.2%. Similarly, the average percent reduction during Jun-Sep 2017 was 47% and it dropped to 43.4% during Jun-Sep 2018.



**Fig 2:** Change in percent reduction in heat flows with the foam-composite over time.

**Albuquerque, NM:** Finally, another set of aging studies is being performed by NanoPore. For this portion, 11"×11"×1" VIPs were produced with four different barrier films. The different barrier films contained EvOH, mPET and Al foil as the primary barrier component. In addition to the barrier films, some VIPs core were incorporated with iron powder (Fe) and calcium oxide (CaO) as oxygen and water vapor getters, respectively. All VIPs are stored in a 30°C constant temperature room and are periodically tested for internal pressure. For pressure measurement, the VIPs are placed in a vacuum chamber and the chamber pressure is lowered until the barrier film relaxes (based on visual examination) as the pressures inside and outside the panels equilibrate. This method has a low-pressure detection limit of 2 mbar and an accuracy of  $\pm 0.5$  mbar. Due to the high stiffness of the Al foil film, those VIPs could not be accurately measured by this method and their testing was discontinued.



**Fig 3:** Aging results of VIPs with EvOH and mPET1 films and getters.

Fig. 3 shows the pressure measurements of EvOH and mPET1 VIPs over time. The first set of measurements were performed after about 30 days of preparing the VIPs. The internal pressure of VIPs is known to increase during the first several days after production due to several reasons related to the sealing methods used and also due to desorption of water vapor from the core and barrier films. PET films are known for such desorption, which might

explain the relatively higher pressure of the mPET VIPs compared to EvOH VIPs. During the first 150 days of measurements, the EvOH VIPs showed a constant rise in internal pressure. Conversely, the mPET VIPs showed a general reduction in pressure during the same time period. The water vapor getter (CaO) appeared to have a beneficial impact on all VIPs during the initial measurement period by absorbing the residual and/or desorbed water vapor from the VIP core and barrier films. After 150 days, during autumn and winter periods in Albuquerque when the ambient RH is low, the pressure within all VIPs was observed to decrease. NanoPore has previously observed similar seasonal behavior; when the ambient RH is low, water vapor will diffuse out of VIPs and will diffuse back in during high RH times.

**CHARACTERIZATION OF THERMAL BRIDGING:** In addition to the aging studies, the impact of the different barrier films on the edge-effects of the VIPs was also investigated. Each composite contained four 11"×11"×1" VIPs sandwiched by 1.3 cm HD PIR and 1.3 cm PIR boards. The composites contained VIPs separated by a PIR foam strip in one direction and the VIPs adjacent to each other in the other direction. The composite samples were tested in a multi-transducer HFM that can map the heat flow distribution across non-homogeneous samples. Fig. 4 shows the heat flow measurements from a set of composite samples with configuration 2. The results show that the edge effects due to EvOH and mPET films were similar, but the Al foil film allowed twice or more heat flows around the VIP edges.

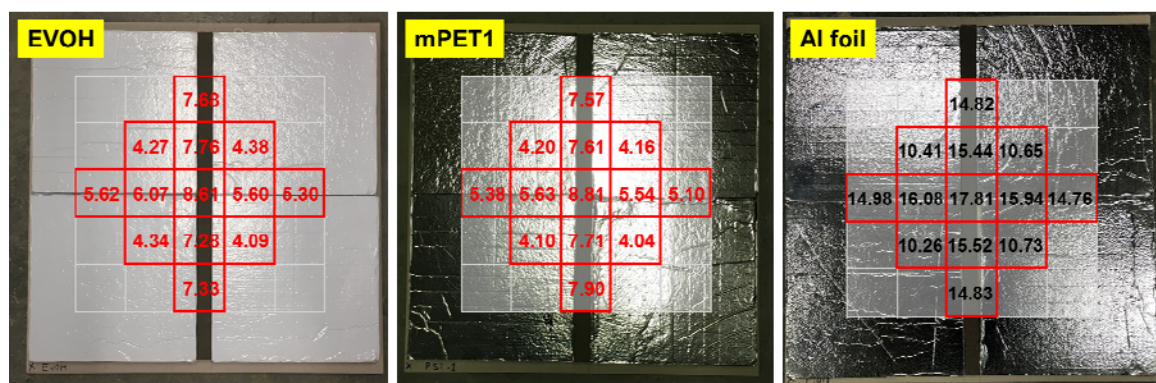


**Fig 4:** Heat flow measurements (in W/m<sup>2</sup>) of small-scale composites.

**CONCLUSIONS:** Aging studies indicated some degradation in long-term performance of VIPs with EvOH films. Thermal characterization indicated that the edge effects due to EvOH and mPET films were similar and much lower than the Al foil film. Thus, mPET films are promising alternatives if the long-term performance of the EvOH film is not adequate.

**ACKNOWLEDGEMENT:** This work was supported by the Building Technologies Office of the U. S. Department of Energy (DOE) under Contract No. DE-AC05-00OR22725 with UT-Battelle, LLC. The authors acknowledge the funding support from Mr. Sven Mumme of the U.S. DOE. Thanks are due to Dr. John Letts, Dr. Jennifer Yao and Mr. Randy Strauser of Firestone Building Products and Mr. Jerald Atchley and Mr. Anthony Gehl of ORNL.

## REFERENCES

1. Biswas, K. et al. (2018). Development and thermal performance verification of composite insulation boards containing foam-encapsulated vacuum insulation panels. *Applied Energy*, 228, 1159-1172.
2. ASTM C518-17, Standard Test Method for Steady-State Thermal Transmission Properties by Means of the Heat Flow Meter Apparatus, ASTM International, West Conshohocken, PA, 2017, [www.astm.org](http://www.astm.org)

## Structural characterization of nanostructured silica ageing: Imaging and analysing particles and pores from a few nanometres up to 100nm

Bruno Chal<sup>1,3\*</sup>, Bernard Yrieix<sup>2,3</sup>, Lucian Roiban<sup>1,3</sup>, Karine Masenelli-Varlot<sup>1,3</sup>, Guilhem Baeza<sup>1,3</sup> and Geneviève Foray<sup>1,3\*</sup>

<sup>1</sup>Univ Lyon, INSA-Lyon, UCBL, MATEIS UMR CNRS 5510, 20 Avenue Albert Einstein, 69621 Villeurbanne Cedex, France

<sup>2</sup>EDF R&D, MMC, Avenue des Renardières –Ecuelles -77818 MORET SUR LOING Cedex, France

<sup>3</sup>Univ Lyon, INSA-Lyon, UCBL, MATeB CNRS UMR5510, F-69621, France

\*[bruno.chal@insa-lyon.fr](mailto:bruno.chal@insa-lyon.fr) ; \*[genevieve.foray@insa-lyon.fr](mailto:genevieve.foray@insa-lyon.fr)

### ABSTRACT

Assessing the durability of super-insulation products is a key step before they can become widespread in the building market. Understanding ageing mechanisms of silica (powders-VIP or aerogels-SIAP) when exposed to temperature and moisture is compulsory to both optimize the synthesis and enlarge applications for these high-end products. Our study includes a large panel of commercial silica (powder, aerogel) which differ by their chemistry (precipitated: hydrophilic SiOH, fumed: rather hydrophobized (SiOSi and SiOH) and intentionally hydrophobized (SiR)) and their structural properties (particles size, specific surface area). These samples are aged for various time in climatic chambers, and then characterized using a wide range of techniques, including gas sorption (N<sub>2</sub>, H<sub>2</sub>O, Ar), FTIR, TGA, TEM and electron tomography, Small Angles Scattering, isostatic (Hg porosimeter) and oedometric compression, thermal measurements. Results obtained allow a discussion on the ageing mechanisms and scenario according to the type of silica. As example, mechanisms such as hydrolysis/condensation at the surface and precipitation/deposition are discussed. They result in changes in the surface hydrophilicity, a decrease in the SSA, a shift of the pore size distribution (loss of the smallest pores), a stiffening of the silica backbone. These evolutions are now imaged (electron tomography) and quantified while ageing.

### KEYWORDS

Ageing, Silica, Mechanisms, Tomography, Small Angles Scattering.

### INTRODUCTION

Reaching the objectives assessed by COP 21 (2015), and even more following the recent recommendations to policymakers given by IPCC, implies to lower the emission of greenhouse quickly. In this perspective, energy saving is part of the equation. New buildings will have to be, at least, low energy ones, and if possible positive energy buildings. However, there is still an important work to do on actual residential buildings. Retrofitting sometimes needs specific solutions due to space hindrance or the impossibility to impair the facade (heritage buildings as example). Superinsulation materials (SIM), with low thermal conductivities are complementary to traditional insulation materials. Understanding and assessing their ageing is a key step to ensure their stability and promote their efficiency. It implies to consider the building scale, the composite scale and the core material. At the material scale, VIP ageing implies both the envelope (Dubelley *et al.* 2017) and the silica used as core material, whereas regarding SIAP

(window-glazing systems, blankets, renders...) only silica aerogels are concerned. This work takes place at this scale, and englobes both silica powders (precipitated, pyrogenic with or without hydrophobic functions) and aerogels, also concerned by ageing even though they include hydrophobic functions on the surface (Chal *et al.* 2018). Rather than having a comparison between different solutions or producers, the aim of this work is to highlight how the nanostructured silica evolves due to an exposition to temperature and moisture. Some mechanisms were already discussed during the last IVIS symposium at Paris (2017) (B. Chal *et al.* 2017) and recently published (Chal *et al.* 2019). They imply chemical and structural modifications along with ageing, the type and intensity of which depends on the nature of the silica. This work offers a specific focus on the structural evolution, probed by different methods including Small Angles Scattering, TEM, electron tomography and mercury porosimetry.

## METHODS

A wide range of commercial products, including silica powders (precipitated, pyrogenic) and silica aerogels (grains, blankets), was part of this study. Samples were aged by the means of climatic chambers, where the temperature and the relative humidity are precisely monitored. Several couples of condition have been used with temperature from 23 to 70°C, and relative humidity going from 0 to 90 %. Some treatments are accelerated ageing, but in a scale that can be encountered, more or less punctually (depending on the application and the location), by the SIM during its service life. Duration spans from 24 days to more than a year. Nitrogen sorptions were performed as routine characterisation, allowing to extract inform about the specific surface area (BET method) and the pore size distribution (BJH method). The aim of the work exposed in this paper is too depend understanding on structural evolutions by the mean of refined tools such as Small Angles Neutrons Scattering (SANS) and electron tomography.

SANS characterisation were performed on the PA20 instrument, at CEA Saclay, France (research reactor Orphée). Pellets of silica sample were shaped by oedometric compression at a  $1\text{mm.min}^{-1}$  loading rate up to 0.6 MPa (Zwick Roell press), following a protocol described in a previous paper (Benane 2019). As aerogels are complicated to shape in pellets, they were placed between two Kapton films instead. Three configurations were used (sample detector distance and wavelength: 1.5 m/15 Å; 8 m/6 Å; 1.5 m/4 Å), allowing the completion of data from  $8.10^{-3}\text{ nm}^{-1}$  to  $4\text{ nm}^{-1}$  (scattering vector  $q$ ). Data were corrected to subtract the incoherent diffusion inherent to the protons in SANS.

Electron tomography and TEM were performed with the ETEM TITAN from FEI, accessible via the CLYM (Lyon/Saint-Etienne consortium of microscopy). This TEM is equipped with a OneView camera (4k\*4k) from Gatan. Samples were prepared using a “dry” protocol to avoid specimen damage. The silica was disposed on a perforated carbon film copper grid with a “300 mesh” (TEM) or “200 mesh” (tomography – with gold nanoparticles (5 nm diameter) deposited previously as fiducial markers). A single-tilt sample holder was used for the tomography. Images were acquired from  $-72^\circ$  to  $72^\circ$  with  $2^\circ$  angle step. The typical pixel size is 0.2 nm. Silica materials are highly sensitive to the electron beam. Therefore, low dose strategies are required to perform the acquisition. First, it implies to use minimum illumination (typically  $10\text{ é.Å}^{-2}.\text{s}^{-1}$  or less). Then, it is necessary to work quickly which is done by using the so-called fast-tomography technique, developed at MATEIS laboratory. With this approach, all the angles (75 images) could be acquired in 2 minutes, lowering the global exposition to less than  $1500\text{ é.Å}^{-2}$ . Irradiation test were previously performed to determine the critical dose and ensure that the sample is neither transformed nor not damaged during the acquisition.

Finally, mercury porosimetry is also a complementary tool to probe the porosity and mechanical behaviour on these highly porous and fragile materials (isostatic compression). These measurements were performed at MATEIS laboratory (Lyon, France), using the AUTOPORE IV 9500 instrument by Micrometrics Instrument Corporation. A powder cell equipped with a



1.131 cm<sup>3</sup> capillary and a 5.913 cm<sup>3</sup> cell volume was used. Samples mass are from 50 to 100 mg depending on the porosity (aerogel or silica powder). Pressure were applied from 3.5 kPa to 408 MPa.

## RESULTS

Several mechanisms are occurring during the application of isostatic compression on highly porous materials. The first one is an unusual regime where the structure is deformed (buckling and/or bending of the pillars/walls) which correspond to a loss of volume without mercury intrusion. One may notes that Washburn formula does not applied to this specific regime. Then, if the residual material is stiff enough, a second regime starts at higher pressure. The shift between the two regimes is often observed by a change of dynamic in the log/log curve (Volume occupied by the mercury VS Pressure). The second region is governed by a rather usual intrusion phenomenon where classical Washburn equation applies. It should be keep in mind that the pores seen in this regime are the consequences of what happened to the material during the first one. Therefore, it includes both the smallest pores pre-existing in the initial material, and those generated by the compression of the larger ones. Most of highly porous aerogels only exhibit the first regime, without intrusion. In this study, our main interest on silica powders is to follow the smallest pore size that can be probe by this technique. This pore size is associated to the neck in-between primary particles. Example of data obtained on unaged and aged silica powders are shown in figure 1.

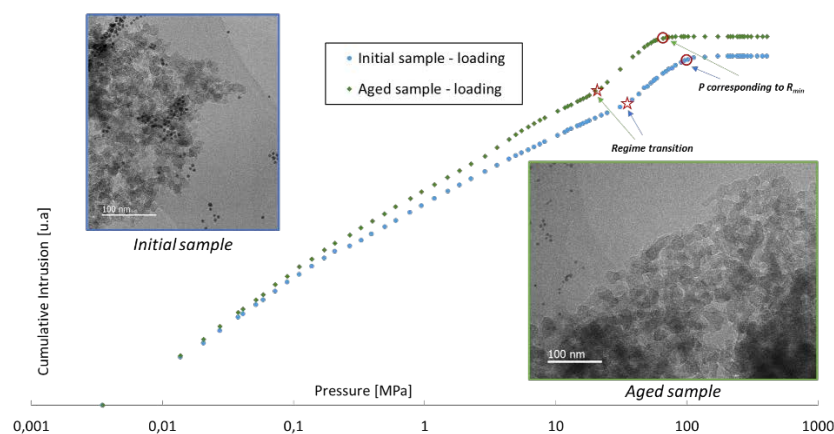


Figure 1. Porosimeter curves and TEM microographies on unaged and aged precipitated silica

The particle size is tracked directly by TEM. So is the pore size, especially regarding aerogels for which the distribution is sharper than silica powders. TEM microographies are depicted in Figure 1 (*black dots are gold particles*). Depending of the initial size, aged silica tends to have higher particle size and larger neck, leading to more elongated primary particles. Electron tomography allows the observation, in three dimensions, of the global architecture, inaccessible with TEM microographies. However, one should keep in mind that TEM is a local technique thus that depends on the object probed. TEM and electron tomography highlight that those commercial products have a dispersion at the primary particle size, both in term of size and shape. To ensure results acquired on TEM and electron tomography, we performed SANS measurements with calibration allowing retrieving the absolute intensity. This technique allows to determine a surface/volume ratio and to estimate a statistical primary particle size, which is in good agreement with TEM observation. This is done using the Porod law and an assumption regarding the shape of the object probed (spherical). SANS also informs on the surface fractal dimension, thus the roughness. However, in the presence a structure factor, which is the case when the object are not dispersed, it is not possible to retrieve a volume fractal dimension corresponding to the aggregates/agglomerates, even though it is often done in the literature.

## DISCUSSIONS

The mercury porosimetry confirms that the smallest pores are closed during the ageing, as already foreseen by sorption measurements (BJH – Chal *et al.* 2019). This observation, along with the increase in particle size (TEM, SANS) and neck enlargement due to ageing is coherent with the loss of specific surface area (BET– Chal *et al.* 2019) already reported on those materials, and going up to a 60 % reduction after 96 days of ageing at 70°C/90%HR. In the meantime, experiments performed with mercury porosimeter also highlight the structure stiffening, which corresponds to a transition between the two regimes at lower pressure for the aged sample. The porosity determined thanks to the electron tomography tends to be lower for aged silica, when comparing objects of similar size (from two to a few hundreds of nanometres). This result is in good agreement with the densification observed at the aggregate size thanks to SANS measurements.

Therefore, additional tools used in this work give a clearer view of the evolution occurring at the particle size during ageing of nanostructured silica. They confirm the mechanism by which the matter is displaced from the hump regions to the neck ones, leading to the loss of the smallest pores, the lowering of the specific surface area and the increase of the statistical particle size.

## CONCLUSIONS

Small angles scattering techniques are rather unusual on amorphous silica, which are dispersed in size and shape. However, this technique succeeds to probe the primary particle size and evolution occurring at the aggregate scale. One of main advantages is that it probes a rather large amount of material. This tool is complementary with electron tomography, which allows the acquisition of an object including several aggregates (agglomerate scale). However, we would like to draw the attention on the fact that silica materials are very sensitive to the electron beam (which also includes SEM) and that micrographies of damaged materials are meaningless. Cautions in the analysis also apply when it comes to mercury porosimeter on these highly porous and fragile materials. The intensity and type of structural evolution depicted in this paper depends on the surface chemistry. As the silica backbone and porosity evolve, so are the skeletal and gaseous conductivities. Additional contributions may also come from physisorbed water.

## ACKNOWLEDGEMENT

The authors would like to gratefully acknowledge funding from ADEME grant 1604C0019.

## REFERENCES

- B. Benane, GP. Baeza, B. Chal, L. Roiban, S. Meille, C. Olagnon, B. Yrieix, G. Foray. 2019. Multiscale structure of super insulation nano-fumed silicas studied by SAXS, tomography and porosimetry. 168. 401-410.
- B.Chal, B. Yrieix, G. Foray, L. Roiban, J-M Chenal, K. Masenelli-Varlot. 2017. Superinsulation material ageing, characterized by combined sorption analysis and thermal measurements. In: *Proceedings of the 13th International Vacuum Insulation Symposium (IVIS 2017)*, Paris, France, September 20–21, 2017
- B. Chal, G. Foray, B. Yrieix, K. Masenelli-Varlot, L. Roiban, J-M Chenal. 2018. Durability of silica aerogels dedicated to superinsulation measured under hygrothermal conditions, *Microporous and Mesoporous Materials*, 272, 61-69
- B. Chal, B. Yrieix, L. Roiban, K. Masenelli-Varlot, J-M Chenal, G. Foray. 2019. Nanostructured silica used in super-insulation materials (SIM), hygrothermal ageing followed by sorption characterizations. 2019, *Energy and Buildings*, 183, 626-638.
- F. Dubelley, E. Planes, C. Bas, E. Pons, B. Yrieix, L. Flandin. 2017. The hygrothermal degradation of PET in laminated multilayer, *European Polymer Journal*, 87, 1-13.

## **Utilization of the vacuum insulation panels in a factory and comparison of long term performance measurement using micro-pressure sensor and prediction value**

Hideya Yamamoto<sup>1,2\*</sup>, Daisuke Ogura<sup>2</sup>

<sup>1</sup>Asahi Fiber Glass Co., Ltd., Kanagawa, Japan

<sup>2</sup>Kyoto University, Kyoto, Japan

\*Corresponding e-mail: [h-yamamoto@afgc.co.jp](mailto:h-yamamoto@afgc.co.jp)

### **ABSTRACT**

Vacuum insulation panels (VIPs) are high-performance heat insulation materials that improve the energy efficiency of various products, including refrigerators, vending machines, and cooler boxes. Glass fiber or fumed silica is covered by a laminated film that forms the core material of the VIP and creates vacuum, making it possible to reduce the gas thermal conductivity to approximately zero and exhibit high thermal performance. There has been recent progress in the application of VIPs to building or housing structures; however, the difficulty lies in accurately predicting its long-term performance. The objective of this research is to clarify the long-term performance of VIPs exposed to the actual environment as well as the environmental conditions surrounding the VIPs constructed on a factory wall. We acquired internal temperature, humidity and pressure measurements using a thermohygrometer and micro-pressure sensor, which were employed to confirm the temperature dependence of the VIP gas permeation at the laboratory scale, and then predicted the long-term VIP performance in the building environment. We also prepared a replaceable VIP and measured the thermal conductivity every three months.

### **KEYWORDS**

Vacuum insulation panel, Long-term performance, Glass fiber, Building scale, Sensor

### **INTRODUCTION**

The insulation performance of porous structures under vacuum conditions has been thoroughly investigated, and its mechanism and physical properties have been clarified [1]. Furthermore, the market of vacuum insulation panels (VIPs) has been gradually expanding since 2000 because of the development of the core materials and barrier films. The VIP core comprises either a glass fiber or fumed silica core. A glass fiber core is primarily used in most of the VIP markets in Japan because of its high insulation performance with internal pressure less than 10 Pa and low cost. This high insulation performance of glass fiber core VIPs denotes the potential of reducing the wall thickness and enhancing the energy savings when they are used in building applications. However, even though many studies have discussed the long-term performance of VIPs in a constant environment, the long-term performance of the VIP itself has not been measured in a building environment. This lack of actual measurement data indicates that the accuracy of the long-term performance predictions in building environments cannot be confirmed. Furthermore, most of these studies focused on fumed silica core VIPs, with only a few studies investigating the glass fiber core VIPs [2-5]. There have also been no reports of cases in which many VIPs were used in building insulation.

The objective of this research was to evaluate the factory environment, where VIPs were installed inside the outer factory wall, as well as to measure and predict the long-term VIP performance. The micro-pressure sensor was inserted inside the VIPs to directly measure the thermal performance of the on-site VIPs by enabling continuous internal pressure

measurements via non-contact power supply technology. Further, the Arrhenius equation in terms of gas permeation was used to predict the long-term VIP performance, where the gas permeation dependence in a constant environment was considered to be the reciprocal of temperature. The internal pressure changes of the VIP were subsequently calculated via the Arrhenius equation and compared with the output values obtained from the pressure sensors.

## METHODS

### Factory details and insulation structure

This building is located at an altitude of 158 m in west Japan. The surrounding climate is classified as a humid subtropical climate. The VIPs were installed on the interior side of the outer wall of the area painted in red (Figs. 1 and 2). The VIP installation area covered ~81% of the outer wall on the south side. There were almost no thermal bridges, with the exception of steel frames, because there were no windows. Polyurethane foam (~15 mm thickness) was applied to the VIP surface. Furthermore, the thermal bridge of the steel frame was thermally insulated using polyurethane foam.

### VIP details and micro-pressure sensor

The VIP composition is presented in Table 2. The VIPs that contained the micro-pressure sensors (Fig. 3) were located to the southwest and southeast of the factory wall. The sensors were located 1.5 m from the ground in the south and ~10 m from the ground in the southeast. Each sensor contained a thermohygrometer and pressure sensors. It stored electricity in a small battery via a non-contact power supply, and the data were wirelessly transmitted to a computer. Further, the relation between the pressure sensor output and ambient pressure is shown in Fig. 4, with the approximate expression provided as equation 1.

$$AD_{tot} = AD_{atm} + \frac{AD_{vac}}{1 + \frac{P_a}{P_{1/2}}} \quad (1)$$

### Environmental measurement

A thermohygrometer (Z2010, HIOKI) and heat flow meter (Energy Eye, DENSO) were installed in the front and back of the VIP in each direction at a wall height of 1–2 m to measure the environmental conditions around the VIP. A thin-film sensor (SHT35, Sensirion) with a thickness of ~1 mm was used between the outer wall and VIP to avoid creating a structural problem by the creation of a space between the outer wall and VIP.

## RESULTS AND DISCUSSION

The VIP measurement results on the south side of factory 2 are depicted in Fig. 6. We predicted the long-term VIP performance up to December 2018 using the temperature dependence of the gas permeation of this VIP (Arrhenius plot). Furthermore, the micro-pressure sensor output values were converted to thermal conductivity via Equations 1 and 2 and compared with the predicted values.

$$\lambda_{cop} = \lambda_{int,sr} + \frac{\lambda_{ga,0}}{1 + \frac{P_{1/2}}{P_a}} \quad (2)$$

The results of the environmental conditions surrounding the VIPs that were used for performing the prediction are summarized in Fig. 7 and Table 3. There was a temperature difference of up to 23 °C between the front and back of the VIP. The maximum temperature differed by 16 °C, and it was difficult to compare the minimum temperatures because of the lack of data. A comparison of the sensor output values with aluminum foil VIP and the calculated values is presented in Fig. 6. The measurement results are in good agreement with the calculated results obtained based on the fact that the film's edge of VIP was constructed to face the outer wall side.



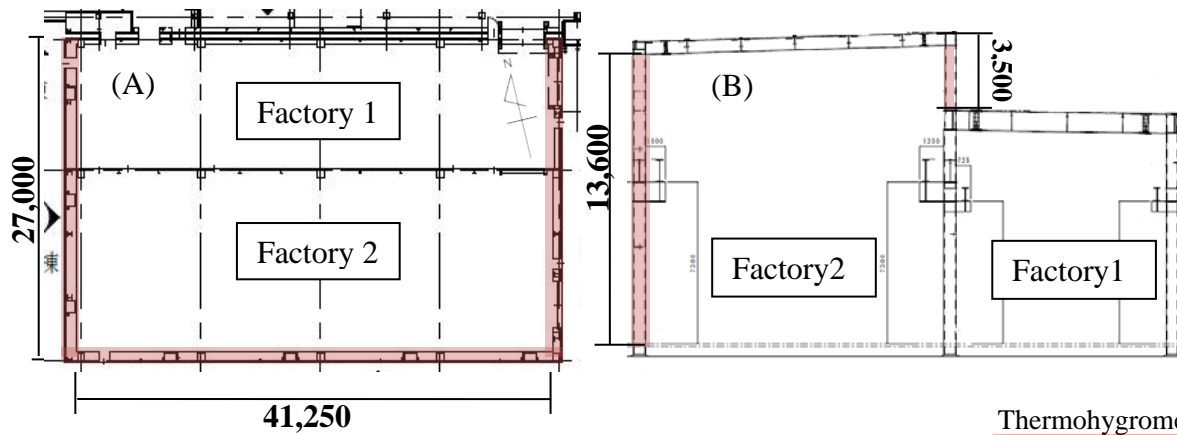


Fig. 1. Top view (A) and north-south sectional view (B) of the factories.



Fig. 2. Wall cross-section. Fig. 3. Factory wall after VIP construction (south side).

Fig. 4. Micro-pressure sensor, thermohygrometer, and heat flow meter placement in the VIP.

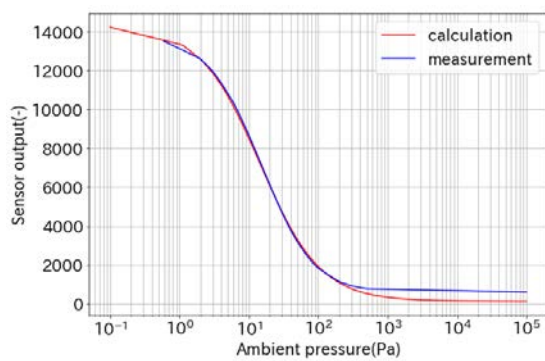


Fig. 5. Relation between the sensor output and ambient pressure. (Left)

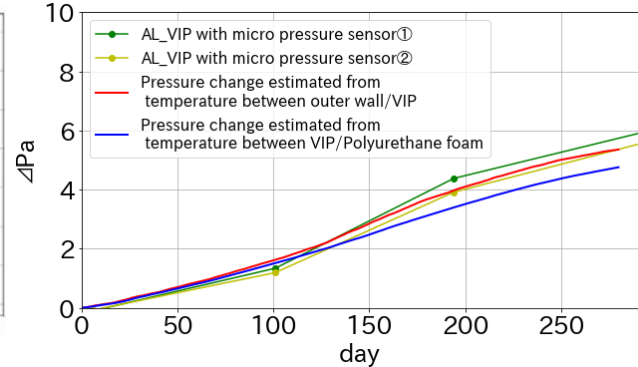


Fig. 6. Long-term performance of VIP with a micro-pressure sensor. (Right)

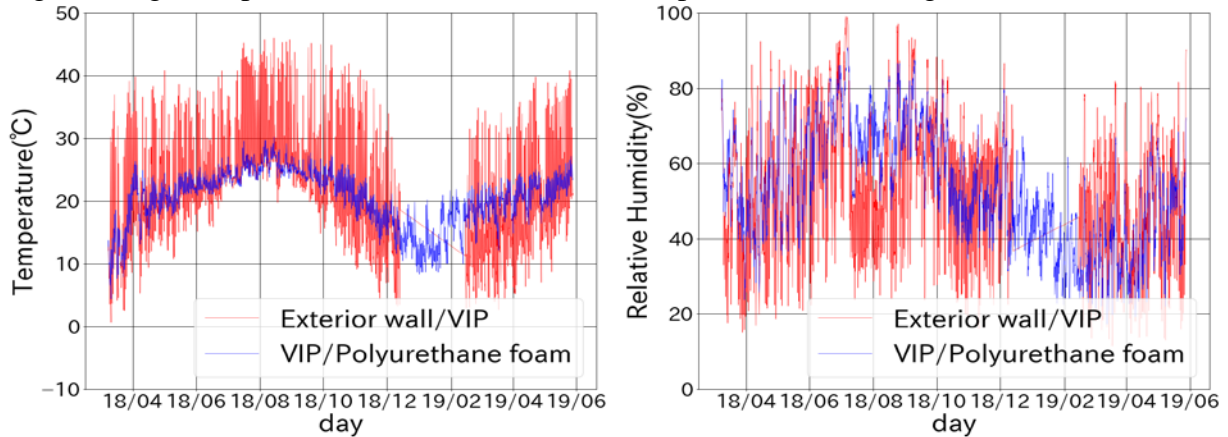


Fig. 7. Temperature and humidity measurements at the front and back of the VIP in the southern wall.

Table 1: Thermal properties of the insulation used in this factory (Fig. 2).

No	Insulation	Thermal Conductivity (mW/mK)	R value (m <sup>2</sup> K/W)
1	Exterior wall	20	1.75
2	VIP	2.5 <sup>*1</sup>	2.4 <sup>*1</sup>
3	Polyurethane foam	38	0.39

\*1:  $\lambda$  cop (center of panel)

Table 2: Specifications of the VIP.

	Factory 1	Factory 2
VIP size	6 × 445 × 875 mm	
Desiccant/Getter	Calcium Oxide 10 g/ Zeolite 5 g	
Film*1	AL foil Type, Hybrid Type	
Micro-pressure Sensor	-	Inserted for 6 panels

\*1: Edge of VIP' film is facing outer wall side

Table 3: Temperature and humidity measurement results at the front and back of the VIP in the southern wall (every 2 h from January 4, 2018, to May 28, 2019).

	Average Temp (°C)	Max Temp (°C)	Min Temp (°C)	Average RH (%)	Max RH (%)	Min RH (%)
Outer wall/VIP <sup>*1</sup>	20.5	46.0	2.6	57.6	99.0	16.0
VIP/Polyurethane foam	20.6	30.2	8.3	53.1	90.9	17.2

\*1: It could not be measured from December 13, 2018, to February 14, 2019, because of the malfunctioning measuring instrument.

## CONCLUSIONS

We measured the environmental conditions of the VIPs installed inside the outer factory wall and the internal pressure of the VIPs using micro-pressure sensors. The output value of the sensor is considered to have sufficient accuracy in the pressure at the life of glass wool VIP. The predicted value calculated by the Arrhenius equation for the aluminum foil VIP and the sensor output value were almost the same considering the edge direction. Based on this result, we will calculate the internal pressure by separating the edge and surface gas permeation in Hybrid VIP. Our future work will include a comparison of the indoor temperature and relative humidity measurements to determine the amount of improvement in the thermal environment of the factory due to the installation of VIPs.

## REFERENCES

- [1] M.G.Kaganer Thermal insulation in cryogenic engineering (1969)
- [2] S.Brunner, H.Simmler, In situ performance assessment of vacuum insulation panels in a flat roof construction (2007)
- [3] P.Mukhopadhyaya, D.Maclean, J.Korn, D.van Reenen, S.Molleti, Building application and thermal performance of vacuum insulation panels (VIPs) in Canadian subarctic climate (2014)
- [4] P.Johansson, B.Adl-Zarrabi, A.S.Kalagasidis, Evaluation of 5 years' performance of VIPs in a retrofitted building facade (2015)
- [5] D.Maclean, P.Mukhopadhyaya, J.Korn, S.Mooney, Design details and long-term performance of VIPs in Canada's North (2016)

## Symbols

$AD_{tot}$ : sensor output [-];  $AD_{vac}$ : sensor output under vacuum conditions [-];  $AD_{atm}$ : sensor output at atmospheric pressure [-];  $P_a$ : ambient pressure [Pa];  $P_{1/2}$ : fitting pressure [Pa];  $\lambda_{cop}$ : thermal conductivity at the center of the panel [mW/mK];  $\lambda_{ini,sr}$ : initial thermal conductivity [mW/mK];  $\lambda_{ga,0}$ : gaseous thermal conductivity [mW/mK]

## **Aging (2011-2019) of Glass Fiber Core VIPs in Arctic Canadian Climate**

Vivian Chan<sup>1</sup>, Phalguni Mukhopadhyaya<sup>1,\*</sup>, Matthew D. Ooms<sup>2</sup>, Juergen Korn<sup>3</sup>, Douglas MacLean<sup>4</sup>, Stephen Mooney<sup>5</sup> and Shane Andre<sup>2</sup>

<sup>1</sup>University of Victoria, Victoria, BC, Canada

<sup>2</sup>Yukon Energy Mines and Resources, Whitehorse, YT, Canada

<sup>3</sup>Yukon Housing Corporation, Whitehorse, YT, Canada

<sup>4</sup>Retired, Yukon Energy Mines and Resources, Whitehorse, YT, Canada

<sup>5</sup>Yukon Research Centre, Whitehorse, YT, Canada

*\*Corresponding e-mail: phalguni@uvic.ca*

### **ABSTRACT**

The uncertainty regarding long-term thermal performance is one of the key barriers which is preventing mass application of vacuum insulation panels (VIPs) in building envelope construction. Numerical modelling, laboratory studies, and field investigations are being conducted by researchers across the world to address this issue. However, a definite answer or a validated procedure to predict the long-term performance of VIPs has yet to be formalized. Lack of closely monitored and reliable long-term field performance data is a major impediment. This paper presents observations from a unique Canadian subarctic field investigation over a period of 9 years where glass fiber core VIPs were used in a building envelope retrofit project. The broad objective of this study is to demonstrate long-term field thermal performance of VIPs in an extreme cold climate. The unique thermal performance data available from field testing (2011-2019) and the accelerated aging results show a significant relationship. There is value in continuing this unique study to further validate this relationship.

### **KEYWORDS**

Vacuum Insulation Panel (VIP), Aging, Glass Fiber Core, Arctic Climate, Retrofit

### **INTRODUCTION**

Glass fiber core vacuum insulation panels (VIPs) can achieve an initial thermal conductivity as low as 0.002 W/m·K, which is among the lowest of all core materials (MacLean et al., 2011). While they have been widely used in aerospace and refrigeration applications, their long-term performance in building construction, which requires a service life of 25 to 50 years, is still questionable. The application of VIPs in building retrofits, particularly in the extreme cold climate of Canada, is an attractive option. In 2011, an existing wall of a commercial building in Whitehorse, Yukon, known for its subarctic climate, was retrofitted with glass fiber core VIPs. Since then, the performance of VIPs in this retrofitted wall assembly has been reported in a number of publications (MacLean et al., 2011; Mukhopadhyaya et al., 2011, 2013, 2014, 2017; MacLean et al., 2017; Chan et al. 2019). This paper presents the most recent field performance observations (until the Winter of 2019) and a critical analysis of the recorded data.

### **METHODS**

In 2011, a concrete block wall (8.4 x 3.7 m<sup>2</sup>) of an existing commercial building in Whitehorse, Yukon was retrofitted with a composite insulation system that consists of VIPs sandwiched between layers of extruded polystyrene foam (XPS). The size of VIPs used were 560 x 460 x 12 mm. The thermal conductivity of the VIPs before construction was found to be 0.0034

W/m·K at the center of the panel using a 600 x 600 mm heat flow meter apparatus with 300 x 300 mm heat flow sensor and an accuracy of  $\pm 2\%$  (Mukhopadhyaya et al., 2014).

The existing concrete block wall was insulated with fiberglass batts, and the thermal resistance of this wall was about  $3.5 \text{ m}^2\cdot\text{K/W}$ . The retrofitting goal was to increase the wall's thermal resistance to  $8.8\text{--}10.6 \text{ m}^2\cdot\text{K/W}$  (Mukhopadhyaya et al., 2014). As shown in Figure 1, first a 0.15 mm polyethylene air vapor barrier was installed over the existing concrete block wall. 25 mm XPS was glued to the polyethylene to provide a smooth surface on which to mount the VIPs. The VIPs were then mounted between horizontal strapping. The VIPs were covered with 6 mm flexible foam material to protect them. 25 mm polystyrene board was placed on the outside of the foam layer to prevent condensation on the VIPs, and to protect them from mechanical damage during and after construction. Steel siding was installed as the exterior finish.

The thermal performance of each additional insulation layer was continuously monitored from the start of the project. Temperature sensors were installed at the interface of each insulation layer. The temperature sensors were located approximately 2 m from the south edge of wall and 1 m down from the top of the wall (Mukhopadhyaya et al., 2014). Three additional temperature sensors were installed on the existing concrete wall to monitor the temperature gradient from the top to the bottom of the wall. These sensors were at about 2 m from the north edge of the wall and were located about 1, 1.5, and 3 m from the top of the wall (Mukhopadhyaya et al., 2014).

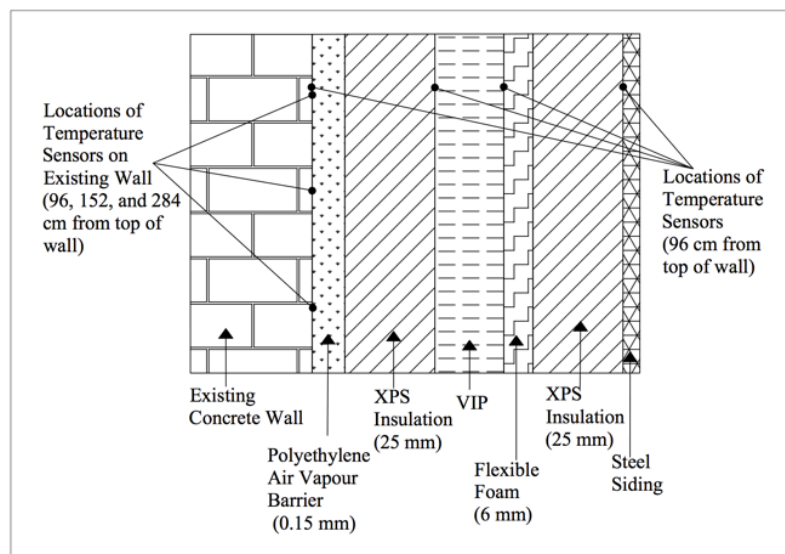


Figure 1. Schematic diagram of the retrofitted wall cross-section starting from cladding onwards and the locations of the temperature sensors. This drawing is not to scale.

## RESULTS AND DISCUSSION

The temperature recordings at the interface of every insulation layer were collected from 2011 to 2019. The temperature drop across each insulation layer (first layer of XPS, VIP, and second layer of XPS) was calculated and expressed as a percentage relative to the composite exterior insulation system (XPS-VIP-XPS) for selected winter months from 2011 to 2017, in the spring of 2018, and in the winter of 2019, as shown in Figure 2.

The average temperature drop is about 66.0% across the VIP layer, and 14.8% and 19.2% across the first and second layer of XPS respectively. The graphical representation in Figure 2 shows

that the thermal performance of the VIP layer is decreasing very slowly, from 69.4% in winter 2011 to 63.1% in winter 2019, at an average rate of about 0.7% per year.

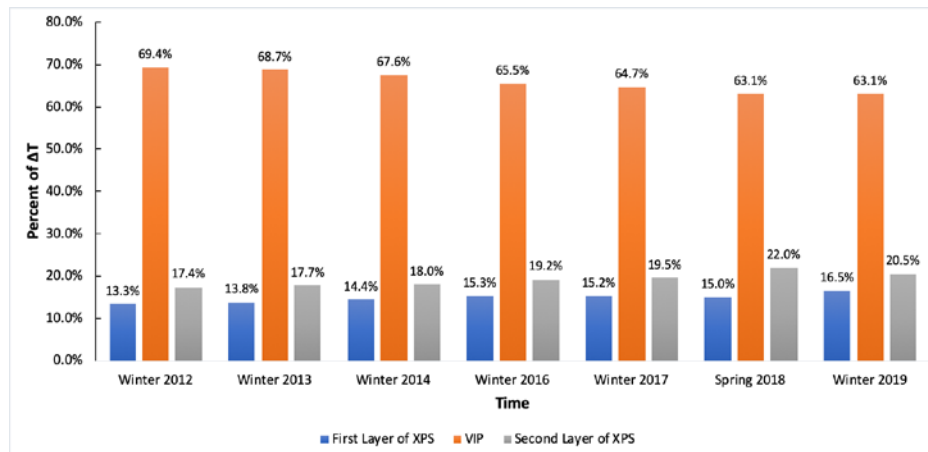


Figure 2. Percentage of temperature drop across wall components, relative to the drop across the entire wall. Data averaged for winter months 2011-2017, spring months of 2018, and winter months of 2019.

Cyclic accelerated aging tests were conducted in a laboratory on glass fiber core VIPs (Mukhopadhyaya et al. 2011). Three VIP specimens were stored under 23°C, 95% RH for a week, then switch to 70°C, 5% RH for the next week, i.e. 2 weeks for 1 cycle (Morlidge, 2012). VIP specimens were subjected to 14 weeks (i.e. 7 cycles) of exposure. The thermal conductivity of the VIPs was measured at the end of each week. The measured thermal resistance values were averaged and expressed as a percentage of initial thermal resistance. The results are plotted in Figure 3 and show a linear trend. The normalized *in situ* VIP aging rate (expressed as a percentage of the initial thermal resistance) is also plotted in Figure 3. The figure shows that the two-year *in situ* aging rate is nearly equal to the 1 cycle (2 weeks) accelerated aging rate. Based on this observation and linear (assumed) extrapolation of the *in situ* data, the thermal conductivity of VIPs is predicted to increase from 0.0034 in 2011 to 0.00429 W/m·K by 2026, or about 21% compared to the initial thermal conductivity.

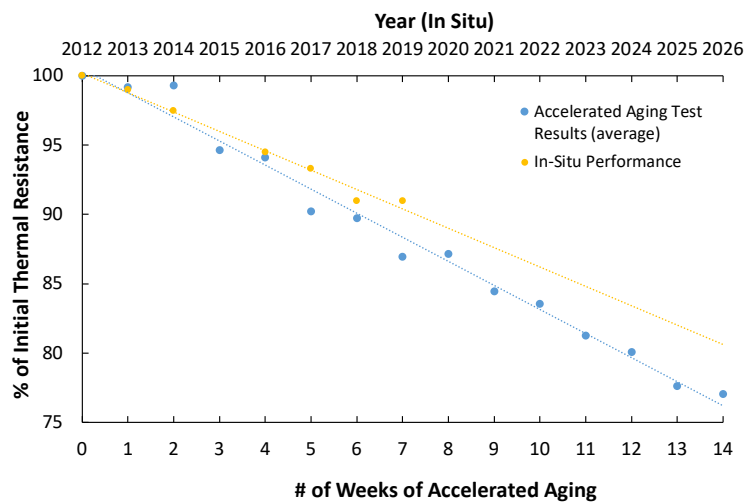


Figure 3. Aging rate of a glass fiber core VIP in terms of its initial thermal resistance as a function of time determined from *in situ* performance and laboratory accelerated aging test results.

## CONCLUSIONS

The results show great promise for the use of a XPS-VIP-XPS composite insulation system in Canada's extreme cold climate. The thermal performance of glass fiber core VIPs changed less than 0.8% per year. The *in situ* aging trend is similar to the accelerated aging test results in a laboratory. Ongoing field monitoring is producing a unique set of test data that is helping and will continue to help researchers to develop a better understanding of the long-term performance of glass fiber core VIPs.

## ACKNOWLEDGEMENT

The authors thank Panasonic Canada Inc. and Panasonic Corporation for supplying the vacuum insulation panels used for this project. The authors gratefully acknowledge the National Research Council Canada (NRCC) for providing technical expertise and financial support. The authors would like to thank Yukon Housing Corporation for providing a wall on one of their buildings for this project, and for providing monitoring equipment and assistance with data collection and handling. Cold Climate Innovation, Yukon Research Centre, Yukon College, and the Energy Solutions Centre must also be credited for providing financial and technical support for this collaborative project.

## REFERENCES

- MacLean, D., Korn, J., Mukhopadhyaya, P. (2011). "Vacuum Insulation Panels (VIPs) Arrive in Northern Canada: Institutional Building Pilot Retrofit in Yukon," in *Proceedings of 10th International Vacuum Insulation Symposium (IVIS-X)* (Ottawa, ON), 10.
- MacLean, D., Mukhopadhyaya, P., Korn, J., Mooney, S. (2017). 'Design details and long-term performance of VIPs in Canada's North', *Energy Procedia*, 111, pp. 481-489.
- Morlidge, M. (2012). Determining the aging performance of vacuum insulation panels: development of a prediction model (*MASc thesis*). Ryerson University, Toronto, ON, Canada.
- Mukhopadhyaya, P., Kumaran M. K., Sherrer G., van Reenen, D. (2011). "An investigation on long-term thermal performance of Vacuum Insulation Panels (VIPs)," in *Proceedings of 10th International Vacuum Insulation Symposium (IVIS-X)* (Ottawa, ON), 10.
- Mukhopadhyaya, P., MacLean, D., Korn, J., van Reenen, D., Molleti, S. (2014). Building application and thermal performance of vacuum insulation panels (VIPs) in Canadian subarctic climate. *Energy Build.* 85, 672–680. doi: 10.1016/j.enbuild.2014.08.038
- Mukhopadhyaya, P., MacLean, D., Korn, J., Mooney, S. (2017). Application of VIPs in Canada's North - Monitoring Results' *ASTM International*, STP1599. West Conshohocken, PA: ASTM International, 122–131.
- Mukhopadhyaya, P., MacLean, D., Korn, J., van Reenen, D., Molleti, S. (2013). "Field application and long-term thermal performance of Vacuum Insulation Panels (VIPs) in Canadian Arctic Climate," in *Proceedings of 11th International Vacuum Insulation Symposium (IVIS-XI)*, 97–98.
- Chan, V.T. T., Ooms, M., Korn, J., MacLean, D., Mooney, S., Andre, S., Mukhopadhyaya, P. (2019). 'Critical Analysis of in situ Performance of Glass Fiber Core VIPs in Extreme Cold Climate' *Frontiers in Energy Research*, May 2019, pp. 1-7. doi: 10.3389/fenrg.2019.00045.

## **The Wall-ACE project: an overview of the in-field monitoring on the novel Aerogel-based products.**

Stefano Fantucci<sup>1</sup>, Elisa Fenoglio<sup>1</sup>, Valentina Serra<sup>1</sup>, Marco Perino<sup>1,\*</sup>, Timea Béjat<sup>2</sup>, Didier Therme<sup>2</sup>, Lori McElroy<sup>3</sup>, Sean Doran<sup>3</sup>, and Jon Hand<sup>3</sup>

<sup>1</sup>Politecnico di Torino - Department of Energy, Torino, Italy

<sup>2</sup>Univ Grenoble Alpes, CEA, LITEN, DTS, LIPV, INES, F-38000 Grenoble, France

<sup>3</sup>Building Research Establishment (BRE) Ltd. UK

*\*Corresponding e-mail: marco.perino@polito.it*

### **ABSTRACT**

The increasing demand for high energy efficient buildings has lead to a growing interest in building envelope solutions characterised by an high level of innovation. The necessity of providing new solutions for the energy retrofit of existing and – especially – old and/or listed buildings is rising great challenges. A promising perspective comes from the implementation of aerogel-based Super Insulating Materials, which can provide added value with respect to current envelope technologies.

In this framework, the EU H2020 research project Wall-ACE aimed at developing a suite of Aerogel-based sustainable insulation solutions for the building market. The five insulation products under development were specifically designed for both the renovation of existing buildings and for the construction of new zero energy buildings. The aim is to achieve for each product a thermal conductivity significantly lower with respect to the state-of-the-art solutions. In this paper, an overview of the research activities which led to the development of these new high insulating products is presented. The products developed were tested through laboratory tests, numerical analysis, small scale and full-scale experimental activities. In this paper, the different large-scale test facilities and the case study buildings selected in different EU countries (Italy, United Kingdom and France) to test the different products developed are showed.

### **KEYWORDS**

Aerogel, thermal insulation, retrofit, plaster, rendering.

### **INTRODUCTION**

The energy saving potential that can be achieved through the building energy retrofit is widely known since about the 80% of the existent stock was built when poor energy saving criteria were in force. To reduce the energy demands related to buildings and to comply with the European target for 2030, innovative insulating materials for the energy retrofit of buildings are needed. The solutions to be developed should carefully consider the number of issues that could be faced during the energy refurbishment, i.e. the use of internal space, historical and technological constraints. So, it is of paramount importance to develop new materials and solutions characterised by very high thermal insulating performance.

The development of aerogel-based super-insulating materials and solutions suitable for new buildings and the energy renovation of existing ones is the aim of the European Horizon 2020 project Wall-ACE. The proposed solutions involve an internal insulating plaster, an internal coating finishing, an external insulating render, an insulating patching filler and aerogel filled bricks; all the solutions developed in the framework of the project are based on the Kwark® aerogel produced by Enersens. The internal plaster and the external render are developed



respectively by Vimark and Quick Mix; these products are suitable for the reduction of the heat losses through the envelope by the application of a few centimetre thick layers. The thermal coating finish, also developed by Vimark, is a product that can be applied in a few millimetres aimed at mitigating the thermal bridge and reduce the mould growth risk. The insulating interior patching filler is developed by Toupret to patch holes, fill cracks and to mitigate the punctual thermal bridges in building elements. Finally, the filled bricks produced by Leipfinger Bader were developed with an optimised geometry to be filled with a high-performance aerogel charged mortar. The goal of the project is to reach a thermal conductivity lower than  $0.03 \text{ W/mK}$  for each material (with the exception of the bricks).

During the first phase of the Wall-ACE project, the development and optimization of the materials were carried on at the laboratory scale; then the products were tested in large-scale laboratory facilities and in-field conditions through the application in different demonstration buildings in Italy, France and United Kingdom. In this paper, an overview of the in-field monitoring activities on the demonstration sites and of the experimental facilities that were adopted to tests the developed products are presented.

## FIELD STUDY

In the following sections, the facilities and the case study building in which the developed materials were tested, divided by country, are presented.

### Italy

The building selected in Italy is located in Turin. It is a 1920' building owned by ATC (Agenzia Territoriale per la Casa del Piemonte Centrale), a social housing organization partner of the project.

The apartment selected is used to measure the thermal performances of the internal plaster and the coating finish applied, respectively, in a thickness of 45 mm and 10 mm. The walls selected for the application of the materials are constituted by a solid brick cavity wall (~52 cm thick). For each aerogel-based material, two walls were selected, one adopted as a reference and the other retrofitted with the developed products. The aim is to compare their thermal resistance and the surface temperature to demonstrate the improvement achieved by the retrofit action.

In addition to the thermal measures, a set of relative humidity sensors were installed to correlate the thermal performance with the hygrometric condition of the aerogel-based materials. Moreover, the RH measurements allowed to identify when the drying process of the products ended, so when it was possible to consider the thermal resistance value reliable.

The monitoring phase on the developed products started in November 2018 and will continue until the end of the project (September 2019).



Figure 1. The Italian case study (ATC building).



## United Kingdom

The approach taken was based on applying the Wall-ACE Insulating Plaster as supplied by project partners Vimark on the inside of an external wall of an apartment at the BRE Innovation Park at Ravenscraig, and adding a layer of insulating coating plaster on the inner side walls to mitigate thermal bridging effects. The plaster was allowed to dry out and afterwards the U-value of the wall was measured (as described below). In a second stage, a building simulation model was developed comparing a base case with uninsulated cavity brick façade and the improved case with the Wall-ACE insulating plaster in place (applied to all of the perimeter walls). The energy demand and occupant thermal comfort were analysed before and after the retrofit.

BRE conducted U-value measurements in an upstairs flat (Flat 'F2'), that is a replica of a typical 1960s four-in-a-block unit, with the Wall-ACE insulating plaster added as a 'retrofit' measure. A first layer of Wall-ACE insulation was applied in September 2018 and a second layer in February 2019. The U-value of the external wall was measured at four positions during March and April 2019. Equipment was installed and heating supplied to the flat, and heat flow and temperatures were monitored at regular intervals.



Figure 2. Case study; the heat flux plates, thermistors and dataloggers recording the readings

## France

Within the WALL-ACE project, several full-scale walls were built at CEA LITEN's INCAS experimental platform in France (Le Bourget du Lac). In FACT (FACade Testing facility) two north facing walls were built on the ground floor (Figure 3). In test cell N°1 an aerogel containing outside render was added to a classic brick wall with a rendering made of plasterboard. In test cell N°2 an aerogel-based thermal plaster was added on the inside surface of a concrete block wall. In a PASSYS test cell, a wall containing all the developed products of the project was installed. The core layer is in aerogel plaster filled bricks, while the outside render was supplied by Quick-Mix and inside thermal coating by Vimark. Some artificial holes were added on the inside to include Toupret's patching filler into this test. Figure 4 presents this installation.

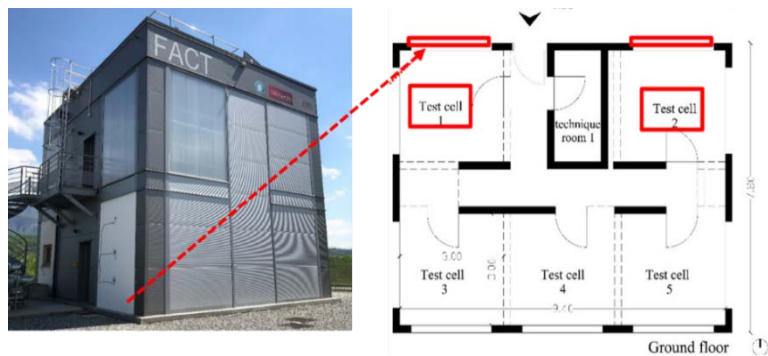


Figure 3. FACT with the two test cells on the North façade



Figure 4. PASSYS test cell installation (all project products)



Figure 5. The French case study (INCAS test houses)

As a demo activity, thermal coating finish was installed in a test room in one of the 4 test houses of INCAS's platform (Figure 5). This house is a recently built high energy performing one, where the test room is compared with a reference room from an environmental quality point of view: thermal comfort and indoor air quality are recorded.

## CONCLUSION

The paper shows the large-scale facilities and the case studies selected and adopted for the in-field measurements of a set of new super insulating materials developed in the framework of a European H2020 project (Wall-ACE). The in-field test of these products allows to define the wall thermal behaviour under different – “real life “ - boundary conditions and when applied to a different substrate. The monitoring results allow comparing the actual performance with the one achieved in the laboratory conditions. Moreover, the monitoring datasets will be used to validate simulation codes used to perform analysis of different scenarios. The measurements in some case study will be performed until the end of the project (September 2019), so a large amount of data will be collected, and a deep analysis of the thermal performance will be possible.

## ACKNOWLEDGEMENT

The research project Wall-ACE has received funding from the EU Horizon 2020 research and innovation programme under the Grant Agreement No. 723574. The authors wish to thank the industrial partner Vimark srl, Quick mix, Toupret, Lepfingerbader and Enersens which have provided/installed the developed materials for the in-field tests.

## REFERENCES

ISTAT 2011, National Census - <http://dati-censimentopopolazione.istat.it/Index.aspx> [last access 04/03/2018]  
Wall-ACE project, <https://www.wall-ace.eu/> [last access 25/06/2019]

## Vacuum Insulation Panels for Fish Box

Sankarshan Verma, Harjit Singh

*Institute of Energy Futures, College of Engineering, Design and Physical Sciences, Brunel University  
London, Uxbridge, UB8 3PH, UK*

### Abstract

Fish is a highly perishable food as it loses quality because of bacterial or enzymatic activity or both with time. The present paper describes a computer model of a fish box, refrigerated with flake ice, developed to study the effect of parameters like fish to ice ratio and box usage time (the time for which the fish remains fresh inside the box) and compare these for two types of insulation i) conventional Expanded Polystyrene ii) Vacuum Insulation Panels. The corresponding economics is also calculated. VIP insulated box, due to the low U-values, could maintain fish to ice ratio of 5 as compared to 3 in EPS boxes, which translates to an added profit of £4 per trip. This could cover the initial cost of VIP insulated box in less than five months.

### Introduction

Increasing popularity of the famous fish dishes like Japanese Sushi and Maldivian Garudiya worldwide has led a rise in demand for the local fresh fish. However, transporting fresh fish is a challenge. Fish is a highly perishable food as it loses quality because of bacterial or enzymatic activity or both with time. The best way to maintain the freshness is by transporting the fish live as the spoilage starts as soon as the fish dies. However, it is difficult to transport live fishes.

Low temperature transportation is a way to increase the shelf life of the harvested fish. According to the ATP treaty on international carriage of perishable foodstuff, the transportation temperature of fresh fish should be as close to 0 °C as possible without freezing the products [1], [2]; the freezing temperature being -1.5 °C to -3 °C for most fish [3]. The harvested fresh fish is usually pre-chilled to about -1 °C using ice or cooled brine and transported to the processing floors, where they are processed (filleting, head removal etc.), packaged and transported further via air, water or road in insulated or refrigerated boxes. Majority of the perishable food, including fish, transported by road or sea face the challenge of lack of refrigeration which accounts for a loss of 20% food worldwide and as high as 9% in developed countries [4]. Also, inadequate handling and processing methods cause loss of nutrients in fish leading to post harvest economic losses [5].

Due to its high latent heat capacity, easy availability and harmless nature, ice, in various forms, is commonly used as a cooling source in the fish box. Chilled Sea Water is extremely efficient cooling medium as it ensures the best contact with the fish but faces temperature stratification over time. Flake ice, which is preferred over block or crushed ice, provides high contact area and prevents temperature stratification.

Recharging the box with ice at regular intervals turns out to be a difficult task because of 'unknown' quantity of ice required or time interval between subsequent rechargings. Also, ice making is an energy intensive process. Burgess et. al. [6] calculated the amount of ice required by correlating the R-value of the box with various box parameters like thickness, and number of layers. Energy balance equation mentioned in [7] can be used to calculate the ice requirements for insulated boxes. However, to determine the effect of factors like dynamic ambient conditions, transient heat transfer coefficients, fish-ice packing and edge effects, finite element thermal modelling provides more reliable results.

Usually fish boxes are insulated with 30-50 mm thick expanded polystyrene (EPS) layers which may or may not be sandwiched between thin plastic sheets. Figure 1 shows typical fish boxes in India for small scale transportation and storage of fish. However, with increased demands due to globalization

and limited transportation capabilities, the storage volume comes at a premium. Vacuum insulation panels (VIPs), due to their super insulating capacity can offer larger fish to ice ratio for the same inner volume of the box, thereby increase revenues by enabling a larger volume of fish transported.

In the present study, a computer model of insulated fish box, refrigerated with flake ice, used to transport fish when subjected to ambient conditions as defined by ISTA 7D [7] has been developed. The effect of different insulation materials, 30 mm thick Expanded Polystyrene and 15 mm thick Vacuum Insulation Panel, on the fish to ice ratio to maintain the average temperature of pre-chilled fish below 0 °C is reported. The corresponding effect on inner volume and the weight of the container is reported.

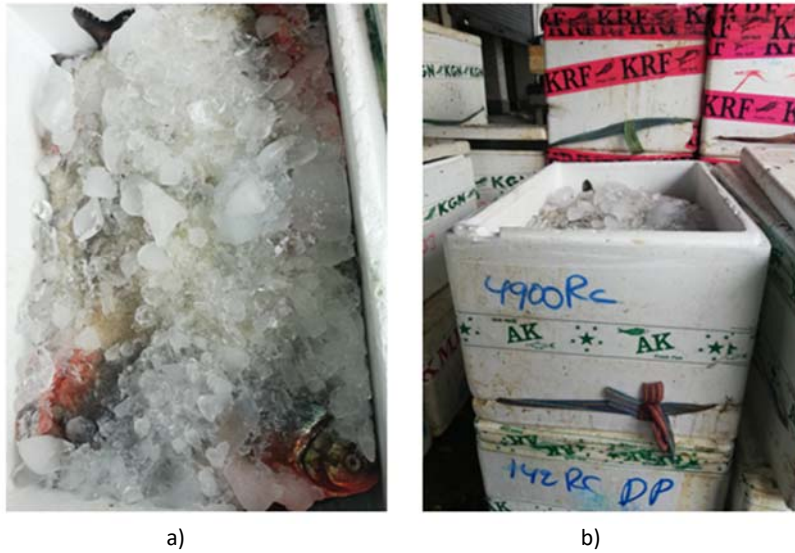


Figure 1 a) Fish preserved inside a fish box with crushed ice b) Fish boxes stored by vendors.

## Methodology

### Geometry

A fully parametric 2-D computer model of a fish box was developed in COMSOL Multiphysics as shown in figure 2. The walls and the lid were modelled as a three phase system consisting of the insulation material sandwiched between an outer and an inner plastic layer. The fish were represented as nine circular entities and the space between the fish was filled with crushed ice. The radius of the fish ( $r$ ) was calculated using the mass ratio of the fish and ice present in the box using equation 1.

$$r = \left( \frac{f \rho_i A_t}{n \pi (\rho_f + f_i \rho_i)} \right)^{\frac{1}{2}} \quad (1)$$

where  $f$  is the mass ratio of fish to ice,  $\rho_i$  the density of crushed ice,  $A_t$  the total inner area of the box, or volume in case of 3D geometry,  $n$  the number of fish and  $\rho_f$  the density of fish. The values for various variables are as given in table 1.

**Table 1: Geometric features of the fish box model**

Internal dimensions of the box ( $l \times h$ )	500 mm $\times$ 500 mm
Thickness of insulation	30 mm (EPS), 15 mm (VIP)
Thickness of inner and outer plastic sheet	1 mm
Density of fish	1081 kg/m <sup>3</sup>
Density of flaked ice	593 kg/m <sup>3</sup>

### Mesh

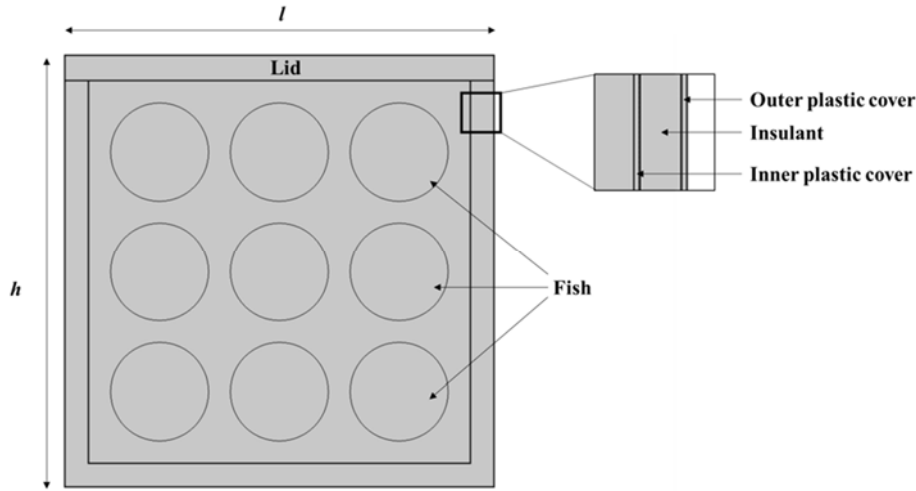


Figure 2 Geometry of the computer model

The geometry was resolved into free triangular elements because of the complexity at the interface of fish and adjoining geometric features. A normal size, predefined by COMSOL, was used which offered a minimum element size of 0.17 mm and a maximum element size of 37.9 mm. The complete mesh consisted of 56325 domain elements and 6418 boundary elements.

### Material

Flaked ice has a density lower than solid ice due to air voids. It can be described as a porous object consisting of two phases (ice and air). Its effective thermal conductivity is calculated by equation 2, until the ice begins melting which causes further reduction in thermal conductivity due to addition of a third phase of lower thermal conductivity (water). The thermal conductivity of this mixture is then calculated by equation 3. After all the ice has melted, the effective thermal conductivity of refrigerant is due to water and air. Figure 3 shows the variation in the effective thermal conductivity of crushed ice with temperature.

$$k = (1 - \theta)k_{ice}(T) + \theta k_{air}(T) \quad (2)$$

$$k = \theta k_{air}(T) + (1 - \theta) \left( \left( \frac{T(^{\circ}C) + 0.5}{1} \right) k_{water}(T) + \left( 1 - \left( \frac{T(^{\circ}C) + 0.5}{1} \right) \right) k_{ice}(T) \right) \quad (3)$$

Where  $\theta$  is the porosity of crushed ice and  $T$  the temperature of the crushed ice. The thermal conductivity values of fish, EPS and VIP were taken as 0.5 W/mK, 0.03 W/mK and 0.006 W/mK respectively.

### Heat transfer

The temperature of contents inside the box rises due to the transfer of heat from surroundings via convection.

The temperature of the fish must be maintained as close as possible to 0 °C without freezing, which can be lowered to -0.9 °C i.e. the freezing temperature of fish. After the fish is harvested, it is processed to lower its

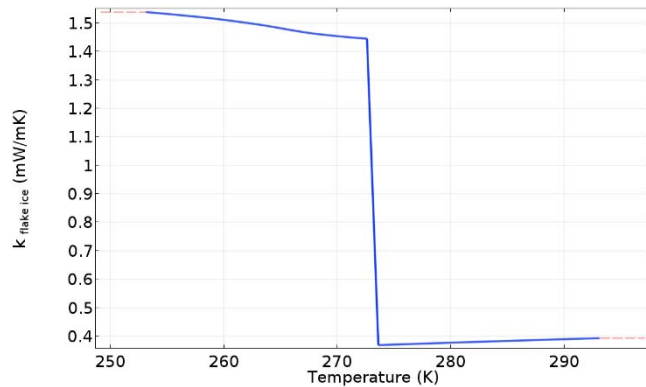


Figure 3 Effective thermal conductivity of crushed ice.



temperature to close to its freezing point. Temperature of fish should initially drop because of ice absorbing heat from it. The initial temperatures of fish, ice and the insulation of the box were set at -1 °C, -5 °C and 5 °C respectively.

Ice serves as the heat sink due to large latent heat capacity of fusion of water (334 kJ/kg). The specific heat of the ice was defined as a piecewise function such that the melting occurred in the temperature range of -0.5 °C to 0.5 °C.

The ambient temperature for summer was set as prescribed by ISTA standards [7] (22 °C for 4h, 35 °C for 2h, 30 °C for 12h and 35 °C for 6h). Heat is transferred from the surrounding environment to the walls of the fish box by laminar natural convection and by conduction through the insulation material to inside of the box. Convection inside the box is neglected as the air is present only in small pores of crushed ice and the temperature gradient along the depth of the box (y-direction) is low. For laminar natural convection, heat transfer coefficients on the external horizontal and the vertical walls can be described as [8]:

$$h_{horizontal} = 1.32 \left( \frac{\Delta T}{x} \right)^{\frac{1}{4}} \quad (4)$$

$$h_{vertical} = 1.42 \left( \frac{\Delta T}{x} \right)^{\frac{1}{4}} \quad (5)$$

where  $\Delta T$  is the difference between ambient temperature and the wall temperature and  $x$  the characteristic length. Surface to surface radiative heat transfer was considered in the study.

As a starting point, the mass ratio ( $f$ ) of the fish was set at 1.5. With the complex input of geometry, ambient temperature and thermal properties of ice, the simulation was run, for a maximum of 30 days, but a stop condition was introduced which stopped the simulation as soon as the average temperature across all the fish reached 0 °C. This time was defined as the box usage time as the fish was assumed to experience thermal abuse after 0 °C. The simulations were performed for both, 15 mm thick VIP and 30 mm thick EPS insulation. The study was extended to find the box usage time with varying  $f$ . The dimensions and the total mass of the box were calculated for each case and compared across insulations.

## Results and discussions

Figure 4 shows the variation of average fish temperature (with  $f = 3$ ) with time for three different cases of insulation. The temperature drops down from the initial temperature to around -1.6 °C within a few hours as ice surrounding the fish absorbs the heat.

Fish temperature again rises up as ice temperature increases to 0 °C. It remains constant for a few days, due to melting of ice, after which it again experiences a shallow kink downwards which can be attributed to reduction in thermal conductivity due to the introduction of liquid water. After most

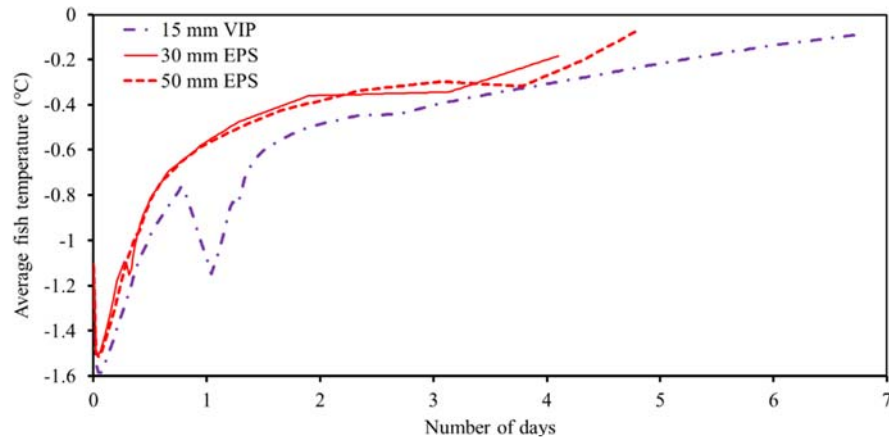


Figure 4 Average fish temperatures for various insulation cases

can be attributed to reduction in thermal conductivity due to the introduction of liquid water. After most

of the ice has melted, the average temperature rises monotonically with little variations due to change in ambient temperature. The corresponding box usage times for the three cases was compared. VIPs, due to their very low thermal conductivity, offer box usage time of more than six days; more than twice than that offered by EPS insulation of the same thickness.

Further, the mass ratio of the fish ( $f$ ) can be optimized according to the required box usage time. Rise

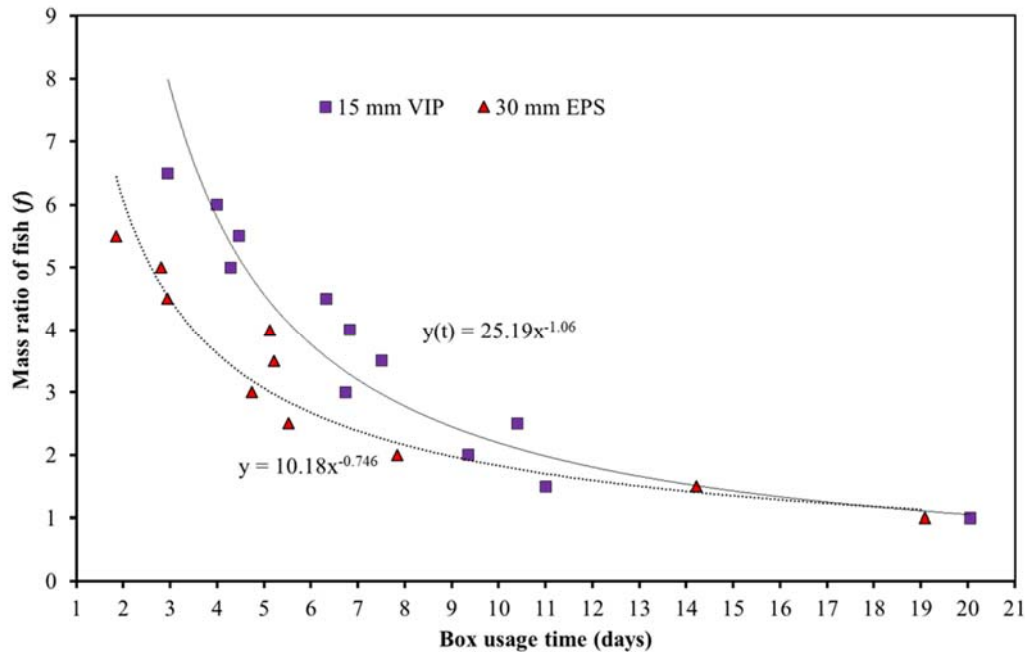


Figure 5 Mass ratio of fish vs box usage time for VIP and EPS insulation.

in  $f$  results in a decrease in the box usage time as can be seen in figure 5 which can be attributed to a lesser amount of ice to absorb the heat. Although the data is spread over a wide range due to varying ambient conditions; trend lines have been generated through a regression analysis ( $R^2 \geq 0.90$ ). Best fit equations shown on figure 5 can be used to estimate the amount of fish that can be transported or, the amount of ice required for a specific box usage time.

The corresponding effect of  $f$  on mass of fish transported and its cost per unit total mass of box is shown in table 2. For a similar box usage time, say 4.5, EPS has an  $f$  value of three and VIP insulated box four and a half. The difference can be translated in terms of economic benefit of around £70 per trip (considering fish price as £12/kg) for a 100 kg box. It is understood VIPs are much more expensive than EPS (at least 5 times). However, considering one trip per day and a modest profit margin of 20%, the cost of a 100 kg box could be recovered in less than two months.

The thickness of the box plays a significant role when a finite capacity of transport systems is considered. A simple calculation shows that the external volume of EPS boxes (30 mm thick) is 1.18 times higher than the VIP insulated boxes (15 mm thick) with same internal dimensions ( $0.5 \times 0.5 \times 0.5 \text{ m}^3$ ). Reduction in overall external volume of the fish box due to the use of VIPs facilitates higher volume being transported enhancing the economic benefit.

**Table 2: Effect of  $f$  on mass of fish transported and revenue generated**

$f$	$r$ (m)	Mass of fish (kg)	Mass of ice (kg)	Revenue per kg of mass of box (£/kg)
1.0	0.029	46.84	46.84	3.500
1.5	0.032	59.34	39.56	4.364
2.0	0.034	68.47	34.24	4.977
2.5	0.036	75.44	30.18	5.436
3.0	0.037	80.94	26.98	5.792

3.5	0.039	85.37	24.39	6.076
4.0	0.039	89.04	22.26	6.308
4.5	0.040	92.11	20.47	6.501
5.0	0.041	94.73	18.95	6.664

## Conclusions

The present study shows the clear advantage of using VIP insulated fish boxes over the conventional EPS insulated ones in terms of increased number of days that fish can be stored, using a complex computer model. It was observed that the box usage time is affected by the type of insulation material as well as the mass ratio of fish. For a similar box-usage time, VIP insulated fish box returned an  $f$ -value of five as compared to three for EPS insulated box. Further, the external volume of the same EPS box will be 1.18 times than that of a VIP insulated box with same internal volume; a factor very important while transporting fish in space constrained conditions.

## Appendix

Derivation of equation 1 to calculate the radius of fish.

$$m_f = f m_i$$

$$\Rightarrow \rho_f A_f = f \rho_i A_i$$

$$\Rightarrow \rho_f A_f = f \rho_i (A_t - A_f)$$

$$\Rightarrow (\rho_f + f \rho_i) A_f = f \rho_i A_t$$

$$\Rightarrow A_f = \frac{f \rho_i A_t}{(\rho_f + f \rho_i)} = n \pi r^2$$

$$\Rightarrow r = \left( \frac{f \rho_i A_t}{n \pi (\rho_f + f \rho_i)} \right)^{1/2}$$

## References

- [1] U. N. E. C. f. Europe, "Agreement on the International Carriage of Perishable Foodstuffs and on the Special Equipment to be Used for such Carriage," United Nations, New York and Geneva, 2018.
- [2] B. Margeirsson, "Modelling of temperature changes during transport of fresh fish products," Faculty of Industrial Engineering, Mechanical Engineering and Computer Science, University of Iceland, Reykjavik, 2012.
- [3] ASHRAE, ASHRAE Handbook - Refrigeration, Atlanta: American Society of Heating, Refrigerating and Air-Conditioning Engineers, Inc, 2006.
- [4] IIR, "The Role of Refrigeration in Worldwide Nutrition," in *5th IIR Informatory Note on Refrigeration and Food*, Paris, France, 2009.
- [5] F. 2001-2019, "Fisheries and Aquatic topics. Utilization and Trade. Topics Fact Sheets.," 06 01 2016. [Online]. Available: [www.fao.org/fishery](http://www.fao.org/fishery). [Accessed 02 04 2019].



- [6] G. Burgess, "Practical thermal resistance and ice requirement calculations for insulating packages," *Packaging Technology and Science: An International Journal*, vol. 12, no. 2, pp. 75-80, 1999.
- [7] ISTA, "7D. Thermal Controlled Transport Packaging for Parcel Delivery System Shipment, ISTA 7 Series Development Test Procedure," ISTA, 2006.
- [8] J. P. Holman, *Heat Transfer-Si Units-Sie*, Tata McGraw-Hill Education, 2002.



# Long-term Performance of Silica Aerogel and Aerogel Based Composites: A Literature Review Highlighting Pathways for Further Studies

Ali Naman Karim<sup>1,\*</sup>, Pär Johansson<sup>1</sup> and Angela Sasic Kalagasidis<sup>1</sup>

<sup>1</sup>Chalmers University of Technology, Gothenburg, Sweden

*\*Corresponding e-mail: ali.karim@chalmers.se*

## ABSTRACT

Aerogels are promising to be used in building materials and insulation products. Among various types of aerogel, silica aerogel is the most commonly type used for building applications. Untreated silica aerogel is hydrophilic, but it can be chemically modified to become hydrophobized. According to the literature review performed in this paper, few studies reporting ageing of hydrophobized silica aerogel under varying hygrothermal (relative humidity and temperature) conditions have been published so far. Among those, studies focused on microstructural evaluation of aerogel during hygrothermal ageing in laboratory conditions reported some reduction of specific surface area and the shift of pore size distribution. This results in a noticeable increase in thermal conductivity of the silica aerogel composite. The objectives of this literature review are to summarize the state-of-the-art studies concerning the impacts of ageing, both accelerated and real-life, in hygrothermal conditions on thermal performance of silica aerogel and aerogel based composite material. The results show that despite the hydrophobic treatment of aerogel, ageing still occur and has, in most cases, a negative impact on thermal performance of aerogel. Relative humidity seems to be the more dominant factor than temperature, concerning the intensity of degradation induced by ageing. Furthermore, a lack of direct correspondence between artificial ageing in laboratory environments and natural ageing is also highlighted.

## KEYWORDS

Silica, Aerogel, Accelerated ageing, Durability, Thermal performance

## INTRODUCTION

Superinsulation materials (SIM) with the advantage of improved thermal properties and reduced required thicknesses are promising options to the traditional insulation materials (Koebel et al, 2012). Among different types of SIMs, various types of opaque and translucent aerogel-enhanced products have been lately developed and commercially introduced to the market (Baetens et al, 2010). As a consequence of the relatively short real-life history of SIM and in particular aerogel and aerogel-enhanced materials, compared to the normal life time of traditional insulating materials which is about 50 years, the durability and long-term performance of aerogel materials is not fully understood (Chal et al, 2018). Beyond that, due to lack of a common and fully standardized ageing test procedure, various test conditions have been utilized in the (hygrothermal) ageing studies performed on these aerogel materials. Within this work, an attempt to systemize and compare the different studies concerning the durability of aerogel and some aerogel-enhanced products has been done. The aim is to identify possible pathways for further research in this field of science. Focus is on the knowledge of thermal performance of these materials when exposed to various types of accelerated hygrothermal ageing.

## METHODS

A literature review was conducted on the published results from studies evaluating the impacts of (accelerated) ageing on the material properties of silica in general and silica aerogel and aerogel-enhanced composites in particular. Generally, an accelerated ageing test is aimed to rapidly evaluate the long-term behavior of a material (Escobar and Meeker, 2006). Among different methods, hygrothermal ageing is a widely used method as weathering is one of the main causes of deterioration. In this artificial ageing process, tested material is exposed to severe hygrothermal conditions, such as elevated temperature, elevated relative humidity (RH), a combination and/or repeated cycles of both elevated temperature and relative humidity. In the studied papers, different authors have been proposed different framework with different hygrothermal conditions. Among the limited number of relevant articles ( $\sim < 20$  articles), 5 articles, specifically focusing on accelerated hygrothermal ageing of silica aerogel and aerogel-enhanced materials have been studied closely in the paper at hand.

### Overview of published ageing tests

In 1976, Bonsack studied long-term performance of silica powder in terms of surface chemical and physical properties by storing in closed containers during one year (Bonsack, 1976). It was shown that the specific surface area (SSA), the total surface area per unit of mass (Everett, 1972), was reduced by 25-60 %. Morel et al. (2009) studied ageing of pyrogenic (fumed) silica under various temperature and relative humidity conditions. A decrement in surface area and an increment in rigidity and hydrophilic capacity were observed. Another study inspected the changes in properties of mesoporous silica and non-porous pyrogenic silica due to ageing in ambient conditions for 32 years (Collins et al, 2008). The pore size distribution (PSD), i.e. the frequency of different pore sizes, was shifted towards larger sizes and the SSA was decreased by approximately 15 %. Balard et al. (2011) studied the ageing phenomenon of pyrogenic silica for 60 days and in conditions of 25 °C and 95 % RH, resulting in a negligible reduction in SSA. In line with the main objectives of this paper, a summary of the articles focusing on hygrothermal ageing of silica aerogel and aerogel-enhanced materials, studied in this paper, are summarized in Table 1.

Table 1. Ageing studies on aerogel and aerogel-enhanced insulation materials.

Article	Studied product(s)	Ageing factors
1. (Ihara et al. 2015)	Granules	Relative humidity, solar radiation
2. (Chal et al, 2018)	Granules and blankets	Relative humidity, temperature
3. (Bellunato et al, 2004)	Tiles	Irradiation, humidity absorption
4. (Chal et al, 2019)	Granules and blankets	Relative humidity, temperature
5. (Alvey et al, 2017)	Blankets	Relative humidity, temperature

In paper number 1, hygrothermal conditions of 35- 65 °C, 100 % RH and a solar radiation simulator with an intensity of  $1200 \text{ W/m}^2$  were chosen for the ageing studies. The tests lasted for 3 months including 300 cycles with a duration of 6 hours each (Ihara et al, 2015). By calculating an acceleration factor, the test period was estimated to correspond to 10-20 years in real-world conditions. Shortly, acceleration factors are calculated based on the conditions used, such as temperature and relative humidity range and other material characteristics such as activation energy and reactions rate, to state the correspondence between accelerated and natural ageing. More information about different acceleration factors can be found in (Escobar and Meeker, 2006). It was concluded that thermal conductivity of the aerogel granules could increase by approximately 10 % due to hygrothermal ageing. Ageing by radiation resulted in a negligible deterioration in the hydrophobicity of the aerogel surface. According to the authors of paper 1, occurrence of silica-network breakage in conjunction with the ageing process was

the main reason for the observed property changes. In paper 2, 5 different commercial products with hydrophobic-treated aerogels, were studied for periods of 96 to 384 days in ageing conditions of 50 °C, 70% RH and 70 °C, 90% RH (Chal et al, 2018). The aerogel products were either granules or blankets, with different initial SSA and different hydrophobic agents. A decrement in the hydrophobicity was observed at the first period of ageing, followed by a reduction of SSA and a shift of PSD towards higher values at the later stages of ageing. The magnitude of these changes varied broadly depending on the product and the hydrophobic treatment of the aerogels. Thermal conductivities of all products were increased by up to 2.5  $mW/mK$ . They also showed that different commercial products responded differently to the ageing process. Hydrophobisation quality and initial PSD were identified as the two governing parameters for thermal efficiency in severe hygrothermal conditions. Paper 3 studied the performance of hygroscopic and hydrophobic aerogels when irradiated with Gamma radiation ( $\gamma$ ), protons and neutrons, and when absorbing humidity (Bellunato et al, 2004). When the aerogels were exposed to  $\gamma$  and protons no changes were observed, while for neutrons a moderate degradation in term of clarity was observed. For the humidity test, aerogels were aged for one week in the conditions of 22-30 °C and 55-80 % RH, resulting in some degradation of the material properties. However, by baking the samples at approximately 500 °C the initial material properties could be restored. In paper 4, several silicas, aerogel and aerogel-enhanced products were aged in conditions of 50-70 °C and 70-90% RH for 24-96 days (Chal et al, 2019). A reduction of SSA and a shift in PSD were observed for all products but with various intensities. The conclusions were that for the short-term ageing of both precipitated and fumed silica, temperature was the governing parameter, while for long-term ageing, relative humidity was the governing one. Similarly, relative humidity was the decisive parameter for aerogel but in that case the intensity of the degradation due to ageing seemed to be product specified. In paper 5, 3 different aerogel blankets were studied for 5 weeks and in conditions of 65.6 °C, 30/60/90 % RH and 32.2 °C, 90 % RH (Alvey et al, 2017). It was found that the increased moisture content in the blankets increased the thermal conductivities of the blanket differently. It was concluded by the authors that parameters such as volume expansion and hygroscopicity have also an impact on the thermal performance of the aerogel blankets.

## DISCUSSIONS

Among the limited number of studies focusing on ageing and long-term performance of aerogels, some characteristic trends can be identified. An increase in SSA and shift in PSD towards larger sizes, negatively affecting the hygrothermal properties, i.e. increasing the moisture capacity and thermal conductivity seem to occur repeatably in different studies. Looking at the ageing effects on thermal property of aerogel it is also clear that ageing can have a negative impact. However, due to the diversities in the results from these studies, in terms of the magnitude of the ageing-induced degradation, it is difficult to state a concrete relation between ageing and aerogel properties. Also, due to the variety of the chosen conditions for the laboratory experiments performed, namely different time intervals, hygrothermal conditions, irradiations (solar radiation) and different products, different production techniques, conditioning, etc., it is difficult to make a direct comparison between the different studies. It is also noted that in some studies, the time of the accelerated ageing is interpreted to real life time by estimating an acceleration factor for the test. However, accuracy and validity of these estimations for materials in nanoscale, such as aerogel seems to be not fully elaborated.

## CONCLUSIONS

Based on the literature review performed, it is concluded that ageing of aerogel can affect the material properties and result in a worsen thermal performance. Variations in relative humidity seems to be one of the most crucial parameters, even if the aerogel particles are hydrophobically

treated. The magnitude of the deterioration by ageing seems to be product depended. It can be concluded that there is a lack of knowledge concerning ageing of aerogel and correlation between accelerated ageing and real time ageing. To fully capture the performance of aerogel-enhanced product and to increase the market penetration of these insulation products, ageing of aerogel needs to be fully understood. Further studies focusing on ageing of aerogel particles, based on standardized frameworks, is therefore recommended.

## ACKNOWLEDGEMENT

The financial support from the Swedish Energy Agency (46822-1) is gratefully acknowledged.

## REFERENCES

- Alvey, Jedediah B., Jignesh Patel, and Larry D. Stephenson. 2017. "Experimental Study on the Effects of Humidity and Temperature on Aerogel Composite and Foam Insulations." *Energy and Buildings* 144: 358–371.
- Baetens, Ruben, Bjørn Petter Jelle, Jan Vincent Thue, Martin J. Tenpierik, Steinar Grynning, Sivert Uvsløkk, and Arild Gustavsen. 2010. "Vacuum Insulation Panels for Building Applications: A Review and Beyond." *Energy and Buildings* 42 (2): 147–172.
- Balard, H., J.-B. Donnet, H. Oulanti, T. Gottschalk-Gaudig, and H. Barthel. 2011. "Study of Aging of Pyrogenic Silicas by Gravimetry and Microcalorimetry." *Colloids and Surfaces A: Physicochemical and Engineering Aspects* 378 (1–3): 38–43.
- Bellunato, T, M Calvi, C Coluzza, G Longo, C Matteuzzi, M Musy, P Negri, and D.L Perego. 2004. "Study of Ageing Effects in Aerogel." *Nuclear Instruments and Methods in Physics Research Section A: Accelerators, Spectrometers, Detectors and Associated Equipment* 527 (3): 319–328.
- Bonsack, J.P. 1976. "Effect of Aging on Surface Properties of Silica Powders Produced by Plasma-Arc Vaporization." *Powder Technology* 15 (1): 53–62.
- Chal, B, G Foray, B Yrieix, ... K Masenelli-Varlot - Microporous and, and undefined 2018. n.d. "Durability of Silica Aerogels Dedicated to Superinsulation Measured under Hygrothermal Conditions." *Elsevier*.
- Chal, Bruno, Bernard Yrieix, Lucian Roiban, Karine Masenelli-Varlot, Jean-Marc Chenal, and Geneviève Foray. 2019. "Nanostructured Silica Used in Super-Insulation Materials (SIM), Hygrothermal Ageing Followed by Sorption Characterizations." *Energy and Buildings* 183 (January): 626–638.
- Collins, K.E., M.C. Gonçalves, R.B. Romero, R.F. Conz, V.R. de Camargo, and C.H. Collins. 2008. "Low Temperature Ageing of Silicas Gasil-I and TK800." *Applied Surface Science* 254 (13): 4029–35.
- Escobar, Luis A., and William Q. Meeker. 2006. "A Review of Accelerated Test Models." *Statistical Science* 21 (4): 552–577.
- Everett, D. H. 1972. "Manual of Symbols and Terminology for Physicochemical Quantities and Units, Appendix II: Definitions, Terminology and Symbols in Colloid and Surface Chemistry." *Pure and Applied Chemistry* 31 (4): 577–638.
- Ihara, Takeshi, Bjørn Petter Jelle, Tao Gao, and Arild Gustavsen. 2015. "Aerogel Granule Aging Driven by Moisture and Solar Radiation." *Energy and Buildings* 103: 238–248.
- Jelle, Bjørn Petter. 2012. "Accelerated Climate Ageing of Building Materials, Components and Structures in the Laboratory." *Journal of Materials Science* 47 (18): 6475–6496.
- Koebel, Matthias, Arnaud Rigacci, and Patrick Achard. 2012. "Aerogel-Based Thermal Superinsulation: An Overview." *Journal of Sol-Gel Science and Technology* 63: 315–339.
- Morel, B, L Autissier, D Autissier, D Lemordant - Powder Technology, 2009. "Pyrogenic Silica Ageing under Humid Atmosphere." *Elsevier*.

## **LCA Analysis of Vacuum Insulation Panels and their Sensitivity to EoL and Future Grid Decarbonisation Scenarios**

Shahaboddin Resalati<sup>1,\*</sup>, Kate Brown<sup>1</sup>, Nuno Simões<sup>2,3</sup>, Márcio Gonçalves<sup>2,3</sup>, Catarina Serra<sup>2,3</sup>

<sup>1</sup> Oxford Brookes University, UK

<sup>2</sup> ADAI – LAETA, Department of Civil Engineering, University of Coimbra, Portugal

<sup>3</sup> Itecons, Portugal

*\*Corresponding e-mail: sresalati@brookes.ac.uk*

### **ABSTRACT**

The current European Energy Performance of Buildings Directive (2018/844/EU) aims at achieving a decarbonised building stock by 2050. Where buildings are constructed to better thermal standards, operational and embodied energy can be equivalent, meaning that it is imperative that embodied energy is considered when specifying optimal insulation strategies. This poses significant development implications for novel insulation technologies (such as VIPs), which are at the verge of upscaling, in relation to their environmental performance. The available EPDs concerning VIPs consider 100% recycling rates for the core material, discounting most of the associated practical constraints. Given that over 90% of the carbon footprint of VIPs is associated with their core material (fumed Silica), this lack of consideration will have significant implications for their true environmental performance representation. A LCA analysis has therefore been applied to VIPs in three European locations presenting their environmental performance in relation to their sensitivity to the core material recycling/reuse rate and future grid decarbonisation scenarios. The study provides a combined operational and embodied carbon payback appraisal. The results demonstrate a direct relationship between future grid intensity, core material recycling/reuse rate and the climatic conditions, delivering a net carbon benefit for effective upscaling.

### **KEYWORDS**

Life Cycle Assessment (LCA); Grid decarbonisation; VIP; Recycling rates, End of Life scenarios

### **INTRODUCTION**

Buildings are the European Union's single largest energy consumer, responsible for around 40% of end-use energy and 36% of CO<sub>2</sub> emissions (EPBD, 2019). According to the latest factsheet of the European Energy Performance of Buildings Directive, around a third of Europe's buildings are energy inefficient. Investment in retrofit (and specifically insulation materials) to improve energy efficiency of buildings is therefore a key policy tool to meet EU's climate change goals, focussing on insulation of existing buildings and strengthening regulations to require better insulation levels in new buildings. Where buildings are constructed and retrofitted to better thermal standards, the relative importance of operational energy emissions is reduced, and the relative contribution of embodied carbon increases. Historically, embodied emissions have been broadly ignored due in part to the belief that they were insignificant within a building's whole life carbon footprint (Ibn-Mohammed et al., 2013), but as operational emissions are reduced due to successes in electricity decarbonisation and measures to reduce heating demand of buildings, embodied carbon is growing in significance. Given that improving the thermal performance of a building is predominantly driven by the building fabric's insulative properties, it is essential to holistically analyse the environmental implications of insulation materials for different building design and

configuration. Novel insulation materials such as VIPs, at the verge of upscaling, are essential to be considered especially where lower R-values are required to be coupled with lower environmental impacts.

Although embodied carbon emissions are not currently legislated in the same way as operational energy, there is a clear trend towards regulating it in the near future. The current French and Belgian legislations are good examples of the move to mandate the compulsory disclosure of environmental characteristics for construction materials. The desire and attempt to quantify the environmental impact of buildings through LCA analyses in recent years has resulted in various environmental certification systems such as the Environmental Product Declaration (EPD), in compliance with EN 15804 and ISO 14025, to accurately and transparently communicate the environmental impact of different products. LCA is an intensively data-driven approach which relies on availability of adequate and high quality data (Takano et al., 2014). Finding reliable data has been an issue for LCA practitioners (De Wolf et al., 2017). This lack of availability of consistent data can be associated with confidentiality issues for manufacturers, the time consuming process of generating reliable data and different methodological approaches to data treatment (Lotteau et al., 2015).

There exist a limited number of EPDs that investigated the Vacuum Insulation Panels and specifically fumed silica based products. The system boundaries of these EPDs only cover cradle to gate stages (module A1-A3) without differentiating between the product's different components and materials. The module-D in these EPDs is mainly a pure assumption of fully recyclable core material and therefore a substantially reduced environmental impact. Such assumptions will have a significant implication for VIPs, as the core material is the key contributor to their environmental impact. This is aligned with findings of studies such as Schonhardt et al. (2003) which have demonstrated that fumed silica as the core material in VIPs is responsible for over 90% of the embodied energy. This paper therefore, presents the results of a comprehensive LCA analysis conducted for VIPs and investigates the results' sensitivity to the recycling rates of the core material and grid decarbonisation. The findings are applied to a combined operational and embodied energy analysis to identify the optimum design configurations associated with improved thermal performance of VIPs and future grid decarbonisation scenarios in three European locations including London, Berlin and Lisbon.

## METHODS

A comprehensive LCA analysis has been conducted in full compliance with ISO norms 14040-14044, and European Standards EN 15804 and EN 15978. The results are then applied to a combined operational and embodied energy analysis in relation to an incremental increase of the building fabric U-value. This is to identify the extent in which the application of VIPs to buildings can lead to a net carbon benefit. The future grid decarbonisation scenarios extracted from Capros et al. (2016) are also accounted for in all locations to demonstrate its impact on the buildings life cycle savings (Table 1). A single-family detached dwelling has been used as the case study building and its fabric's thermal properties has been accordingly adjusted based on each locations' requirements. The system for space heating and cooling is a heat pump with a Coefficient of Performance (COP) for heating of 3.4 and an Energy Efficiency Rating (EER) for cooling of 2.8.

Table 1. Electricity grid carbon intensity scenarios

<i>kgCO<sub>2</sub>/kWh</i>	2015	2020	2025	2030	2035	2040	2045	2050
United Kingdom (London)	0.42	0.20	0.16	0.11	0.10	0.11	0.10	0.08
Germany (Berlin)	0.41	0.42	0.42	0.37	0.32	0.28	0.22	0.14
Portugal (Lisbon)	0.32	0.15	0.10	0.05	0.05	0.03	0.03	0.02



## RESULTS

The results on a cradle to gate basis demonstrate that 86% of the environmental impact is associated with the core material in all impact categories (Figure 1). On a cradle to gate basis, the GWP values for VIPs are substantially higher than other conventional insulation materials. However, given the significant contribution of the core material, EoL scenarios are essential to be considered for VIPs in order to truly represent their environmental performance.

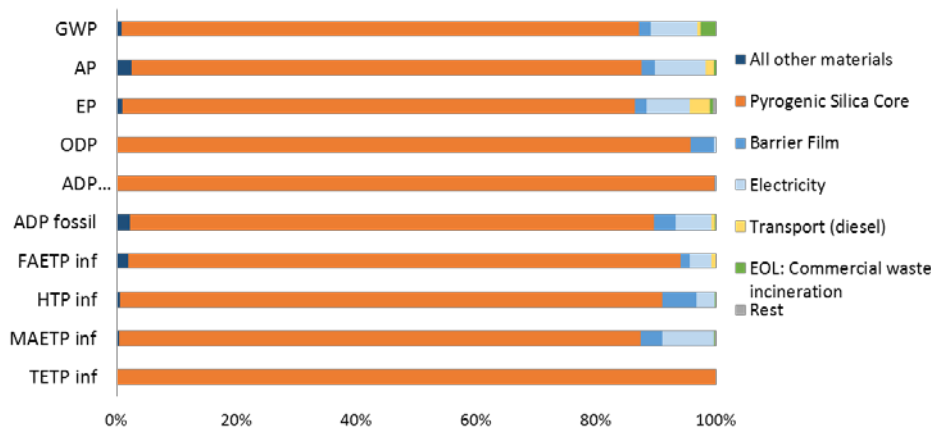


Figure 1. Contribution of different VIP processes to each environmental impact category

Figure 2 illustrates the sensitivity of VIPs' GWP to the recycled content of the core material.

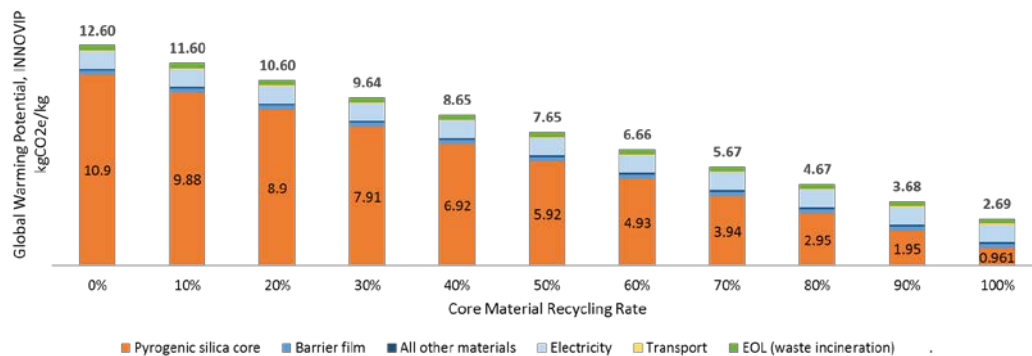


Figure 2. GWP (kgCO<sub>2</sub>e/kg) at various EoL recycling rates (core recycling only)

Figure 3 demonstrates that, by applying the values extracted from Figure 2 to all studied locations, when likely future electricity grid decarbonisation is accounted, the only VIP recycling concept which will deliver a net benefit emissions savings is 100% core material reuse. In the warmer climate zone of Lisbon, grid carbon intensity is already below the level where increasing insulation can provide a net annual emissions benefit. Germany is likely to experience a much slower fall in grid carbon intensity, which makes performance of VIPs more attractive. VIPs with 50% recycled core would offer a net benefit with grid intensity above 0.22kgCO<sub>2</sub>/kWh (not likely to be reached before 2045). 100% recycled core would continue to offer net benefit until grid intensity fell below 0.08kgCO<sub>2</sub>/kWh, a scenario not forecast in Germany before 2050. VIPs with no core recycling would not offer a net benefit from increased insulation thickness under any UK grid carbon scenario (2015 intensity=0.42kgCO<sub>2</sub>/kWh) which is broadly where 0% recycled panel offers no benefit. Within lifespan of product (30 years is assumed), UK grid intensity likely to fall to 0.08kgCO<sub>2</sub>/kWh, at which even 100% recycled core material would be unlikely to offer a net benefit of improved insulation thickness.

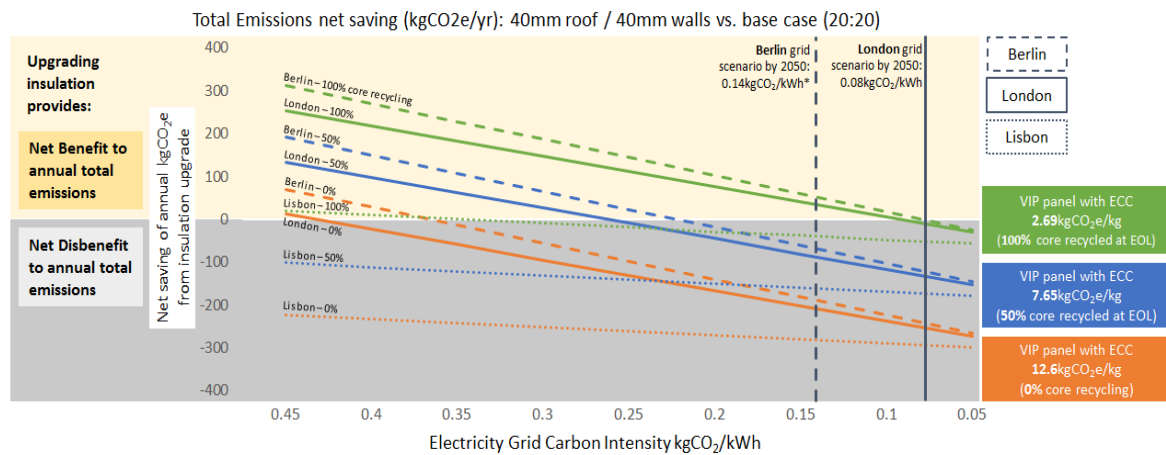


Figure 3. Annual emissions savings kgCO<sub>2</sub>e of insulation upgrade in 3 locations, under different grid carbon intensity scenarios

## CONCLUSIONS

The findings of the LCA analyses are in agreement with the results from the available EPDs for VIPs, with fumed silica used as the core material, in relation to the contribution of the core material to the overall environmental impact of VIPs. The analyses have demonstrated that quantifying the optimum net carbon savings associated with VIPs requires proper analytical and predictive understanding of the influencing factors such as the LCA assumptions and grid decarbonisation scenarios. Practice and standards based on such analyses however, could realistically deliver very significant energy/carbon savings across the life of a building. Such analyses can contribute to informing the maximum levels of insulation that can be incorporated into buildings or that may in the future be required by standards, and can indicate limits to the amount by which current approaches to energy thrift can be escalated using specific products.

## ACKNOWLEDGEMENT

This work has been developed under the European Union's Horizon 2020 research project INNOVIP under grant agreement No 723441.

## REFERENCES

- Capros, P. et al. (2016). EU Reference Scenario 2016: Energy, Transport and GHG emissions trends to 2050. European Commission. European Union. <https://doi.org/10.2833/9127>
- De Wolf, C., Pomponi, F. and Moncaster, A. (2017) 'Measuring embodied carbon dioxide equivalent of buildings: A review and critique of current industry practice', *Energy and Buildings*, 140, pp. 68-80.
- EPBD (2019) 'Building performance factsheet': EU Commission. Available at: [https://ec.europa.eu/energy/sites/ener/files/documents/buildings\\_performance\\_factsheet](https://ec.europa.eu/energy/sites/ener/files/documents/buildings_performance_factsheet)
- Ibn-Mohammed, T., et al. (2013) 'Operational vs. embodied emissions in buildings—A review of current trends', *Energy and Buildings*, 66, pp. 232-245.
- Lotteau, M., et al. (2015) 'Critical review of life cycle assessment (LCA) for the built environment at the neighborhood scale', *Building and Environment*, 93, pp. 165-178.
- Schonhardt, U., Binz, A., Wohler, M., & Dott, R. (2003). *Ökobilanz eines Vakuum-Isolations-Panels (VIP)*. University of Applied Sciences, Institute of Energy, Basel, German.
- Takano, A., Hughes, M. and Winter, S. (2014) 'A multidisciplinary approach to sustainable building material selection: A case study in a Finnish context', *Building and Environment*, 82, pp. 526-535.

## **Molecular dynamic measurements, a tools to assess how surface chemistry modifies mechanical properties of mesoporous silica**

Wassim Kassem<sup>1,2</sup>, Julien Morthomas<sup>1,2,\*</sup>, Patrice Chantrenne<sup>1,2</sup> and Genevieve Foray<sup>1,2</sup>

<sup>1</sup>INSA-Lyon, MATEIS CNRS UMR5510, Villeurbanne, France

<sup>2</sup>Université Claude Bernard Lyon 1, Villeurbanne, France

*\*Corresponding e-mail: genevieve.foray@insa-lyon.fr*

### **ABSTRACT**

Silica aerogels have some of the best thermal insulation properties. Their low thermal conductivity is due to their fractal morphology characterized by a distribution of pore sizes between 2 and 50 nm as well as a very high surface area. Unfortunately, this characteristic structure is also responsible for their brittleness. At the mesoscale, aerogels are described as a network of interconnected silica nano-spheres also known as primary particles, with dead dangling arms. Moreover, the presence of surface hydroxyl groups (Si-OH) and surface methyl groups (Si-O-CH<sub>3</sub>) on silica is known to influence both surface morphology and the macroscopic properties of the aerogels through some simple simulations as well as experiments. Here, we conduct molecular dynamics simulations of silica nano-structures, such as nano-wires and nano-spheres under various silanol (Si-OH) concentrations. The nanostructures represent the underlying building blocks of the aerogel morphology. Using a recent powerful inter-atomic potential (ReaxFF) we can also accurately model hydroxyl-silica interactions and then characterize the microstructural evolution. Using the aerogels generated with various substitution level, we have measured mechanical properties for several cylinder (3 L/D). Those results can then be used as input-data for models at larger scale.

### **KEYWORDS**

Molecular Dynamics, Silica, ReaxFF, Mechanical properties, Aerogels

### **INTRODUCTION**

Silica aerogel are the lightest solids known to man. Their unique fractal structure can be thought of as a 3D network of interconnected nanoparticles (NPs) with a size distribution of 3 to 100 nm. Smaller particles called Primary Particles. They are essentially nano-sized spheres of silica with dense amorphous structure. Secondary Particles are then agglomerations of Primary Particles. The Secondary Particles link up at contact points to form the macro-scale solid network which is the aerogel [1].

The thermal properties of such a solid are indeed fascinating. Silica aerogels have some of the best insulating properties known. In fact, their insulation properties can be better than air. Their unique fractal microstructure impedes heat transfer via conduction (through the solid backbone) as well as convection (through the air particles diffusing through the nanopores). Their main weakness; on the other hand, is their poor mechanical properties. They have low mechanical strength and their fracture behaviour is brittle. This has impeded their widespread use especially in monolith form, and their cost efficiency ratio for overall applications.

Chemistry plays a big part in the tailoring aerogel thermo-mechanical properties. Different chemical treatments before and after ambient air or supercritical drying, as well as the

procedure for drying, affect properties such as density, mechanical strength, and surface characteristics [2]. It is believed that controlling surface hydroxyl and methyl groups, such as -OH and -COH, is the key to controlling network connectivity and stiffness. This might tailor the thermal/ mechanical antagonism of the aerogel.

Our aim in this work is to measure how surface chemical groups modify mechanical properties using molecular dynamics simulations (MD) with a reactive inter-atomic potential. Reactive-MD is one of the best choices for a problem like this one. It offers atomic-scale resolution of deformation events with the important function of modelling chemical reactions. Reactions must include bond creation and bond failure because they are essential for modelling defect structures and dangling arms in a material like  $\text{SiO}_2$ . Here we have characterized nanowires a few nm in diameter and a few nanometre in length as well as spherical particles to catch how surface chemistry change mechanical behaviour.

## METHODS & MATERIALS

We used the LAMMPS code with the included reax/c package for simulation and inter-atomic forces. The initial atomic coordinates are random, so the system is relaxed using a combination of energy minimization and dynamic relaxation using a heating-quenching scheme. Once the system has equilibrated, we performed either indentation or tension-compression simulations. Some mechanical indexes (stiffness, modulus, ultimate strength) were computed to quantify the effect of surface OH groups on the mechanical response. We compared our results for finite-T and 0-T simulations where T is the temperature.

System stability was a big concern as the ReaxFF potential was originally developed independently from LAMMPS, and contains quite a lot of control parameters. We performed a parametric study and chose to use the default ones with no modifications. We use a 100fs Qeq relaxation time. In addition, it was noted that the Nosé-Hoover thermostat was not always the best choice. Reaching a stable configuration of atoms even after repeated attempts at relaxing the atoms requires practice. Hence, a Langevin thermostat was sometimes used as it proved to be more stable. This could be due to the additional damping force.

We have generated several materials. The first set are spheres with diameter equals 4, 6 and 7 nm. Those are subjected to compression tests with and without surface hydroxyl groups using a reflective wall. The second samples set are nanowires with diameter equals 4 or 6 nm, and a length equal to 5 or 10nm. Those were axially loaded and unloaded using affine deformation of the simulation box. The samples generated contained 2000 to 14000 atoms with our largest simulation box containing about 250000 in the form of a bulk periodic configuration used to carve out nanowires.

We used the KOKKOS and MPI libraries to accelerate performance. We carried out simulations using Nvidia GPUs (GTX 1080Ti, Titan V) and Intel Xeon CPUs.

## RESULTS

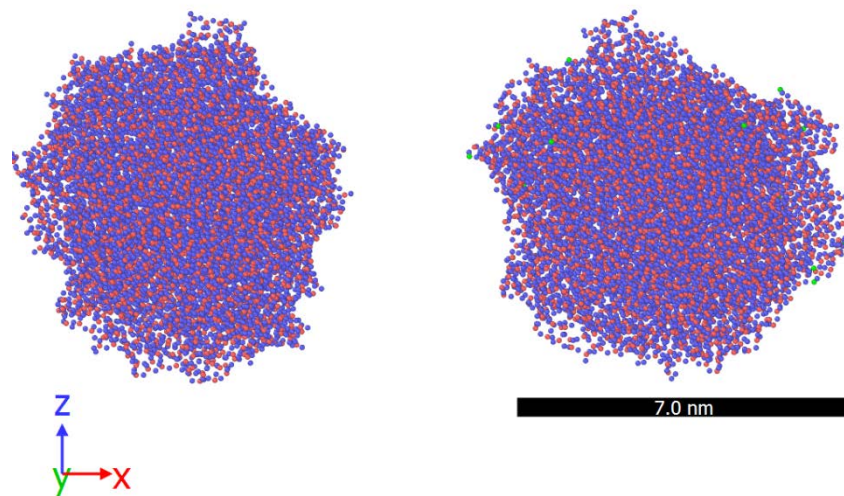


Figure 1. Initial configuration of a D=7nm silica nanosphere with and without surface OH groups (silicium in red, oxygen in blue, OH in green)

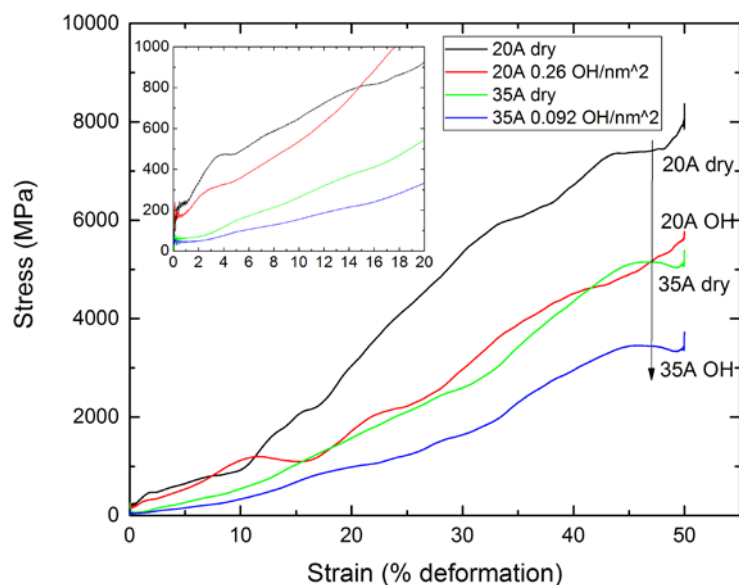


Figure 1. Effect of size and wetting on the compressive behaviour if silica nanospheres

## DISCUSSIONS

Compression testq are first performed on small dense spherical samples. Initial results did confirm that hydroxyl groups decrease their overall mechanical behavior. Our simulations show that increasing the radius of our nano-spheres effectively lowers their stiffness by a non-negligible amount. This has important consequences on the rigidity of the solid aerogel backbone. But mechanical analysis of such simulation is quite difficult. We thus performed simulation on nanowire under axial compression. Those performed on unmodified samples confirmed that REAXFF simulation gives mechanical results similar to those gained with MD and a BKS potential [3].

In addition, we noted that even at relatively low surface OH concentrations of 0.09 and 0.26 OH/nm<sup>2</sup> we can still observe a reduction in the stiffness of our nano-spheres. The reduction is more marked for larger diameter spheres and at larger strains.

## CONCLUSION

A procedure was developed so as to generate mesoporous sample either nanowire or spherical like samples with REAXFF potential. Textural properties of such samples are fully characterized ( bond length, ring size, bond angle).

The generated mesoporous sample are then cloned, and modified with substituted chemical surface groups (OH or hydrophobants). Location and overall density of those groups are tailored.

Mechanical test were then performed as well as failure analysis. First results show that below a given content substitution decreases the ultimate strength and the stiffness.

The mechanical analysis of nanowire is under completion so as to understand if failure depends on the overall content of substitution or is rather link to their local concentration ( isolated, double or block substitution)

## ACKNOWLEDGEMENT

Thanks are due to AURA Region France that granted the COMPASS superinsulation project.

## REFERENCES

- [1] Roiban L, Foray G, Rong, Q, Perret A, Dris I., Masenelli-Varlot K., Maire E. and Yrieix B., Advanced 3 D characterization of silica based ultraporous material, *RCS Advance*, 6, 2016, p.10625 DOI: 10.1039/C5RA26014K
- [2] Chal B, Foray G, Roiban L., Masenelli-Varlot K., Durability of silica aerogels dedicated to superinsulation measured under hygrothermal conditions, *Microporous and Mesoporous materials*, p.61-69, 2017,
- [3] **Gonçalves W**, Morthomas J, Chantrenne P, Perez M, Foray G, Martin C, Elasticity and strength of silica aerogels: a Molecular Dynamics study on large volumes, *Acta Materialia* , 2018, p. 165-74, DOI: [10.1016/j.actamat.2017.12.005](https://doi.org/10.1016/j.actamat.2017.12.005)

## **Calibration Method on the Thermal Conductivity Measurement in the Central Part of Vacuum Insulation Panels (VIP) by Heat Flow Meter Apparatus**

Kensaku Mabuchi<sup>1,\*</sup>, Atsushi Iwamae<sup>2</sup>, Daisuke Ogura<sup>3</sup> and Taichi Tasaka<sup>1</sup>

<sup>1</sup>Japan Testing Center for Construction Materials, Saitama, Japan

<sup>2</sup>Kindai University, Higashi-Osaka, Japan

<sup>3</sup>Kyoto University, Kyoto, Japan

*\*Corresponding e-mail: mabuchi@jtccm.or.jp*

### **ABSTRACT**

The guarded hot plate (GHP) apparatus and the heat flow meter (HFM) apparatus are used in measurements of the thermal conductivity in the central part of vacuum insulation panels (VIP). Although the HFM apparatus has a slightly lower measurement accuracy than the GHP apparatus, it has a more reasonable price and a shorter measurement time.

Basically, it is necessary to calibrate the calibration factor of the HFM of an HFM apparatus by setting a calibration board whose thermal conductivity is close to that of a test specimen. However, VIP has unusually low thermal conductivity of about 1/10 that of a general calibration standard board (e.g. glass wool).

In this research, we studied a method for checking and setting the calibration factor of the HFM. In order to obtain a similar density of heat flow rate in the calibration process and the test process, we reduced the temperature difference in the calibration process. The results clarified the relationship between the heat flow rate density and the calibration factor of the HFM.

### **KEYWORDS**

Thermal conductivity, Heat flow meter, Calibration factor, Test method

### **INTRODUCTION**

The most general evaluation index for vacuum insulation panels (VIP) is the thermal conductivity of the central part of VIP. Therefore, measurement of thermal conductivity is important. The guarded hot plate (GHP) apparatus and the heat flow meter (HFM) apparatus are used in measurements of the thermal conductivity in the central part of VIP.

The measurement principles of the two apparatuses are similar, and only the method of measuring the heat flow is different. Of these two methods, because the heat flow measurement by the GHP apparatus is a direct method that does not require calibration or correction, it is considered possible to apply this apparatus simply to VIP, which is an ultra-high performance heat insulating material. On the other hand, because the HFM apparatus uses an indirect method, in which the calibration factor of the heat flow meter is set by using a calibration standard board (e.g. glass wool), it is necessary to check whether simple application to VIP is possible.

The purpose of this research is to study a method for checking the calibration factor of HFM apparatuses under the condition of a low density of heat flow rate like that when measuring VIP.



## METHODS

The HFM apparatus is a thermal conductivity measurement device in accordance with ISO (1991). Figure 1 shows the configuration of a general HFM apparatus. When performing measurements, a test specimen having a flat plate shape is placed between a heating plate and a cooling plate, and a temperature differential between the front and back sides of the specimen is applied. The density of heat flow rate at that time is measured by the heat flow meter, and thermal conductivity is calculated by Eq. (1).

The heat flow meter is a sensor that outputs a voltage proportional to the heat flow rate, and that proportionality coefficient is set in advance by a calibration procedure. Calibration is performed by setting a calibration standard board having a thermal conductivity value determined by a GHP apparatus, etc. in the HFM apparatus, and the calibration factor  $f$  of the HFM is calculated by Eq. (2).

$$\lambda = \frac{f \cdot e \cdot d}{\Delta T} \quad (1)$$

$$f = \frac{q}{e} \quad (2)$$

where  $\lambda$  is the thermal conductivity of the test specimen [ $\text{W}/(\text{m} \cdot \text{K})$ ],  $f$  is the calibration factor of the HFM [ $\text{W}/(\text{m}^2 \cdot \text{mV})$ ],  $e$  is the output voltage from the HFM (mV),  $d$  is the thickness of the test specimen (m),  $\Delta T$  is the temperature difference of the test specimen (K) and  $q$  is the density of heat flow rate of the calibration standard board ( $\text{W}/\text{m}^2$ ).

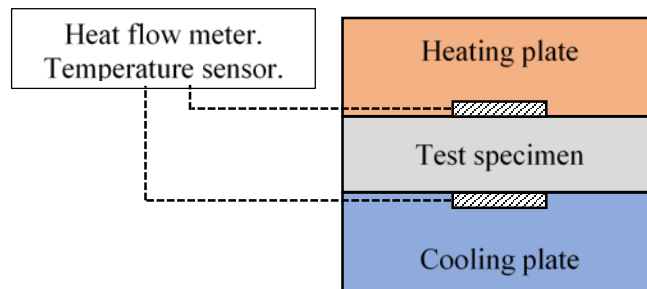


Figure 1. Configuration of a general HFM apparatus

ISO (1991) recommends that the calibration factor of HFMs should be a function of temperature, which is obtained by performing calibrations under multiple levels of temperature conditions using a calibration standard board having thermal conductivity close to that of the object of measurement. However, due to the unusually small thermal conductivity of VIP, no suitable calibration standard board for VIP exists.

Therefore, referring to ASTM (2015), we performed calibrations with the density of heat flow rate reduced to approximately the same level as VIP by reducing the temperature difference of a conventional calibration standard board. The calibrations were performed three types of HFMs (A, B, C), and in all cases, high density glass wool was used as the calibration standard board.

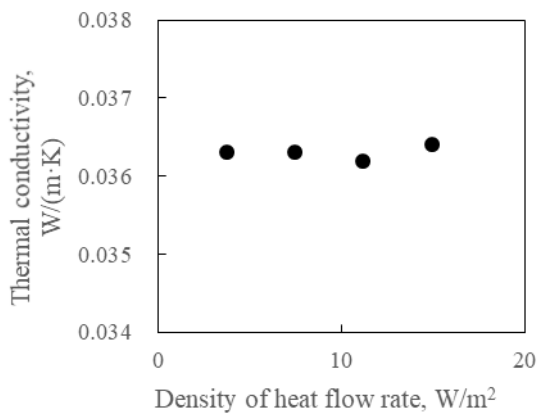
## RESULTS

Table 1 and Figure 2 show the results of the thermal conductivity measurements of the calibration standard board for each of the HFM apparatuses. It should be noted that the thermal

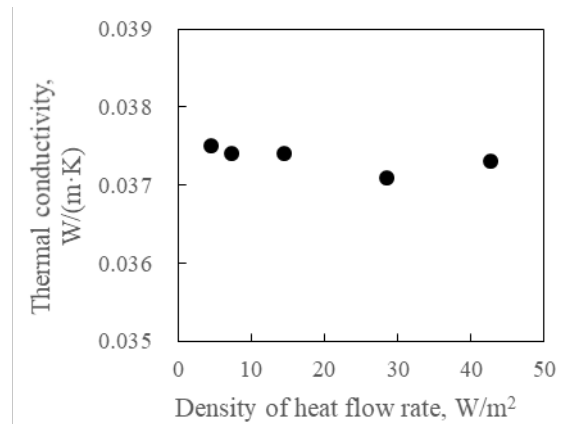
conductivities of the calibration standard board shown in Table 1 and Figure 2 are values that were calculated using a calibration factor set under the condition of a density of heat flow rate on the order of 20 to 30 W/m<sup>2</sup>. The density of heat flow rate when the thermal conductivity of VIP is measured is estimated to be 3 to 5 W/m<sup>2</sup>.

Table 1. Relationship between measured thermal conductivity and density of heat flow rate

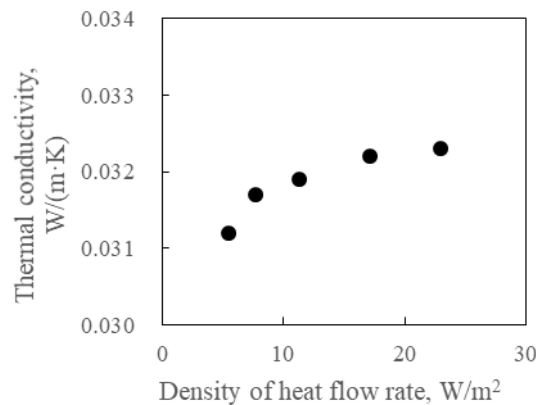
Apparatus	Calibration standard board	Mean temperature, °C	Density of heat flow rate, W/m <sup>2</sup>	Measured thermal conductivity of calibration standard board, W/(m·K)
A	GW1	23	14.97	0.0364
			11.18	0.0362
			7.46	0.0363
			3.74	0.0363
B	GW2	23	42.64	0.0373
			28.40	0.0371
			14.36	0.0374
			7.25	0.0374
C	GW3	23	4.44	0.0375
			22.95	0.0323
			11.09	0.0322
			11.27	0.0319
			7.75	0.0317
			5.46	0.0312
			3.04	0.0298
			1.96	0.0283



a) Apparatus A



b) Apparatus B



c) Apparatus C

Figure 2 Relationship between measured thermal conductivity and density of heat flow rate

## DISCUSSIONS

The following study was carried out based on the results shown in Table 1 and Figure 2.

It is considered that the A and B apparatuses can be used to measure VIP without correction of the calibration factor, as no obvious effect of differences in the density of heat flow rate on the measured values of thermal conductivity can be seen.

With the C apparatus, the effect of differences in the density of heat flow rate on the measured values of thermal conductivity could be seen, and the degree of that effect became remarkable as the density of heat flow rate became smaller. For this reason, this HFM apparatus should not be used to measure the thermal conductivity of VIP without resetting its calibration factor. In order to reset the calibration factor of the HFM as a function that depends on the density of heat flow rate, it is also necessary to consider temperature dependency at the same time. This means that a large number of temperature conditions must be set in the calibration. In this case, it is thought that the calibration should be conducted by an organization which also has a GHP apparatus and can set the values for the calibration standard plate in detail.

## CONCLUSIONS

The calibration factors at low density of heat flow rate, assuming measurement of VIP, were confirmed with three types of HFM apparatuses. As a result, it was found that the tendencies differed depending on the apparatus, indicating that it is necessary to perform a calibration assuming a low density of heat flow rate before measuring the thermal conductivity of VIP.

## ACKNOWLEDGEMENT

This research was carried out as part of a commissioned project of the Ministry of Economy, Trade and Industry (METI) of Japan, “FY2017-FY2018 Commission for Project for International Standardization and Dissemination of Energy Conservation (Development of International Standards for Energy Conservation, Etc. (International Standards Field) International Standardization of Measurement Methods, Etc. for Specific Heat of Thermal Insulation Materials,” Vacuum Insulation Materials Standardization Subcommittee, Chair: Prof. Atsushi Iwamae, Kindai University, Secretariat: Japan Testing Center for Construction Materials). We would like to take this opportunity to thank the members of the committee and all other related persons and organizations for their cooperation.

## REFERENCES

- ASTM. 2015: *ASTM C 1667-15*, Standard Test Method for Using Heat Flow Meter Apparatus to Measure the Center-of-Panel Thermal Resistivity of Vacuum Panels.
- ISO. 1991: *ISO 8301:1991*, Thermal insulation -- Determination of steady-state thermal resistance and related properties – Heat flow meter apparatus.

## Methods for renovation of Kyomachiya dwellings using vacuum insulation panels and evaluation of thermal-insulation performance

Yui Nakazawa<sup>1</sup>, Daisuke Ogura<sup>1</sup>, Chiemi Iba<sup>1</sup>, Hideya Yamamoto<sup>2,1</sup>

<sup>1</sup> Kyoto University, Kyoto, Japan

<sup>2</sup> ASAHI FIBER GLASS CO., LTD., Japan

\*Corresponding e-mail: nakazawa.yui.43m@st.kyoto-u.ac.jp

### ABSTRACT

The conservation of Kyomachiyas is required because the number of these traditional dwellings in Kyoto, Japan, has been decreasing year by year. One of the reasons is their poor thermal environment. Awareness of thermal-insulation retrofit is improving; however, applying a general retrofit method to Kyomachiya structures is difficult because of unique structural features such as the Shinkabe and narrow space between neighboring houses. Herein, we actually retrofitted a Kyomachiya by affixing vacuum insulated panel (VIP) on walls of compacted soil and embedded VIP to the Shinkabe. This study aimed to evaluate the insulating performance of thermally renovated walls using VIP and investigate temperature and humidity inside the insulated walls that affect long-term VIP performance. We found that the surface temperature of the inside walls was kept relatively constant compared to the uninsulated walls, and we gained an understanding of the properties of temperature and humidity inside the VIP-enhanced soil walls. We are proposing this renovation method as a way to help maintain these culturally important traditional dwellings, and in the future we would like to further research the connection between the temperature and humidity inside the walls and the long-term VIP performance.

### KEYWORDS

Insulation retrofit method, Vacuum insulation panels, Evaluation of thermal-insulation performance, Traditional dwelling, Soil wall

### INTRODUCTION

Today, the preservation of Kyomachiyas, a kind of traditional dwelling in Kyoto, Japan, has become a priority policy in Kyoto City (2017) from the several viewpoints, particularly cultural heritage and preservation of the townscape. However, the number of Kyomachiyas has been reduced because of demolition and several rebuilding reasons such as unsuitable room layout for the modern lifestyle, deterioration of traditional building material, and poor thermal environment. Additionally, because of the increasing awareness regarding importance of indoor health and energy conservation, concerns about thermal-insulation retrofitting have been rising. However, applying the prevailing retrofit methods to Kyomachiyas is difficult because of their unique structural features, such as the uninsulated soil wall with exposed timber pillars (hereafter referred to as Shinkabe) and the extremely narrow space between neighboring houses. Therefore, new renovation techniques are required.

In this research, we applied following two proposed thermal-insulation retrofit methods using vacuum insulated panel (VIP) to the thermal-insulation renovation of an existing Kyomachiya. First, installing VIPs inside the existing soil walls to achieve high insulation performance even in an outer wall, where attaching insulation panels from the outside is difficult. Second,

embedding VIP in the soil wall between the pillars to maintain unique appearance of a Shinkabe structure.

This study aims to evaluate the thermal-insulation performance of renovated walls using VIP by measuring the temperature and humidity inside the wall that affect the long-term performance of VIP. Specific methods and results are presented below.

## METHODS

The survey site for this research is a two-story Kyomachiya located in Kyoto. The total floor area is 74 m<sup>2</sup>. Figure 1 shows the locations where thermal insulation was applied, Table 1 lists the specifications of the VIP used for the thermal-insulation renovation, and Figure 2 shows the appearance of the VIP renovation construction. The thermal-conductivity value of the VIP used herein is the average value considering the thermal bridge effect. We calculated the thermal-conductivity considering area ratio of thermal resistance of VIP part and other parts. VIPs were added to the north wall of the first-floor toilet and south wall of the bedroom with average thermal conductivities, 13.6 and 21.4 mW/m·K, respectively. A micro-vacuum sensor was mounted inside the VIP of the north wall of the first-floor toilet, and pressure in the VIP was measured at certain intervals. Above the living-room window, VIP (thermal conductivity, 4.11 mW/m·K) wrapped by a nonwoven fabric film was embedded in the east soil wall with extra wall mud. Sensors were attached to the indoor and outdoor surfaces of the embedded VIP, and the temperature and humidity inside the soil wall were measured every 30 min.

## RESULTS and DISCUSSION

Temperature and humidity of the soil wall in which the VIP had been embedded, measured in the summer of 2018, are shown in Figure 3. When we compared the surface temperatures of the outer and inner sides of the embedded VIP, we found that the inner surface was 1°C–3°C cooler. When we compared the inner surface temperature of the uninsulated soil wall with that of the VIP, the uninsulated soil wall was 2°C warmer during the daytime. The temperature in the VIP-embedded soil wall varied less than that in the uninsulated soil wall, thereby confirming the improved thermal-insulation performance afforded by VIP. The relative humidity in the VIP-embedded soil wall remained at 50%–60%, and was kept relatively constant in spite of changed humidity of the outside air, apparently because of sufficient humidity buffering performance of the soil walls. Table 2 shows the change in pressure and thermal conductivity in the VIP in the north-side wall of the first-floor toilet. To calculate thermal conductivity, we used the equation

$$\lambda_{cop} = \lambda_{sr,ini} + \lambda_{ga,0} / (1 + \frac{P_{1/2}}{P_a}), \quad (1)$$

where  $\lambda_{cop}$  is thermal conductivity at the center of the panel,  $\lambda_{sr,ini}$  is initial thermal conductivity,  $\lambda_{ga,0}$  is gaseous thermal conductivity,  $P_{1/2}$  is fitting pressure, and  $P_a$  is pressure inside the VIP (H. Simmler, S. Brunner, 2005). Immediately after construction, the internal pressure increased rapidly, but the amount of increase thereafter was relatively small (Table 2). The final thermal conductivity of VIP in the panel was about 2.88 mW/m·K, which is slightly higher than the design value. No major performance degradation of VIP was confirmed during about eight months of measurements.

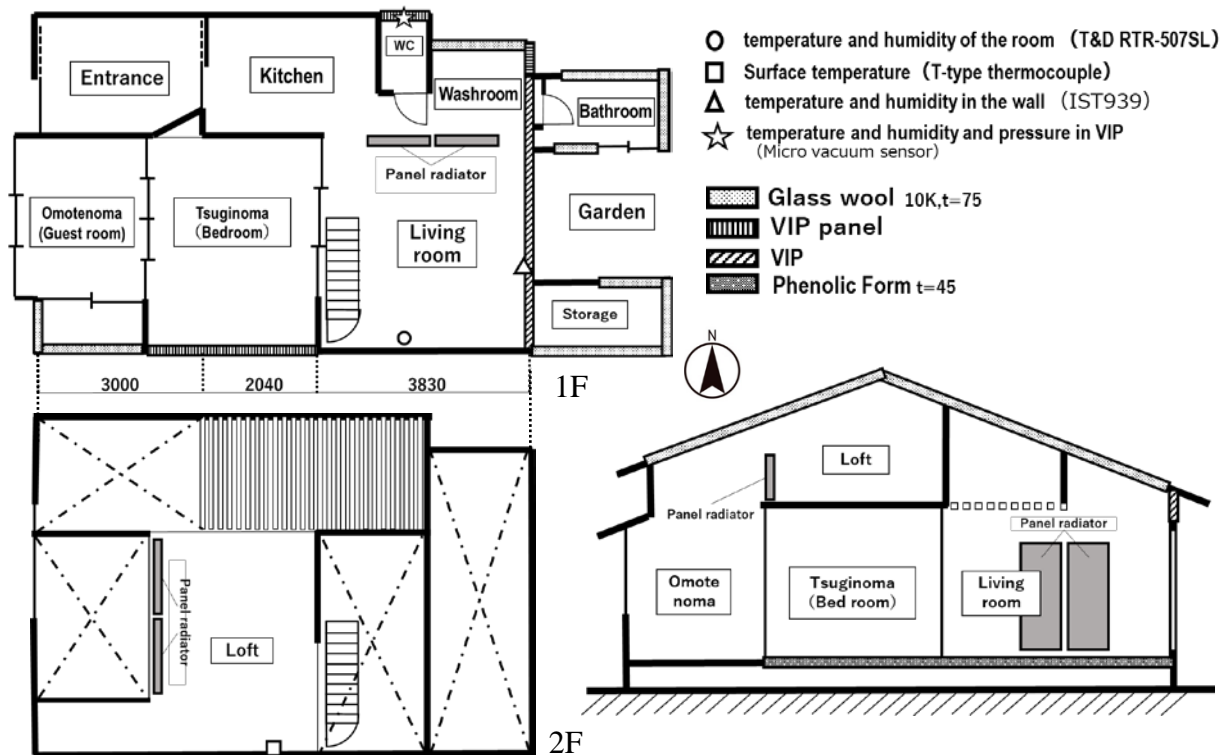


Figure 1 Locations of thermally renovated walls and measurement points

Table 1 Specification of VIP used for thermal-insulation renovation. [EVOH, ethylene vinyl alcohol; VIP, vacuum insulated panel]

Location	In clay walls	North wall of 1st floor toilet		South wall of bedroom	
Type	VIP	VIP	VIP panel	VIP	VIP panel
Thickness [mm]	6	12	18	11	18
Width [mm]	240–750*	735	850	355	910
Length [mm]	220–1010*	795	1820	355	1820
Thermal conductivity* [mW/m·K]	4.11	2.73	13.6	4.5	21.4
Core material	Fumed silica	Glass fiber		Fumed silica	
Film	EVOH film A (with nonwoven surface)	EVOH film B		EVOH film B	

\* Average thermal conductivity considering thermal bridge effect

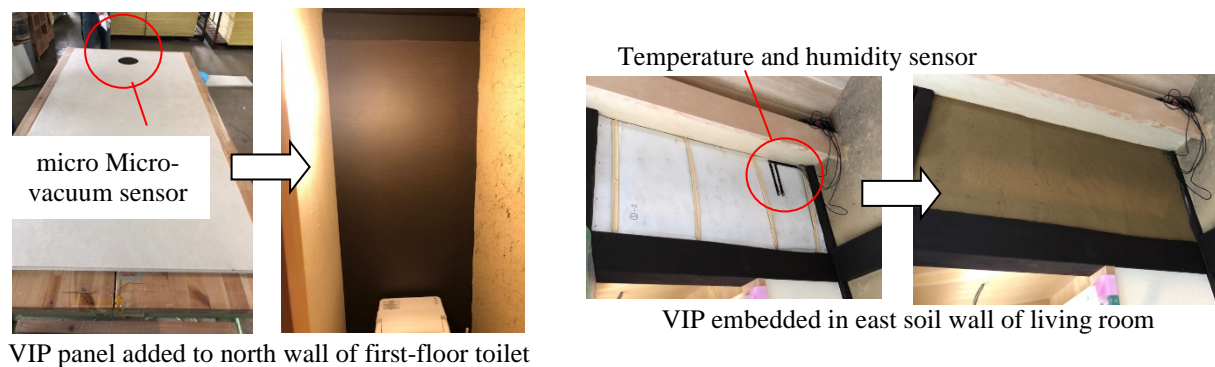


Figure 2 Appearance of VIP renovation construction

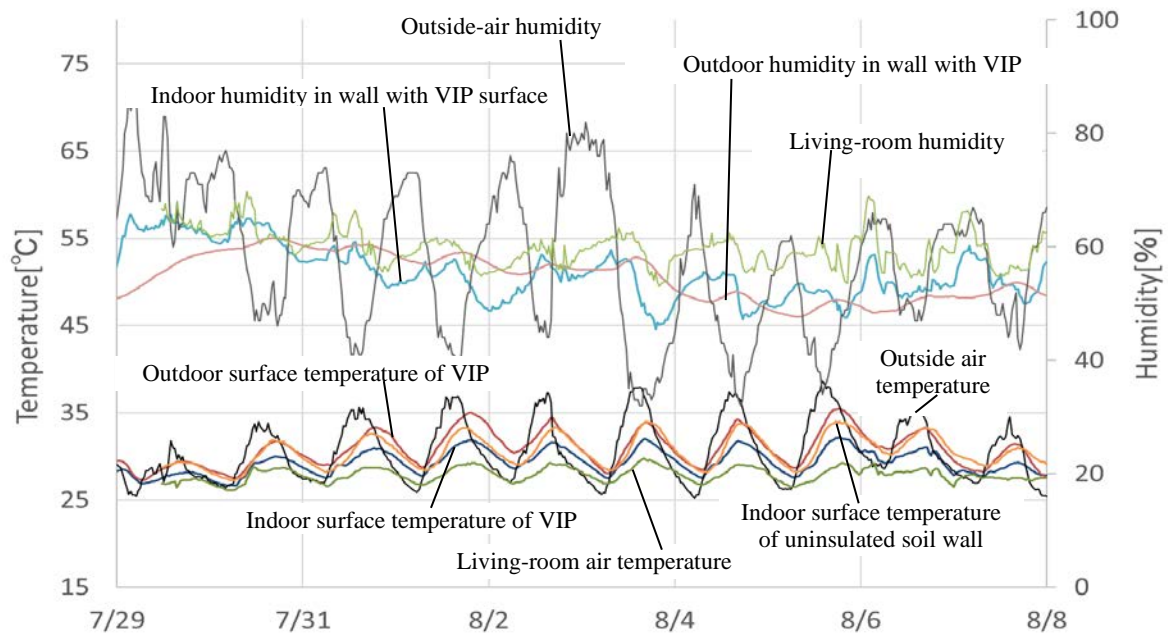


Figure 3 Measurement results of temperature and humidity in VIP-embedded soil wall, summer 2018

Table 2 Change in pressure and thermal conductivity in VIP

Day	Internal pressure [Pa]	Thermal conductivity [mW/m·K]
6/1/2018	4.8	2.19
6/6/2018	8.1	2.44
9/10/2018	12.3	2.77
1/31/2019	13.8	2.88

## CONCLUSIONS

As shown by measurement results for the renovated Kyomachiya, the inner-surface temperature of the thermally insulated wall was kept relatively constant compared to the uninsulated wall, and the characteristics of temperature and humidity changes inside the VIP-embedded soil wall were clarified. Although we already propose this renovation method as one that preserves the townscape of the traditional Kyomachiya house, we suggest further research in the future. The relation between temperature and humidity in the wall and long-term performance of VIP should be examined in more detail to measure thermal transmissivity using thermal-imaging methods.

## ACKNOWLEDGEMENT

The authors would like to express their appreciation to the Kyomachiya residents for their generous cooperation.

## REFERENCES

- H. Simmler, S. Brunner, 2005. Vacuum insulation panels for building application Basic properties, aging mechanisms and service life.
- Kyoto City, 2017. About the results of the follow-up survey pertaining to the Kyomachiya town development survey.
- Sustainable open Innovation Initiative, 2018. Next-generation energy saving building materials support project.

## Prediction on Long-term Thermal Performance of VIP using Glass Fiber Core Considering Influence of Getter

Taichi Tasaka<sup>1,\*</sup>, Daisuke Ogura<sup>2</sup>, Atsushi Iwamae<sup>3</sup>, Kensaku Mabuchi<sup>1</sup> and Hideya Yamamoto<sup>4</sup>

<sup>1</sup>Japan Testing Center for Construction Materials, Saitama, Japan

<sup>2</sup>Kyoto University, Kyoto, Japan

<sup>3</sup>Kindai University, Osaka, Japan

<sup>4</sup>Asahi Fiber Glass Co., Ltd., Kanagawa, Japan

*\*Corresponding e-mail: tasaka@jtccm.or.jp*

### ABSTRACT

Recently, various studies have been conducted on methods for predicting long-term thermal performance of VIP. However, the long-term thermal performance of VIP using glass fiber core is not sufficiently clarified in terms of influence of adsorbent (especially getter). Therefore, we conducted an aging test under various conditions and clarified the trend of thermal conductivity change. In addition, a prediction method was constructed based on these results; it was confirmed that the long-term thermal performance of VIP with getter under the standard condition can be roughly predicted from the ratio of the VIP with getter under the accelerated condition and the amount of inner pressure change of the VIP without getter.

### KEYWORDS

Long-term thermal performance, Glass fiber core material, Getter

### INTRODUCTION

Our previous report <sup>[1]</sup> clarified the thermal conductivity change of glass fiber core material VIP without getter under constant temperature and humidity environments, and also proposed a method for prediction of its long-term performance. Although the thermal conductivity changes of glass fiber core material VIP with getter is small in comparison with that of glass fiber core material VIP without getter, the effect of getter on the thermal conductivity change of glass fiber core material VIP is still largely unknown. Moreover, methods for prediction of the long-term performance of glass fiber core material VIP with getter also have not been studied.

Therefore, in this research, we measured the thermal conductivity change of glass fiber core material VIP under various constant temperature and humidity environments, and clarified the effect of the presence or absence of getter on the thermal conductivity change of the glass fiber core material VIP. In addition, we studied a method for prediction of the long-term performance of glass fiber core material VIP with getter based on the results of measurements of the thermal conductivity change.

### MEASUREMENTS ON THERMAL CONDUCTIVITY CHANGE TEST SPECIMENS

An outline of the samples is shown in Table 1. A total of four samples were studied, with specifications comprising two types of glass fiber core material VIP with or without getter. In all the samples, the envelope material is an aluminized (aluminium vapour-deposited) composite film using EVOH film as the base material, and the getter is a zeolite-based physical adsorption-type adsorbent. It may be noted that No.1 and No.2 are different products.



## TEST METHOD

Measurements were performed by the following procedure.

- (1) Measure the initial thermal conductivity for centre of panel in accordance with ISO 8301. The measurement conditions shall be a mean temperature of 23 °C and a temperature difference of 20 K.
- (2) Condition the sample in a constant temperature and humidity chamber set to the temperature and humidity shown in Table 1 for a period of from 3 months to 6 months.
- (3) Remove the sample from the constant temperature and humidity chamber at appropriate time intervals, and measure the thermal conductivity for centre of panel after the passage of time in accordance with ISO 8301.
- (4) Separately, obtain the relational expression for the thermal conductivity and inner pressure of a glass fiber core material VIP of the same specification as the sample.
- (5) Using the relational expression for the thermal conductivity and inner pressure, convert thermal conductivity to inner pressure, and obtain the amount of change in inner pressure per unit time for the sample.

Table 1 Test specimens and test conditions

No.	Adsorbent		Size of core material (mm)	Thickness (mm)	Quantity (pieces)	Environmental conditions <sup>Note)</sup>		
	Desiccant	Getter				23 °C / 50 %	50 °C / dry	80 °C / dry
1	○	—	300 × 500	15	3	○	○	○
	○	○	300 × 500	15	3	○	○	○
2	○	—	200 × 300	15	3	○	○	○
	○	○	200 × 300	15	3	○	○	○

Note) For 50 °C / dry and 80 °C / dry (hereinafter, called “accelerated conditions”), the absolute humidity was set to the same level as used with 23 °C / 50 % (hereinafter, called the “standard condition”).

## TEST RESULTS AND DISCUSSION

The measurement results of the thermal conductivity change are shown in Fig. 1, and the calculation results of the inner pressure change are shown in Fig. 2. With both No.1 and No.2, the samples with the getter showed a tendency to have smaller thermal conductivity change than the samples without the getter under the same test conditions. In particular, in the case of No.1 with the getter, no clear change in thermal conductivity could be observed under the standard condition.

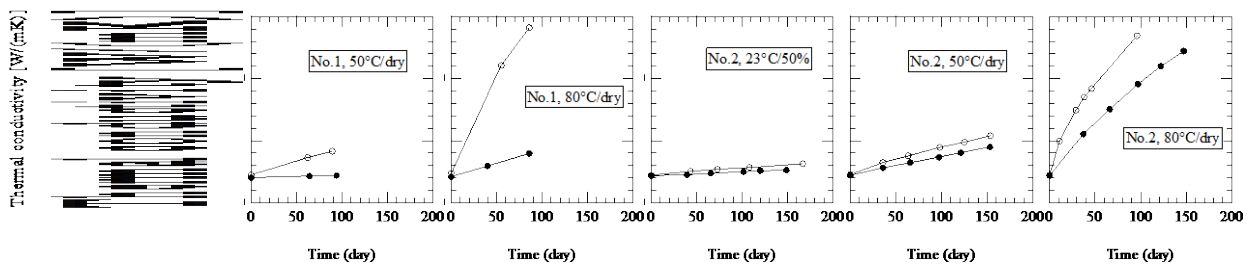


Figure 1. Measurement results of thermal conductivity change

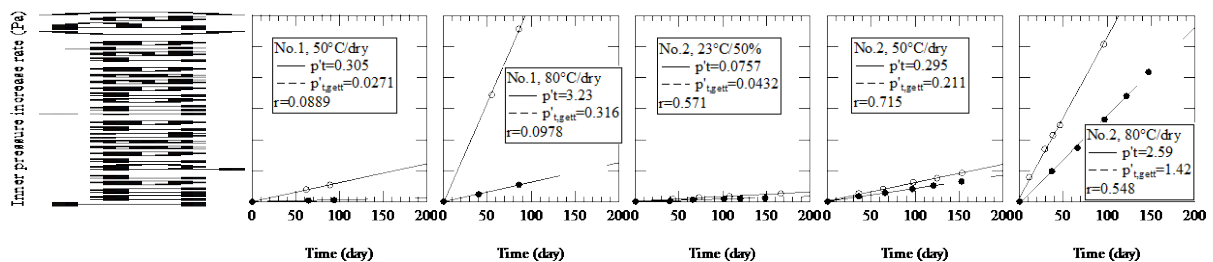


Figure 2. Calculation results of inner pressure change

## PREDICTION ON LONG-TERM PERFORMANCE OF VIP WITH GETTER STUDY ON PREDICTION METHOD

In our previous report <sup>[1]</sup>, we showed that it is possible to predict the long-term performance of glass fiber core material VIP without getter by Eq. (1). On the other hand, in glass fiber core material VIP with getter, inner pressure increases due to gaseous components which are contained in dry air that leaks into the VIP but cannot be adsorbed by the getter. For this reason, Eq. (1) cannot be applied as-is to glass fiber core material VIP with getter. Moreover, under the standard condition, there were cases in which no clear thermal conductivity change could be recognized. Precise estimation of the proportion of residual dry air is difficult in this case. Therefore, we studied a method for prediction of the long-term performance of glass fiber core material VIP with getter based on the thermal conductivity change under accelerated conditions. The study was carried out under the following assumed conditions, based on the measured results of thermal conductivity change.

- Assumption 1: Penetrated gases through the film into the VIP can be adsorbed by the getter instantaneously.
- Assumption 2: The relationship between the inner pressure of dry air and thermal conductivity remains if the dry air components is absorbed by the getter.
- Assumption 3: The proportion of the gas component of the dry air remaining in the VIP with getter do not depends on the surrounding environment. It is constant irrespective of conditions.

As shown in Fig. 2, the inner pressure change of the glass fiber core material VIP is regarded as roughly constant with or without getter. Moreover, even if there are changes in the temperature and humidity conditions of the atmosphere, the relationship in Eq. (2) is materialized if the component ratio of the dry air remaining in the VIP is assumed to be constant. Accordingly, the change of the thermal conductivity of the glass fiber core material VIP with the getter is expressed by Eq. (3), and in case the three above-mentioned assumed conditions are satisfied, the change of thermal conductivity under the standard condition can be predicted from the results of measurements under the accelerated conditions.

$$\lambda_{cop} = \lambda_{sr} + \frac{\lambda_{ga,0}}{1 + \frac{p_{1/2}}{p(0) + p'_{t,air} \cdot t}} \quad (1)$$

$$r = \frac{p'_{t,air,gett,23/50}}{p'_{t,air,23/50}} = \frac{p'_{t,air,gett,acc}}{p'_{t,air,acc}} \quad (2)$$

$$\lambda_{cop} = \lambda_{sr} + \frac{\lambda_{ga,0}}{1 + \frac{p_{1/2}}{p(0) + p'_{t,air,gett} \cdot t}} = \lambda_{sr} + \frac{\lambda_{ga,0}}{1 + \frac{p_{1/2}}{p(0) + p'_{t,air} \cdot r \cdot t}} \quad (3)$$

Where,  $\lambda_{cop}$  : thermal conductivity for centre of panel [W/(m·K)],  $\lambda_s$  : solid thermal conductivity [W/(m·K)],  $\lambda_g$  : gaseous thermal conductivity [W/(m·K)],  $\lambda_r$  : radiative thermal conductivity [W/(m·K)],  $r$  : ratio of inner pressure increase rate with / without getter (-),  $p'_{t,air,gett,23/50}$  : inner pressure increase rate of the sample with getter under the standard condition (Pa/day),  $p'_{t,air,23/50}$  : inner pressure increase rate of the sample without getter under the standard condition (Pa/day),  $p'_{t,air,gett,acc}$  : inner pressure increase rate of the sample with getter under the accelerated conditions (Pa/day),  $p'_{t,air,acc}$  : inner pressure increase rate of the sample without getter under the accelerated conditions (Pa/day),  $\lambda_{sr}$  : solid and radiative thermal conductivity [W/(m·K)],  $\lambda_{ga,0}$  : dry air thermal conductivity [W/(m·K)],  $p_{1/2}$  : inner pressure of VIP, where increases by 1/2 of the thermal conductivity of still air (Pa),  $p(0)$  : initial value of the inner pressure (Pa),  $t$  : time (day)

## PREDICTION RESULTS AND DISCUSSION

To verify the appropriateness of the prediction model studied here, the thermal conductivity change over a 25-year period under the standard condition was predicted using the results of calculations of the proportion of residual dry air under the standard condition and the accelerated conditions. The prediction results are shown in Fig. 4. Prediction results 1, 2 and 3 are the results of predictions of the thermal conductivity change over the 25-year period by Eq. (3) using  $r_{23/50}$ ,  $r_{50/dry}$  and  $r_{80/dry}$ , respectively. Comparing the average thermal conductivity over the 25-year period, the difference of the prediction results was within 15 % for both No.1 and No.2. Thus, the obtained results were approximately in agreement.

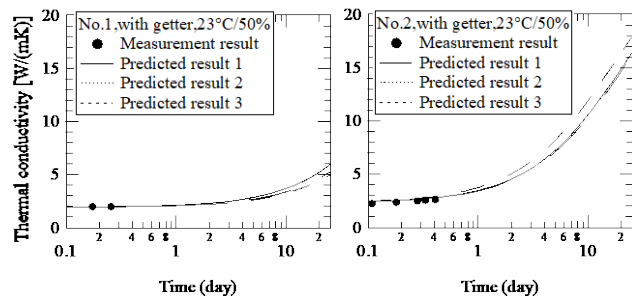


Figure 4. Result of prediction of change in thermal conductivity over 25-year period

## CONCLUSION

The thermal conductivity changes of glass fiber core material VIP with and without getter was measured. The results clarified the fact that the change in thermal conductivity of the glass fiber core material VIP with getter is small in comparison with the same glass fiber core material VIP without getter.

In addition, a method for prediction of the thermal conductivity change of glass fiber core material VIP with getter was studied based on the measured results of the thermal conductivity change, and the measured results of the thermal conductivity change were analyzed using the prediction method studied here. The results confirmed that the thermal conductivity change under the standard condition can be predicted with approximate accuracy from the results of measurements of the thermal conductivity change under accelerated conditions by a prediction method using the proportion of residual dry air. However, the question of whether this prediction method can also be applied in the case of getters having adsorption characteristics different from those of the getter used in the research is a problem for future study.

## ACKNOWLEDGEMENT

This research was carried out as part of a commissioned project of the Ministry of Economy, Trade and Industry (METI) of Japan, “FY2017-FY2018 Commission for Project for International Standardization and Dissemination of Energy Conservation (Development of International Standards for Energy Conservation, Etc. (International Standards Field) International Standardization of Measurement Methods, Etc. for Specific Heat of Thermal Insulation Materials,” Vacuum Insulation Materials Standardization Subcommittee, Chair: Prof. Atsushi Iwamae, Kindai University, Secretariat: Japan Testing Center for Construction Materials). We would like to take this opportunity to thank the members of the committee and all other related persons and organizations for their cooperation.

## REFERENCES

- [1] Ogura D., Iwamae A. et al. 2017. Prediction on Long-term Thermal Performance of Vacuum Insulation Panels (VIP) using Glass Fiber Core Considering Differences in Hygrothermal Environment and Size of VIP and Influence of Desiccant. In: Proceedings of the 13th International Vacuum Insulation Symposium (IVIS 2017), Paris, France, September 20-21, 2017, pp. 142-144.

## Wood-fibre panels as core material for VIP

Sebastian Treml<sup>1,\*</sup>, Max Engelhardt<sup>2</sup> and Elisabeth Windeisen-Holzhauser<sup>2</sup>

<sup>1</sup>Forschungsinstitut für Wärmeschutz e. V. München, Gräfelfing, Germany

<sup>2</sup>Technische Universität München, Holzforschung München, München, Germany

\*Corresponding e-mail: [treml@fiw-muenchen.de](mailto:treml@fiw-muenchen.de)

### ABSTRACT

The utilization of wood-fibre panels (WF) as core materials for vacuum insulation panels (VIP) can provide advantages in terms of LCA, costs and process of manufacture. To clarify the principle feasibility, this paper describes preliminary studies to compare the thermal conductivity, the sorption isotherms and the outgassing behaviour of evacuated WF panels with conventional fumed silica-based (SI) core materials. The thermal conductivity of the exemplary chosen standard WF panel in the evacuated state reaches values of ca. 0.007 W/(m·K). A comparison of the sorption isotherms shows higher moisture contents of the WF but distinct hysteresis effects are measured also for SI that should be considered with respect to annual variations in moisture distribution. The outgassing behaviour shows higher pressure increase rates for the WF panels.

### KEYWORDS

Sustainable core material, renewable resources, wood fibre boards

### INTRODUCTION

WF panels are available in a variety of densities (50 – 220 kg/m<sup>3</sup>), thicknesses (10 – 300 mm), as well as mechanical and microstructural characteristics, offering a cheap, homogenous and easily machinable raw material with only a little dust formation during the handling. In comparison to conventional core materials made from SI or mineral fibre, the utilisation of WF panels is generating a carbon sink over the lifetime of the VIP panel and can thereafter be recycled or used for CO<sub>2</sub>-neutral energy production. Despite these advantages in terms of availability, costs and LCA, the natural wood extractives are likely to outgas over time if kept under vacuum conditions and sorption behaviour has to be considered.

### MATERIAL AND METHODS

For the exemplary study described in this paper, a wet process board (WF) with a nominal thickness of 22 mm and a raw density of ca. 170 kg/m<sup>3</sup>, as well as standard silica (SI) core materials are used.

#### Thermal performance of wood fibre insulation boards in evacuated condition

For thermal conductivity measurement the guarded hot plate method acc. to DIN EN 12667 is applied (< 2 % uncertainty for standard insulation materials). A vacuum-tight connector similar as described in Carmi 2013 allows evacuation and equipping a pressure gauge. With the adapter base and the WF panel (directly out of the dry kiln at 103 °C) placed next to each other, the barrier film bag is sealed (Figure 1, left). The panel is evacuated for 24 h prior to and during the measurements to an internal pressure equilibrium of ca. 0.03 mbar. At this pressure and at 20 °C, the mean free path of residual air molecules is greater than 2 mm (cf. table 17.6 in Wutz et al., 2000, p. 668), which is well above the average scale of cavities in wood insulations. Therefore, gaseous thermal convection can be considered approximately

zero. The measurements are conducted at a temperature difference of 10 K and average specimen temperatures of -50 °C and +40 °C.

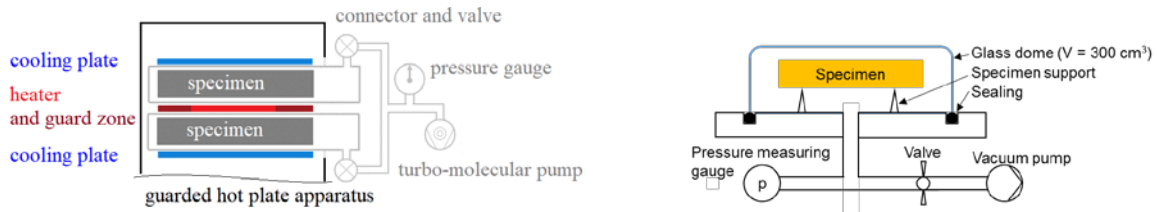


Figure 1. Left: Principle sketch of measurement equipment to determine the thermal conductivity of evacuated wood fibre insulation at known internal pressure. Right: Principle sketch of measurement equipment to determine the outgassing intensity of several core materials with a gas flow-rate measurement

### Outgassing of vacuum insulation core material

To compare the outgassing of the WF panel with standard SI based core materials under vacuum condition, a gas flow-rate measurement was performed acc. to Figure 1 (right). The glass dome has a volume of ca. 300 cm<sup>3</sup>. Underneath, the specimens with dimensions ca. 60 x 60 x 20 mm are placed on a support. The glass dome is sealed to a valve cluster for evacuation and equipping a pressure gauge. After inserting the test specimen the valve to the vacuum pump is opened immediately. Thus the pressure in the glass dome is going down to a specific end value dependent from the outgassing of the specimen and the surrounding environment. To eliminate moisture desorption during the test run, the specimens are pre-conditioned for ca. 12 h in a ventilated oven at 103°C. The temperature and time frame is chosen to ensure absolute drying of the wood-based specimen without provoking pyrolytic disintegration of the constitutive parts of the cell wall (cellulose, hemicellulose, lignin and extractives) respective the binder and additives of the wood based material. For reference, the empty glass dome and a standard SI core material are examined with similar dimensions and identical pre-conditioning.

### Determination of sorption isotherms

Sorption isotherms of the WF panel and an exemplary SI core material were measured by means of a proUmid SPSx-1μ “high load” dynamic vapour sorption analysis for a temperature of 23 °C and a relative humidity in the range of 0 – 98 %.

## RESULTS

### Thermal performance of WF insulation boards in evacuated condition

The measurements of thermal conductivity in evacuated state and at standard atmospheric pressure are shown in table 1. For the thermal conduction of the solid material, a constant thermal conductivity can be assumed. Therefore, the equivalent thermal conductivity of the evacuated specimen at different temperatures is fitted to a function of  $\lambda_{evac}(T) = \lambda_{r+s}(T) = k_{rad} \cdot T^3 + \lambda_s$  (simplified radiative heat transfer model, cf. Cremers 1972). The difference to the equivalent thermal conductivity  $\lambda_{atm} - \lambda_{evac}$  represents the remaining heat transfer mechanisms of conduction and convection of the gases as well as coupling effects and is fitted with a good approximation to  $\lambda_{g+c} = AT^2 + BT$ . Thus, the contributions of the different heat transfer are estimated for a mean temperature of 10 °C. The conduction in the solid phase contributes only 0.002 W/(m·K), the radiation between cavities contributes 0.005 W/(m·K) and the majority of 0.031 W/(m·K) is due to the prevalent air. The evacuation is reducing the thermal conductivity of the WF board by over 80 %.

Table 1. Results of thermal conductivity measurement on evacuated and non-evacuated WF panels in W/(m·K)

average temperature	-48 °C	-20	+10	+38
evacuated state	0.0047	0.0054	0.0073	0.0089
standard pressure	–	–	0.384	0.416

### Outgassing of vacuum insulation core material

Low outgassing rates of the core material are crucial for the development of VIP panels with durable low thermal conductivity. Compared to the reference empty glass dome latest after 1000 sec. of evacuation time the final pressure of the test setup is reached for both WF and SI core materials (Figure 2). However, the WF core material shows higher outgassing during the first 1000 s of total 22.4 mol compared to SI with total 3.7 mol (calculated acc. to the exhaustion rate of the vacuum pump and based on the assumption of ideal gas behaviour).

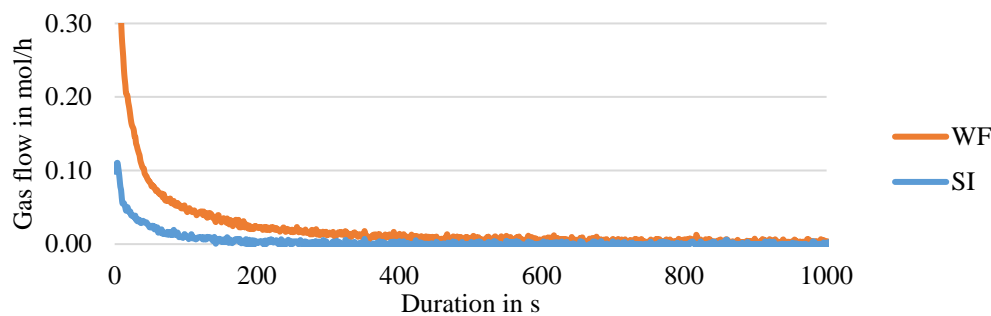


Figure 2. Outgassing of WF and exemplary SI core material

### Sorption behaviour

Although similar mass related moisture contents (m-%) in the range of ca. 27 – 33 m-% are reached by both materials for a relative humidity of 98 %, the course of the isotherm functions differs clearly. The WF insulation board shows in general, a higher level of moisture uptake compared to silica core materials. However, remarkable is the distinct hysteresis effect with values between 1.5 – 2.5 m-% in the relevant range of relative humidity, visible also for the SI core materials.

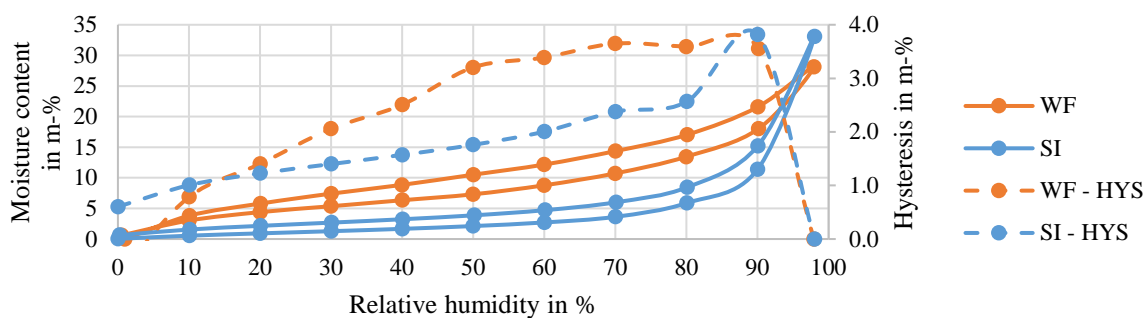


Figure 4. Sorption isotherms and hysteresis at 23°C for WF and exemplary SI core material

### DISCUSSIONS

The thermal conductivity of evacuated WF board offers a competitive performance compared to other alternative core materials like perlite, while on the other hand the hygroscopic behaviour will induce higher moisture contents compared to standard SI cores, at least for the expected mean relative humidity of 50 % representative for long term applications in the construction sector (Tremel et al. 2017). However, also for SI core materials the annual cycle of water uptake due to dewing phenomena on the cold side of the VIP panel and subsequent

redistribution of the moisture in the transitional period, leads to moisture contents acc. to the desorption curve. In this manner, also the high hysteresis effects for SI based core materials have to be considered.

Outgassing behaviour of WF shows potentially more severe pressure increase rates by time, presumably due to volatile organic compounds of the wood fibres or additives, which should be mitigated by the application of suitable pretreatment procedures. The applied outgassing method is only suitable to detect short term desorption effects. The detection of slow rate and long term desorption phenomena requires modified setups.

## OUTLOOK AND CONCLUSION

To assess the impact of the outgassing processes and the moisture uptake on thermal performance during the lifetime of the VIPs, the relationship between internal pressure, moisture content and thermal conductivity of the core material is of importance. Therefore thermal conductivity measurements in the range of  $10\text{E-}2$  mbar to 1 atm and moisture contents up to 10 m-% (desorption curve for 50 % r.h.) will be conducted for typical WF insulation products.

As wood contains numerous extractives it is important to identify the mixture of substances that evaporate from the WF boards to develop adequate methods for stabilization of the internal pressure. Therefore the outgassing effects will be investigated via chemical analysis e. g. by evolved gas analysis (EGA, cf. Heigenmoser et al., 2011) in the lower temperature range to quantify the amounts of volatile compounds depending on core material and pre-treatment. By utilizing highly sensitive solid-phase extractions elements for gas chromatography/mass spectrometry (GCMS) or via pyrolysis–GCMS those compounds can be identified.

Provided that internal pressure can be stabilized, WF boards based on renewable resources can be identified as an interesting alternative to standard core materials like SI or mineral fibre.

## ACKNOWLEDGEMENT

The authors are grateful that parts of the work were funded by the German Federal Ministry of Food and Agriculture due to a decision of the German Parliament.

## REFERENCES

- Carmi Y. 2013 Accurate Prediction of the Lifetime Performance of VIPs: Challenges and Working Solutions. In: Proceedings of the 11th International Vacuum Insulation Symposium -, Dübendorf, Switzerland, September 19–20, 2013, pp. 55-57.
- Cremers, C. J. 1972 Thermal Conductivity of Apollo 14 Fines. In: Proceedings of the Lunar Science Conference, 3:2611–2617.
- Heigenmoser A., Fuchs R., Windeisen E., Wegener G. 2011 Characterization of different wood samples using a new combined method of evolved gas analysis and pyrolysis–gas chromatography/mass spectrometry. In: *Wood Sci Technol* 46, Springer, Berlin, p. 637f.
- Treml S., Sprengard C., Engelhardt M. 2017 Calculation of increase of thermal conductivity of Vacuum Insulation Panels (VIP) acc. to differing climate influences. In: 13<sup>th</sup> International Vacuum Insulation Symposium, September 20-21, 2017, Abstract Book
- Wutz M., Adam H., Walcher W., Joustel K. 2000 *Handbuch Vakuumtechnik Theorie und Praxis* 7., erweiterte Auflage, Friedr. Vieweg

## Studying the effect of surface chemistry on the mechanical properties of silica nano-structures through atomistic simulations

Wassim Kassem<sup>1</sup>, Julien Morthomas<sup>1,2,\*</sup>, Patrice Chantrenne<sup>1,2</sup> and Genevieve Foray<sup>1,2</sup>

<sup>1</sup>INSA-Lyon, MATEIS CNRS UMR5510, Villeurbanne, France  
France

<sup>2</sup>Université Claude Bernard Lyon 1, Villeurbanne, France

*\*Corresponding e-mail: julien.morthomas@insa-lyon.fr*

### ABSTRACT

Silica aerogels have some of the best thermal insulation properties. Their low thermal conductivity is due to their fractal morphology characterized by a distribution of pore sizes between 2 and 50 nm as well as a very high surface area. Unfortunately, this characteristic structure is also responsible for their brittleness. At the atomic level, the fibrous structure of aerogels is described as a network of interconnected silica nano-spheres also known as primary particles, with dead dangling arms. Moreover, the presence of surface hydroxyl groups (Si-OH) and surface methyl groups (Si-O-CH<sub>3</sub>) on silica is known to influence both surface morphology and the macroscopic properties of the aerogels through some simple simulations as well as experiment.

Here, we conduct molecular dynamics simulations of silica nano-structures, such as nano-wires and nano-spheres under various silanol (Si-OH) concentrations. The nanostructures represent the underlying building blocks of the aerogel morphology. Using a recent powerful inter-atomic potential (ReaxFF) we can also accurately model hydroxyl-silica interactions and see how it affects the connectivity and “bulk” properties of a network of interconnected silica nano-spheres. Using the information derived from atomistic simulations, we are able to draw useful conclusions and link mechanical properties with textural ones. Those results can then be used as input-data for models at larger scale.

### KEYWORDS

Molecular Dynamics, Silica, ReaxFF, Mechanical properties, Aerogels

### INTRODUCTION

Silica aerogel are the lightest solids known to man. Their unique fractal structure can be thought of as a 3D network of interconnected nanoparticles (NPs) with a size distribution of 3 to 100 nm. Smaller particles called Primary Particles. They are essentially nano-sized spheres of silica with a glass-like or dense amorphous structure. Secondary Particles are then agglomerations of Primary Particles. The Secondary Particles link up at contact points to form the macro-scale solid network which is the aerogel.

Their unique fractal microstructure impedes heat transfer via conduction (through the solid backbone) as well as convection (through the air particles diffusing through the nanopores). Their main weakness; on the other hand, is their poor mechanical properties. They have low mechanical strength and their fracture behaviour is brittle.



Chemistry plays a big part in the tailoring aerogel thermo-mechanical properties. Different chemical treatments before and after supercritical drying, as well as the procedure for drying, affects properties such as density, mechanical strength, and surface characteristics (Buratti, 2019). It is believed that controlling surface hydroxyl and methyl groups, such as -OH and -COH, is the key to controlling network connectivity and stiffness and plays an important role in determining the final mechanical strength of the aerogel.

Our aim in this work is to study this link between surface chemical groups and mechanical properties of silica Primary NPs using molecular dynamics simulations (MD) with a reactive inter-atomic potential. Reactive-MD is one of the best choices for a problem like this one, and has successfully reproduced both the mechanical properties of amorphous silica (Chowdhury et al., 2016; Yu et al., 2016) and hydroxylation kinetics (Rimsza et al., 2016; Yeon and van Duin, 2016). It offers atomic-scale resolution of deformation events with the important benefit of modelling chemical reactions. The reactions in question are the key to modification of surface properties they include bond creation and breaking and are essential for modelling defect structures and dangling bonds in  $\alpha$ -SiO<sub>2</sub>. Previous studies have alluded to the effect of surface structure on the mechanical properties of amorphous silica nanoparticles (Gonçalves et al., 2018).

In this work, we would like to shed light on how surface chemistry, and then surface properties, impede the mechanical behaviour of silica NPs and nanowires (Zhang et al., 2015).

## METHODS

The materials studied are silica aerogel nanowires and nanospheres,

For the nanowires (NWs) we vary the diameter and height as well as the amount of OH substituted on the surface (between 0.1 and 0.7 OH/nm<sup>2</sup>). The NWs are created using a cutting method from a bulk sample. Typical volumes studied are a few 10 of cubic nanometers in dimension, and up to 50000 atoms. The nanowires are deformed at a constant strain rate of 10<sup>9</sup> s<sup>-1</sup> using an affine transformation of the simulation box.

For the spheres (SPs) we numerically create R=2.0, 3.0 and 3.5 nm spheres that are subjected to compression tests; again with and without surface hydroxyl groups. Simulations contained between 2000 and 15000 atoms including Si, O, and H. The compression tests were performed using a virtual platen indenter.

We used the LAMMPS code with the included reax/c package for simulation and inter-atomic force calculation. The initial atomic coordinates were random, so the system is relaxed using a combination of energy minimization and dynamic relaxation using a heating-quenching scheme.

After equilibration we performed either indentation or tension-compression simulations to evaluate the effect of surface OH groups on the mechanical response. We compared our non-hydroxylated samples to published studies which use the same potential.

For acceleration we used the KOKKOS and MPI libraries provided with LAMMPS. We carried out our simulations using either Nvidia GPUs (GTX 1080Ti and Titan V) or Intel Xeon CPUs. Runtimes varied from a few hours to a few days depending on the thermostat used.

## RESULTS

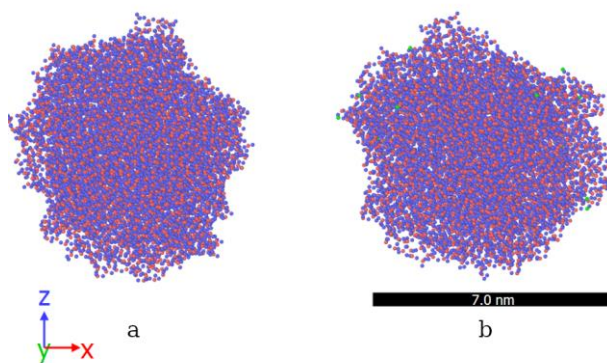


Figure 1. Initial configuration of a  $R=3.5\text{nm}$  silica nanosphere: a) without grafted OH groups and b) with surface OH groups at a  $0.092$  density by  $\text{nm}^2$ . Blue:Si, red: O, green: H.

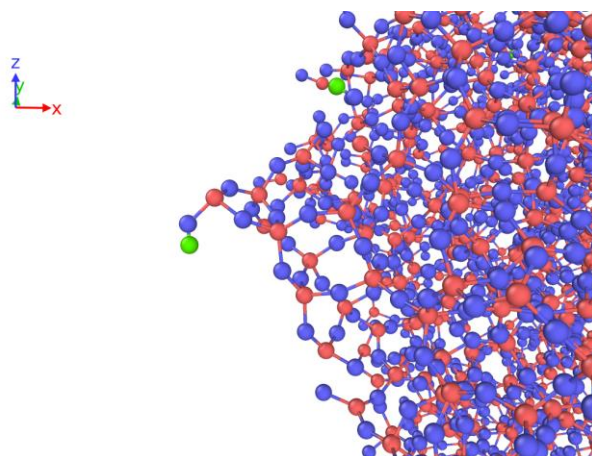


Figure 2. Close up of the surface of a partially hydroxylated silica nanosphere showing an isolated silanol group ( $-\text{SiOH}$ ).

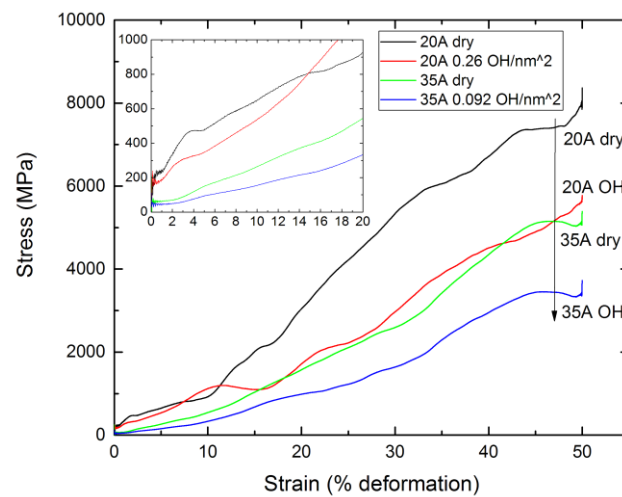


Figure 3. Effect of size and wetting on the compressive behaviour of silica nanospheres

## DISCUSSIONS

The sphere including hydroxyl group grafted on surface at a density equal to  $0.092 \text{ OH/nm}^2$  (Fig. 1b), has a quite larger roughness, and some differences are observed in the nearby rings. Initial results indicate that surface effects on the mechanical behavior of nanospheres are significant. Our simulations show that increasing the radius of our nano-spheres effectively lowers their stiffness by a non-negligible amount.

In addition, we note that even at relatively low surface OH concentrations of  $0.09$  and  $0.26 \text{ OH/nm}^2$  we can still observe a reduction in the stiffness of our nano-spheres. The reduction is more marked for larger diameter spheres and at larger strains.

## CONCLUSION

A refined strategy was designed to represent small nanowires of silica aerogel with the ReaxFF potential.

Spheres of aerogel up to a few tens of cubic nanometers were numerically designed. Grafting of hydroxyl groups with increasing quantities of OH up to  $2 \text{ per nm}^2$  were performed.

First results confirmed that those surface groups highly modify mechanical properties of the material.

## ACKNOWLEDGEMENT

Thanks are due to the AURA program that granted the COMPASS program in the societal energy fields.

## REFERENCES

- Chowdhury, S.C., Haque, B.Z., Gillespie, J.W., 2016. Molecular dynamics simulations of the structure and mechanical properties of silica glass using ReaxFF. *Journal of Materials Science* 51, 10139–10159. <https://doi.org/10.1007/s10853-016-0242-8>
- Gonçalves, W., Morthomas, J., Chantrenne, P., Perez, M., Foray, G., Martin, C.L., 2018. Elasticity and strength of silica aerogels: A molecular dynamics study on large volumes. *Acta Materialia* 145, 165–174. <https://doi.org/10.1016/j.actamat.2017.12.005>
- Rimsza, J.M., Yeon, J., van Duin, A.C.T., Du, J., 2016. Water Interactions with Nanoporous Silica: Comparison of ReaxFF and *ab Initio* based Molecular Dynamics Simulations. *The Journal of Physical Chemistry C* 120, 24803–24816. <https://doi.org/10.1021/acs.jpcc.6b07939>
- Yeon, J., van Duin, A.C.T., 2016. ReaxFF Molecular Dynamics Simulations of Hydroxylation Kinetics for Amorphous and Nano-Silica Structure, and Its Relations with Atomic Strain Energy. *The Journal of Physical Chemistry C* 120, 305–317. <https://doi.org/10.1021/acs.jpcc.5b09784>
- Yu, Y., Wang, B., Wang, M., Sant, G., Bauchy, M., 2016. Revisiting silica with ReaxFF: Towards improved predictions of glass structure and properties via reactive molecular dynamics. *Journal of Non-Crystalline Solids* 443, 148–154. <https://doi.org/10.1016/j.jnoncrysol.2016.03.026>
- Zhang, C., Duan, F., Liu, Q., 2015. Size effects on the fracture behavior of amorphous silica nanowires. *Computational Materials Science* 99, 138–144. <https://doi.org/10.1016/j.commatsci.2014.12.020>



## Ultralight carbon-based composites foam with considerable thermal insulation

Zhang Junxiong<sup>1,2</sup>, Chen Zhaofeng<sup>1,\*</sup>, Xue Songbai<sup>1</sup>

<sup>1</sup>International Laboratory for Insulation and Energy Efficiency Materials, Nanjing University of Aeronautics and Astronautics, Nanjing, P. R. China

<sup>2</sup>Jiangsu Collaborative Innovation Center for Advanced Inorganic Function Composites, Nanjing University of Aeronautics and Astronautics, Nanjing, P. R. China

<sup>3</sup>Kyushu University, Kasuga-Fukuoka, Japan

\*Corresponding e-mail: zhaofeng\_chen@163.com

### ABSTRACT

Ultralight carbon-based composites foam is fabricated by the CVD method in this research. The composites foam possesses a typical microstructure formed by the hairy composite's cells consisted of the carbon foam and the SiC nanowires. Results show that this composites foam is ultralight with a minimum density of 5.56 mg/cm<sup>3</sup> as 4.3 time as the standard air. Meanwhile, this ultralight foam possesses considerable thermal insulation in a temperature range of ~900°C, where its minimum thermal conductivity is 0.055 W m<sup>-1</sup> K<sup>-1</sup> about 3.2% of that of carbon foam matrix at 900°C. And, it's a kind of promising material of this ultralight composite foam for the application of the thermal insulation of the spacecraft.

### KEYWORDS

Ultralight, thermal insulation, composites foam, SiC nanowires

### INTRODUCTION

Carbon foam is a class of carbon materials consisted of over 99% open-cell porous. And, the porous forms a three-dimensional (3D) interconnected network with a porous diameter of 10~20μm. In general, this material is compressible, flexible and sponge-like macroporous materials with specific characteristics for thermal insulation, acoustic insulation, great absorptivity and low density [1, 2]. A reported of novel carbon foam is fabricated by pyrolyzing the melamine foam directly, and this foam shows non-graphitic skeletons with a 3D elastic/flexible interconnected network [3].

SiC<sub>nw</sub> are an important ceramic nanowire with great compressive resistance, which draws a series of attentions for its excellent mechanical properties [4] and low thermal conductivity [5]. Meanwhile, reports showed that the SiC<sub>nw</sub> could play a positive role on reducing the thermal conductivity of the composite by varying the volume fraction, size and orientation of the SiC<sub>nw</sub>[6,7]. In this work, flexible MCF was employed as matrix to fabricating 3D interconnected SiC<sub>nw</sub>/MCF composites foam with hairy skeletons by a simple process of CVI process with Ni catalyzed.

### METHODS

The preparing process of SiC<sub>nw</sub>/MCF composites aerogel includes three steps. Firstly, the MCF preparation. Firstly, the MCF was obtained by pyrolyzing MF at a temperature range of ~1100°C with an argon gas flow of 400 sccm. The Ni/MCF was obtained by soaking MCF in the different catalyst solutions and dried at 60°C for 12h, where catalyst solutions with Ni<sup>2+</sup> were made of ethanol (AC, ≥ 99.7%) and Ni(NO<sub>3</sub>)<sub>2</sub>·6H<sub>2</sub>O (AC, ≥ 98%). Subsequently, the

Ni/MCF was put in a LPCVI furnace to fabricate  $\text{SiC}_{\text{nw}}$  with a gas mixture of  $\text{CH}_3\text{SiCl}_3$  (MTS),  $\text{H}_2$  and Ar for 2~5h, which obtained ultralight  $\text{SiC}_{\text{nw}}$ /MCF composites with different densities.

Morphologies of samples were observed by scanning electron microscopies (S4800 Hitachi SEM). Phases of MCF and  $\text{SiC}_{\text{nw}}$ /MCF were characterized by X-ray diffraction (XRD, D8 Advance). For the thermal conductivity, the MCF and the  $\text{SiC}_{\text{nw}}$ /MCF were cut into rounds with a diameter of 12.5 mm and a thickness of 1.5 mm for the thermal diffusivity measurement. Thermal conductivity was calculated from  $\kappa = D \cdot \rho \cdot C_p$ , where  $D$  was the thermal diffusivity in a temperature range of  $100^\circ\text{C} \sim 900^\circ\text{C}$  and measured by the laser flash diffusivity method in a LFA427 (NETZSCH, LFA427, Germany).

## RESULTS AND DISCUSSION

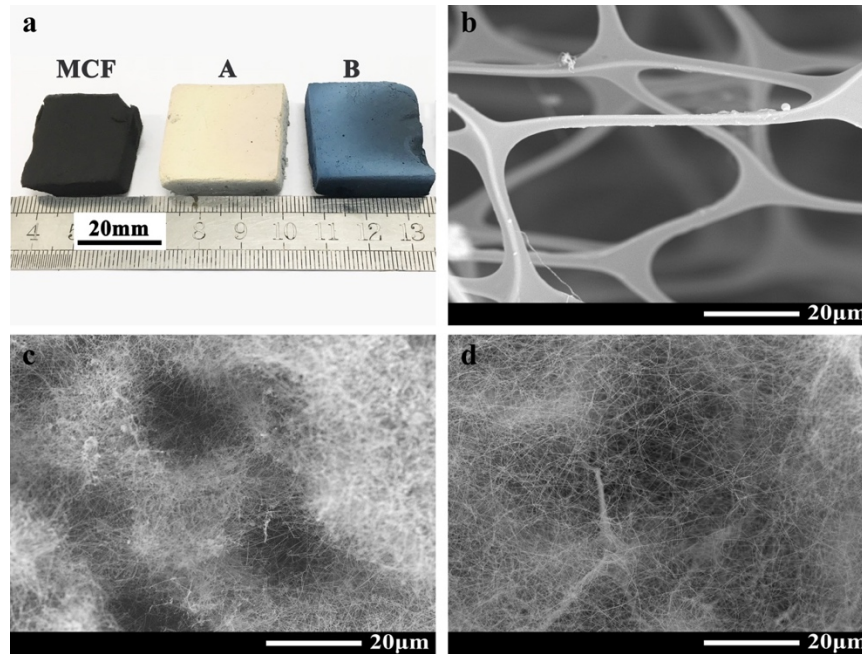


Figure 1. Photos of samples and relative morphology of  $\text{SiC}$  nanowires covered on the MCF skeleton, (a) Photos of samples, (b)~(d) morphology of MCF, sample A and sample B

Figure.1 displayed the photos of samples and their relative morphology of from SEM. It was obvious that the MCF shown in figure.1(b) possessed a 3D interconnected network consisted of surface smooth carbon skeletons. And, the microstructure of sample A and B were exhibited in fig1(c) and (d). Compared to fig1(b), the morphologies of sample A and B with 3D network were unusual with lots of nanowires sprouted from the carbon skeletons and covered on them, but they were still with visible macroporous outlines of original MCF. However, the figure.1(d) showed a better 3D network than figure.1(c) for it possessing much longer nanowires to fill with the macroporous and cutting it into micropores. Densities of sample MCF, A and B are  $4.12 \pm 0.08 \text{ mg/cm}^3$ ,  $5.56 \pm 0.12 \text{ mg/cm}^3$  and  $31.30 \pm 3.54 \text{ mg/cm}^3$ . Obviously, the sample A possesses a lowest density of  $5.56 \pm 0.12 \text{ mg/cm}^3$ .

Figure.2a exhibited the microstructure of  $\text{SiC}_{\text{nw}}$  in sample A. Outlines of each  $\text{SiC}_{\text{nw}}$  was clearly visible. Measuring by Image Pro Plus software, it indicated that the  $\text{SiC}_{\text{nw}}$  were with an average diameter of  $38.06 \pm 13.37 \text{ nm}$  and tens of microns in lengths. Meanwhile, it could be found from the enlarged scale that there stood a microsphere at the tip of each nanowire obviously, which demonstrated that the growth of  $\text{SiC}_{\text{nw}}$  followed the VLS growth mechanism in the CVI process.

As shown in figure.2b, the result exhibited the three greatest diffraction peaks of  $\text{SiC}_{\text{nw}}$  located at  $35.6^\circ$ ,  $59.9^\circ$  and  $71.5^\circ$  corresponding to the crystal faces of the  $\beta$ - $\text{SiC}$  of the (111), (220) and (311), respectively [8]. However, a series of strong diffraction peaks of  $\delta$ - $\text{Ni}_2\text{Si}$  occurred in the XRD pattern either, and it was an interesting phenomenon. Therefore, we



thought that the  $\delta$ -Ni<sub>2</sub>Si occurring was because of the overweight and maldistribution on the Ni catalyst on the MCF.

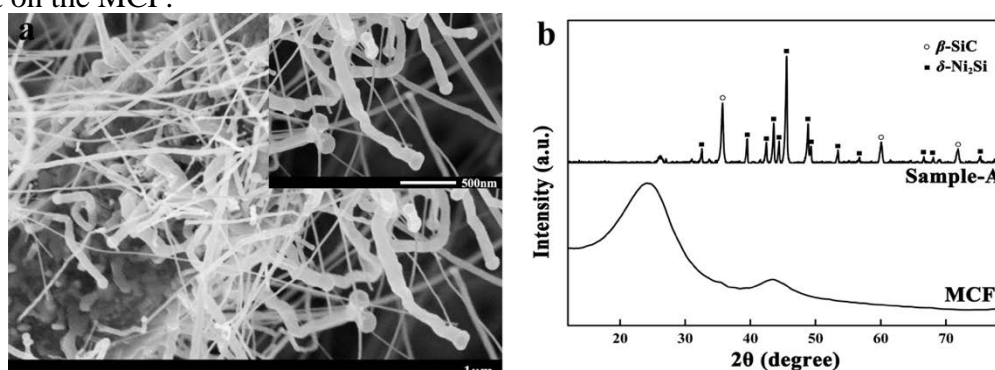


Figure 2. Microstructure of SiC nanowires in sample A and its XRD

According to the results of XRD, it involved that there  $\sigma$ -Ni<sub>2</sub>Si occurred in the SiC<sub>nw</sub>/MCF composites foam, but the existence form of  $\sigma$ -Ni<sub>2</sub>Si was unknown and needed to investigate. The HRSEM of sample A showed that a bulk of phases covered on the MCF, where few SiC<sub>nw</sub> was found to sprout from it. Obviously, the bulk was formed on a branch node of MCF skeleton. Meanwhile, lots of SiC<sub>nw</sub> were covered on MCF skeletons nearby this node. The EDS results displayed the elemental compositions of areas P1 and P2, it proved the SiC<sub>nw</sub> and Ni<sub>2</sub>Si. Therefore, we thought this phenomenon was because of the catalysis gathering on the node.

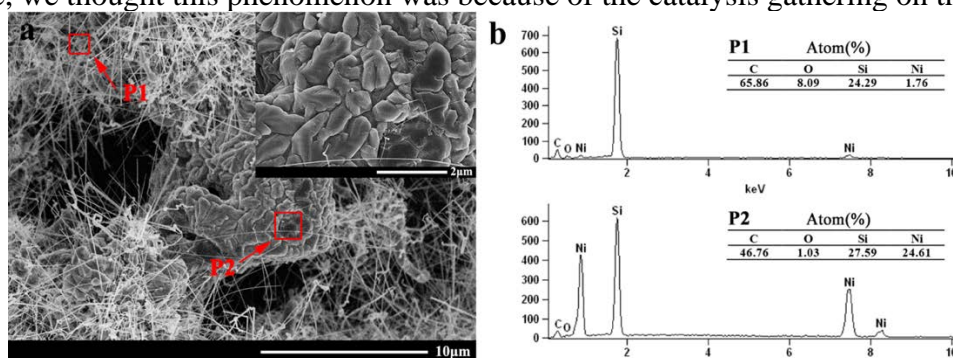


Figure 3. Morphology of and EDS of SiC nanowires

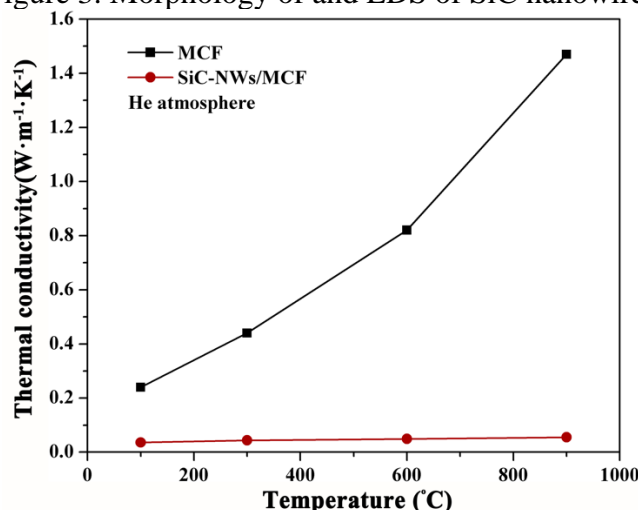


Figure 4. Thermal conductivities of MCF and SiC<sub>nw</sub>/MCF composites

Furthermore, thermal insulation of both MCF and SiC<sub>nw</sub>/MCF were investigated. Figure.4 exhibited the results of their temperature dependent thermal conductivities at He atmosphere. It was clear that the SiC<sub>nw</sub> /MCF composites possessed much higher thermal conductivity than that of the MCF at low and high temperatures, where its thermal conductivity was 0.036 W·m<sup>-1</sup>·K<sup>-1</sup> at 100°C, just 15% of that of the MCF (0.24 W·m<sup>-1</sup>·K<sup>-1</sup>). At 900°C, the thermal



conductivity of SiC<sub>nw</sub>/MCF composites was around  $0.055 \text{ W} \cdot \text{m}^{-1} \cdot \text{K}^{-1}$  increasing by 55.55% compared to that of result as  $100^\circ\text{C}$ , however, that of MCF increased to  $1.475 \text{ W} \cdot \text{m}^{-1} \cdot \text{K}^{-1}$ , 29.34 times than that of the SiC-NWs/MCF. Apparently, it meant that the SiC-NWs/MCF possessed a perfect thermal insulation property at low and high temperature. Therefore, it was meaningful to apply this material for high temperature thermal insulation.

## CONCLUSIONS

In this paper, SiC<sub>nw</sub>/MCF composites foams were synthesized by CVI with Ni catalyst using flexible MCF as template. For the SiC<sub>nw</sub>/MCF composites foams, their distinct morphologies were observed that crooked SiC<sub>nw</sub> sprouted from the MCF skeletons and covered it accompanying with Ni catalyst microspheres standing on each SiC<sub>nw</sub> tip. The pores in the SiC<sub>nw</sub>/MCF composites foams were much smaller than that of MCF due to the segmentation effect of the SiC<sub>nw</sub>. For the sample A and B, they were with their density controlled at 5.56 mg/ml and 9.97 mg/ml. It was a potential material of this SiC<sub>nw</sub>/MCF composites foams for utilization as an ultralight porous catalyst carrier and so on. The SiC<sub>nw</sub>/MCF composites possessed perfect thermal insulation that its thermal conductivity was  $36.1 \text{ mW} \cdot \text{m}^{-1} \cdot \text{K}^{-1}$  (at  $100^\circ\text{C}$ ) and  $55.5 \text{ mW} \cdot \text{m}^{-1} \cdot \text{K}^{-1}$  (at  $900^\circ\text{C}$ ) respectively, much better than that of MCF matrix.

## ACKNOWLEDGEMENT

The present work was supported by the National Natural Science Foundation of China (Grant No. 51772151, 51761145103). This work was also supported the Priority Academic Program Development of Jiangsu Higher Education Institutions.

## REFERENCES

- [1]. Li, S., Guo, Q., Song, Y., Liu, Z., Shi, J., Liu, L., & Yan, X. Carbon foams with high compressive strength derived from mesophase pitch treated by toluene extraction. *Carbon* 45, 2843-2845, doi: 10.1016/j.carbon.2007.09.035 (2007).
- [2]. Zani, A., Dellasega, D., Russo, V., & Passoni, M.. Ultra-low density carbon foams produced by pulsed laser deposition. *Carbon* 56, 358-365, doi: (2013).
- [3]. Zhang, H., Zhou, Y., Li, C., Chen, S., Liu, L., Liu, S., Yao, H., & Hou, H. Porous nitrogen doped carbon foam with excellent resilience for self-supported oxygen reduction catalyst. *Carbon* 95, 388-395, doi: 10.1016/j.carbon.2015.08.025 (2015).
- [4]. Pei, B., Zhu, Y., Yuan, M., Huang, Z., & Li, Y. Effect of in situ grown SiC nanowires on microstructure and mechanical properties of C/SiC composites. *Ceramics International* 40, 5191-5195, doi: 10.1016/j.ceramint.2013.10.077 (2014).
- [5]. Roewer, G., Herzog, U., Trommer, K., Müller, E., & Frühauf, S. Silicon carbide—a survey of synthetic approaches, properties and applications. In *High performance non-oxide ceramics I* (pp. 59-135). Springer, Berlin, Heidelberg, (2002).
- [6]. Xu, Y., Tanaka, Y., Murata, M., Kamihira, K., Isoda, Y., & Yagi, K. Thermal conductivity of unidirectionally aligned SiC whisker reinforced Al alloy matrix composite with interfacial thermal resistance. *Materials transactions* 46, 148-151, doi: 10.2320/matertrans.46.148 (2005).
- [7]. Geng, L., Ochiai, S., Wang, B., & Yao, C. K. Effect of whisker volume fraction on the coefficient of thermal expansion and thermal conductivity of SiCw/6061Al composites. *Journal of materials science letters* 17, 403-405, doi: 10.1023/A:1006539318554 (1998).
- [8]. Ge, Y. C., Liu, Y. Q., Shuai, W. U., Huang, W. U., Mao, P. L., & Yi, M. Z. Characterization of SiC nanowires prepared on C/C composite without catalyst by CVD. *Transactions of Nonferrous Metals Society of China* 25, 3258-3264, doi: 10.1016/S1003-6326(15)63962-0 (2015).

Platinum Level Sponsorship

VACUUM INSULATION PANEL



Gold Level Sponsorship



Silver Level Sponsorship



Bronze Level Sponsorship

